SMIP95

SMIP95 SEMINAR ON SEISMOLOGICAL AND ENGINEERING IMPLICATIONS OF RECENT STRONG-MOTION DATA

San Francisco, California
May 16, 1995

PROCEEDINGS

Sponsored by

California Strong Motion Instrumentation Program
Division of Mines and Geology
California Department of Conservation

Supported in Part by

California Seismic Safety Commission

DEPARTMENT OF CONSERVATION
Division of Mines and Geology

The California Strong Motion Instrumentation Program (CSMIP) is a program within the Division of Mines and Geology of the California Department of Conservation and is advised by the Strong Motion Instrumentation Advisory Committee (SMIAC), a committee of the California Seismic Safety Commission. Current program funding is provided by an assessment on construction costs for building permits issued by cities and counties in California, with additional funding from the California Department of Transportation, the Office of Statewide Health Planning and Development, and the California Department of Water Resources.

SMIP95

SMIP95 SEMINAR ON SEISMOLOGICAL AND ENGINEERING IMPLICATIONS OF RECENT STRONG-MOTION DATA

San Francisco, California
May 16, 1995

PROCEEDINGS

Edited by

M.J. Huang

Sponsored by

California Strong Motion Instrumentation Program
Division of Mines and Geology
California Department of Conservation
801 K Street, MS 13-35
Sacramento, California 95814-3531

Supported in Part by

California Seismic Safety Commission

PREFACE

The California Strong Motion Instrumentation Program (CSMIP) in the Division of Mines and Geology of the California Department of Conservation promotes and facilitates the improvement of seismic codes through the Data Interpretation Project. The objective of this project is to increase the understanding of earthquake strong ground shaking and its effects on structures through interpretation and analysis studies of CSMIP and other applicable strong-motion data. The ultimate goal is to accelerate the process by which lessons learned from earthquake data are incorporated into seismic code provisions and seismic design practices.

Since the establishment of CSMIP in early 1970s, over 600 stations, including 400 ground-response stations, 140 buildings, 20 dams and 35 bridges, have been installed. Significant strong-motion records have been obtained from many of these stations. One of the most important sets of strong-motion records is from the 1994 Northridge earthquake. During this earthquake strong-motion records were obtained from 116 ground-response stations and 77 extensively-instrumented structures. In addition to these records, CSMIP is cooperating with the City of Los Angeles and other agencies to collect and process accelerograms recorded at over 300 high-rise buildings during the Northridge earthquake. These buildings were instrumented by the building owners as required by the City's Building Code. The strong-motion records from the Northridge earthquake have been and will be the subject of CSMIP data interpretation projects.

The SMIP95 Seminar is the seventh in a series of annual events designed to transfer recent interpretation findings on strong-motion data to practicing seismic design professionals and earth scientists. In both oral presentations and poster sessions, investigators of four CSMIP-funded data interpretation projects presented the results from interpretation studies of CSMIP data during the past year. In addition, CSMIP staff presented a study on near-real-time strong-motion monitoring, and three invited speakers presented topics related to strong-motion data. One paper was on strong-motion records from the 1995 Kobe, Japan earthquake, and two were on analysis of the response of steel frame buildings during the Northridge earthquake. Professor Bruce Bolt of UC Berkeley presented a keynote address at the luncheon on the prediction of seismic ground motion.

The papers in this Proceedings volume presented by the investigators of four CSMIP-funded data interpretation projects represent interim results. Following this seminar the investigators will be preparing final reports with their final conclusions. These reports will be more detailed and will update the results presented here. CSMIP will make these reports available after the completion of the studies.

TABLE OF CONTENTS

SMIP95 SEMINAR ON

SEISMOLOGICAL AND ENGINEERING IMPLICATIONS

OF RECENT STRONG MOTION DATA

San Francisco Airport Radisson Hotel, California
May 16, 1995

PROGRAM

8:30-9:30	**Registration**
9:30-9:40	**Welcoming Remarks** *Wilfred Iwan*, Seismic Safety Commission, and Chair, Strong Motion Instrumentation Advisory Committee (SMIAC) *James Davis*, State Geologist, Division of Mines and Geology
9:40-9:45	**Introductory Remarks** *Anthony Shakal*, Manager, Strong Motion Instrumentation Program
SESSION I	**Ground Response** **Moderator:** *Bruce Bolt*, UC Berkeley Chair, SMIAC Ground-Response Subcommittee
9:45-10:10	**CSMIP Near-Real-Time Strong Motion Monitoring System: Rapid Data Recovery and Processing for Event Response** *A. Shakal, C. Petersen, A. Cramlet and R. Darragh*, CSMIP
10:10-10:35	**Ground Motion Prediction for Thrust Earthquakes** *P. Somerville and N. Abrahamson*, Woodward-Clyde Federal Services, Pasadena
10:35-11:00	Break
SESSION II	**Building Response** **Moderator:** *Wilferd Peak*, Consulting Engineering Geologist Chair, SMIAC Data Interpretation Subcommittee
11:00-11:25	**Evaluation of Seismic Code Provisions using Strong-Motion Building Records from the 1994 Northridge Earthquake** *J. De la Llera* and *A. Chopra*, University of California, Berkeley
11:25-11:50	**Response of Base-Isolated Buildings during the 1994 Northridge Earthquake** *S. Nagarajaiah*, University of Missouri, Columbia
11:50-12:20	**Poster Session**

12:20-2:10 **Lunch**
Introduction *Wilfred Iwan*, Chair, SMIAC
Keynote Address: **The Prediction of Seismic Ground Motion**
Bruce Bolt, UC Berkeley

SESSION III **Lifeline Structure Response and Kobe Earthquake**
Moderator: *Vern Persson*, Division of Safety of Dams, DWR
Chair, SMIAC Lifelines Subcommittee

2:10-2:35 **Effect of Contraction Joint Opening on Pacoima Dam in the 1994 Northridge Earthquake**
G. Fenves and S. Mojtahedi, University of California, Berkeley

2:35-3:00 **Strong-Motion Records from the Kobe, Japan Earthquake of January 17, 1995 and Implications for Seismic Hazards in California**
P. Somerville, Woodward-Clyde Federal Services, Pasadena (Invited)

3:00-3:20 Break

SESSION IV **Steel Moment Frame Buildings**
Moderator: *Chris Poland*, H.J. Degenkolb Associates
Chair, SMIAC Buildings Subcommittee

3:20-3:45 **Assessment of the Performance of Steel Moment Frame Buildings during the 1994 Northridge Earthquake: Task 3 of SAC Steel Program**
J. Malley, H.J. Degenkolb Associates, San Francisco (Invited)

3:45-4:10 **Dynamic Analysis of a 13-story Steel Frame Building Instrumented and Damaged in the 1994 Northridge Earthquake**
C.-M. Uang, Q. Yu, A. Sadre, D. Bonowitz, and N. Youssef,
University of California, San Diego (Invited)

4:10-4:15 **Closing Remarks**

CSMIP NEAR-REAL-TIME STRONG MOTION MONITORING SYSTEM: RAPID DATA RECOVERY AND PROCESSING FOR EVENT RESPONSE

A.F. Shakal, C.D. Petersen, A.B. Cramlet and R.B. Darragh

California Department of Conservation
Division of Mines and Geology
Strong Motion Instrumentation Program

ABSTRACT

Recent developments in accelerographic instruments and communication technology have made possible significant advances in the monitoring and reporting of earthquake strong motion. The California Strong Motion Instrumentation Program (CSMIP) has developed and implemented an economical system for near-real-time data recovery from strong-motion stations in its network. The system can guide earthquake response and provide shaking data rapidly to emergency responders, engineers and seismologists. The system has extensive redundancy and can be easily expanded as more stations are added. The data recovered are automatically processed to produce the ground motion parameters most useful for engineering assessment of the earthquake impact. Distribution channels for the rapid strong-motion information continue to be developed and will include local and state emergency response officials as well as earthquake seismology and engineering agencies.

INTRODUCTION

During the minutes and hours after a strong earthquake in California, little information has been available on the levels of shaking that occurred. The traditional seismic monitoring networks (weak motion) have developed capabilities over the last five years that allow rapid determination of the earthquake epicenter and magnitude and rapid distribution of that information (e.g., Caltech USGS Broadcast of Earthquakes (CUBE) and the Rapid Earthquake Data Integration (REDI) system). However these networks are mostly comprised of instruments designed to record the thousands of small to moderate earthquakes that occur every year in California. These instruments can provide only limited information on large earthquakes because the shaking exceeds their measuring range.

In contrast, strong-motion networks do accurately measure the strong shaking, using instruments specialized for recording the strongest motions. However, these instruments were originally designed to provide data for strong-motion research, and not designed to provide the data they record quickly. As a result of these two aspects, very little strong shaking information has been available after an earthquake in a time frame useful to guide emergency response activities.

An example from the 1994 Northridge earthquake dramatizes the problem. The Santa Monica area was shaken with unexpected severity relative to neighboring areas. Yet this was not widely known for some time, since most attention was focused on the epicentral area and the San Fernando Valley. The strong-motion instrument on the grounds of the Santa Monica City Hall did accurately record the severe shaking. However, the data from that analog

instrument could not be recovered and provided to regional and state officials for several days.

The 1989 Loma Prieta earthquake provided another example. The Santa Cruz and Watsonville areas were heavily damaged during the event, but that was not known for several hours because the focus was on the San Francisco Bay area. Oakland was more heavily shaken than could have been expected, while in contrast, San Jose, closer to the event, was shaken less. These shaking levels were all recorded by strong-motion instruments, but the data could not be provided in a timely enough manner to be useful in strategic coordination of the available response resources or in developing early earthquake damage estimates. With expansion of the system described here, the important information can be provided to emergency officials within a few minutes.

SEISMIC NETWORKS AND EARTHQUAKE DATA TIME SCALES

In order to clarify the difference between the system described here and the traditional seismic networks, some of their differences are highlighted. One aspect is the instrument type, as discussed below. Another key aspect is that seismic networks operate in real-time, while the strong-motion system described here operates in near-real-time. These two time scales are important to consider in post-earthquake data reporting.

Real-Time Real-time seismic data are available at a central location at the same time shaking at a field station occurs. This is data-as-it-happens, being recorded at a central site and available for processing. Real-time data requires a continuous, dedicated telemetry or other communication link from the station to the central site. Once data is available at the central site, the epicenter and magnitude can be quickly determined.

The development of techniques for rapid determination and dissemination of the location and magnitude of an earthquake was a significant improvement in seismic monitoring in California. The CUBE system initiated in 1990 in southern California was the pioneer project in this effort (Kanamori et al., 1993). In Northern California, the REDI system (Romanowicz, 1993), a joint project of UC Berkeley and the USGS, now parallels the CUBE capability.

CUBE and REDI rely primarily on the existing real-time weak-motion seismic monitoring networks in California. These instruments and networks were designed to detect and locate small events on fault systems in California. For large earthquakes these sensitive instruments are overdriven and can provide little information beyond duration. The instruments go off-scale because of their limited dynamic range, and their narrow frequency response means they do not measure the long-period motion of larger events well. These instruments are not poorly designed, rather they are well designed for their original function, monitoring the seismicity of California. Much of what is known about the seismicity and deep geologic structure of California comes from analyses of the recordings made by these instruments. These weak-motion instruments are monitored continuously, transferring the data in real time, to a central site in both the CUBE and REDI approaches. As a result, these systems can determine very rapidly the locations of the many small earthquakes that occur in California. Speed is the strength of a real-time system, and the potentially high ongoing cost of the dedicated communication link is its price.

Near-Real-Time Near-real-time strong-motion data is available at a central facility not at the same time the shaking happens, but within seconds to minutes after earthquake shaking begins at a field station. The strong-motion monitoring system discussed here uses non-dedicated telephone links to transmit data that are recorded. The short delay, required for the data to be communicated via a non-dedicated telephone link, allows a major reduction in the cost of the information without reducing its value for many applications (Shakal et al., 1995).

The occurrence of strong shaking at a given station is quite rare in California. It is common for a period of several years to elapse between recordings of more than a few percent g at most strong-motion stations. This infrequency of significant data makes the high cost of continuous real-time data telemetry a deterrent. In contrast, the economy of near-real-time data transmission makes that approach cost effective for most strong-motion applications. This approach is the primary focus of the system described here. Before the system is described, certain characteristics of strong-motion instruments are reviewed.

DEVELOPMENTS IN STRONG-MOTION INSTRUMENTS

Until the introduction of modern designs, strong-motion instruments had little application for near-real-time seismic monitoring. Traditional accelerographs are analog, photographic-film recorders and thus they can make no contribution to rapid data recovery. Modern accelerographs are digital and store the record in solid-state memory. These instruments record the strong motion and, with minor auxiliary equipment, can transmit the record to a central facility by modem and telephone line. These instruments are very useful in a near-real-time system, since information on peak acceleration and other key parameters can be available within a few minutes after the shaking occurs. The full, complete record can also be transmitted within a few minutes. This capability can be obtained with a small incremental upgrade to existing digital instruments.

The most modern high-end accelerographs have a dual capability. They can record strong motion, like a classic accelerograph, while at the same time providing an output data stream to a digital telemetry system for continuous seismic monitoring, like a traditional weak motion system. Stations with these instruments can play a dual role, both as part of a strong-motion network and a traditional seismic network and they revolutionize strong-motion/weak-motion monitoring in that aspect. However, these units have been more expensive and have not yet been integrated into the CSMIP system described here.

CSMIP NEAR-REAL-TIME STRONG-MOTION MONITORING SYSTEM

The CSMIP strong-motion monitoring system uses the standard digital accelerographs at field stations throughout the State. These stations transmit data via high-speed dial-out communication links to Sacramento using conventional phone lines. Cellular phone links are used at remote strong-motion stations without land-line phone service. The ancillary equipment at the station consists of a high-speed modem and logic controls. The equipment at Sacramento includes a bank of standard personal computers (PCs) attached to modems and running monitoring code. The CSMIP system is illustrated

schematically in Figure 1.

At the onset of strong shaking (P-wave arrival) at a station, the field instrument system establishes a telephone connection with the central monitoring system in Sacramento (the unit at the site performs the equivalent of taking the phone off the hook and dialing a number). This ensures that a connection is established before the phone system is compromised or saturated with calls. The central monitoring system has a rolling phone line bank with the lines connected to a series of PCs with modems and backup power. When a field station calls in, the next available PC answers the call and begins to interrogate the instrument. The PC directs the instrument to identify itself and transmit a compressed file of the recorded accelerogram. Once the accelerogram has been transmitted, which may take 30-60 seconds, the PC releases the field instrument to return to monitoring strong motion at the site. The PC then begins automatic processing of the data, discussed further below. If the field instrument was unsuccessful in getting one of the PCs to answer because they were all busy or for some other reason, it tries again repeatedly after certain delays. Some of the key logic components are also used in a similar system developed by the Bureau of Reclamation in Denver for strong motion instruments located at dams through the U.S. (Viksne et al., 1995)

The design of the CSMIP monitoring system incorporates redundancy, since the PCs function in parallel and independently, and each operates with uninterruptible power systems (UPS) for backup power. This design also allows the recovery and processing of the shaking data from multiple stations to occur simultaneously. The entire system is scalable, and as the number of field instruments increases the central monitoring system is easily expanded by the proportional addition of more PCs.

The communication links being used in this project already existed at many of the recently-installed CSMIP stations. These phone lines were in use because of their value in communicating with the stations for maintenance activities. This approach yields reduced maintenance costs through more targeted maintenance work, and higher overall instrument performance levels.

Near-real-time strong ground motion data is now available from 50 CSMIP stations in California. The distribution of CSMIP stations and near-real-time stations are shown in Figure 2 for northern California.

AUTOMATED DATA PROCESSING

When a central computer has requested and received an accelerogram file from a field instrument, it begins unattended automated processing. The processing proceeds through several steps, each with careful quality control checks. The file is first uncompressed and converted from binary counts to raw acceleration data. The acceleration data is next integrated and high-pass filtered in the frequency domain to calculate the velocity. The data is once again integrated and high-pass filtered in the frequency domain to yield the estimated displacement. In normal processing selection of the optimal filtered bandwidth is a careful and time consuming process (e.g., Darragh et al., 1995). In contrast, automated processing in the near-real-time system assumes a more limited central bandwidth of 5 seconds period to 46 Hz. At the completion of processing, the system provides through pagers the peak

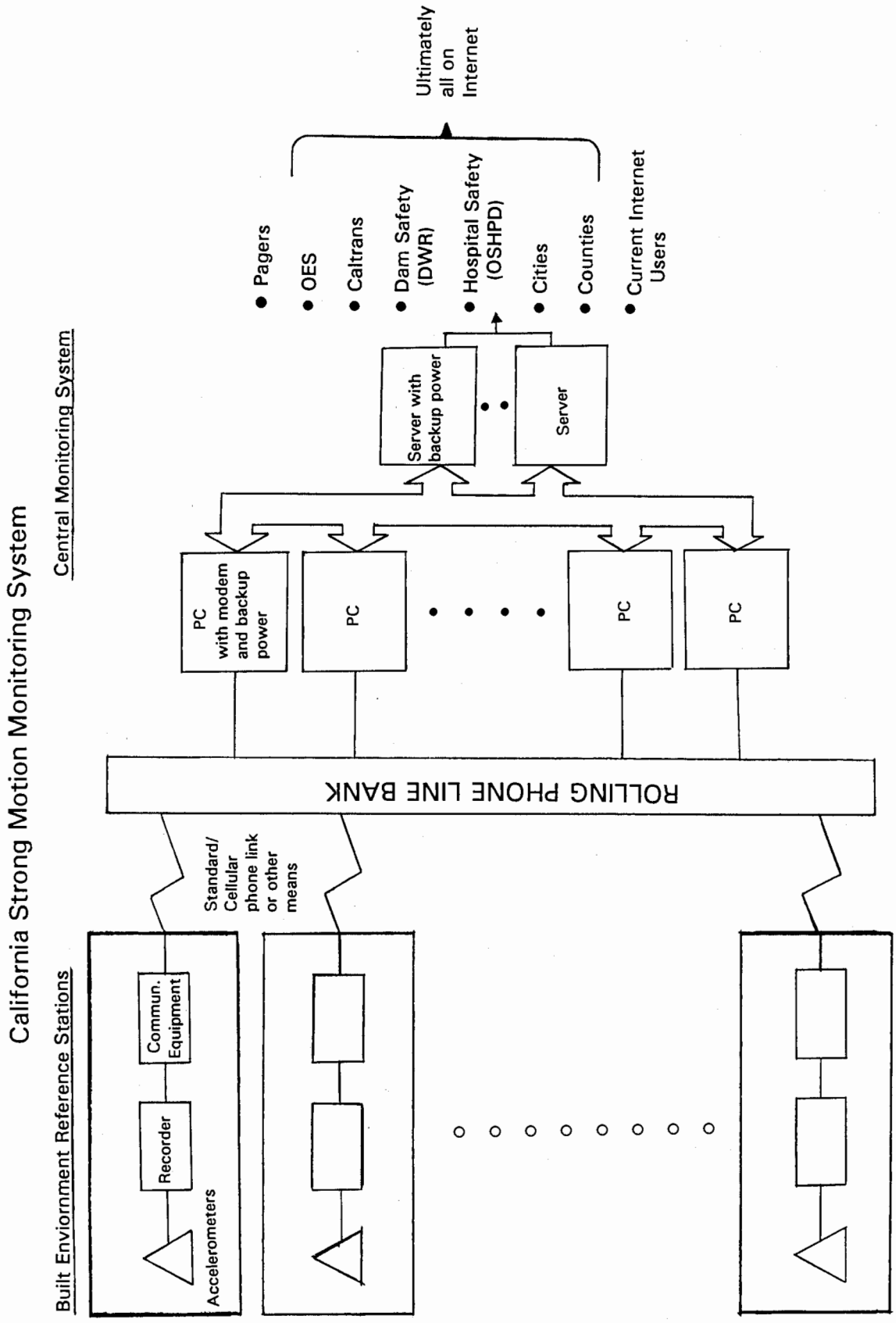

Fig. 1. Schematic of the CSMIP near-real-time strong motion monitoring system.

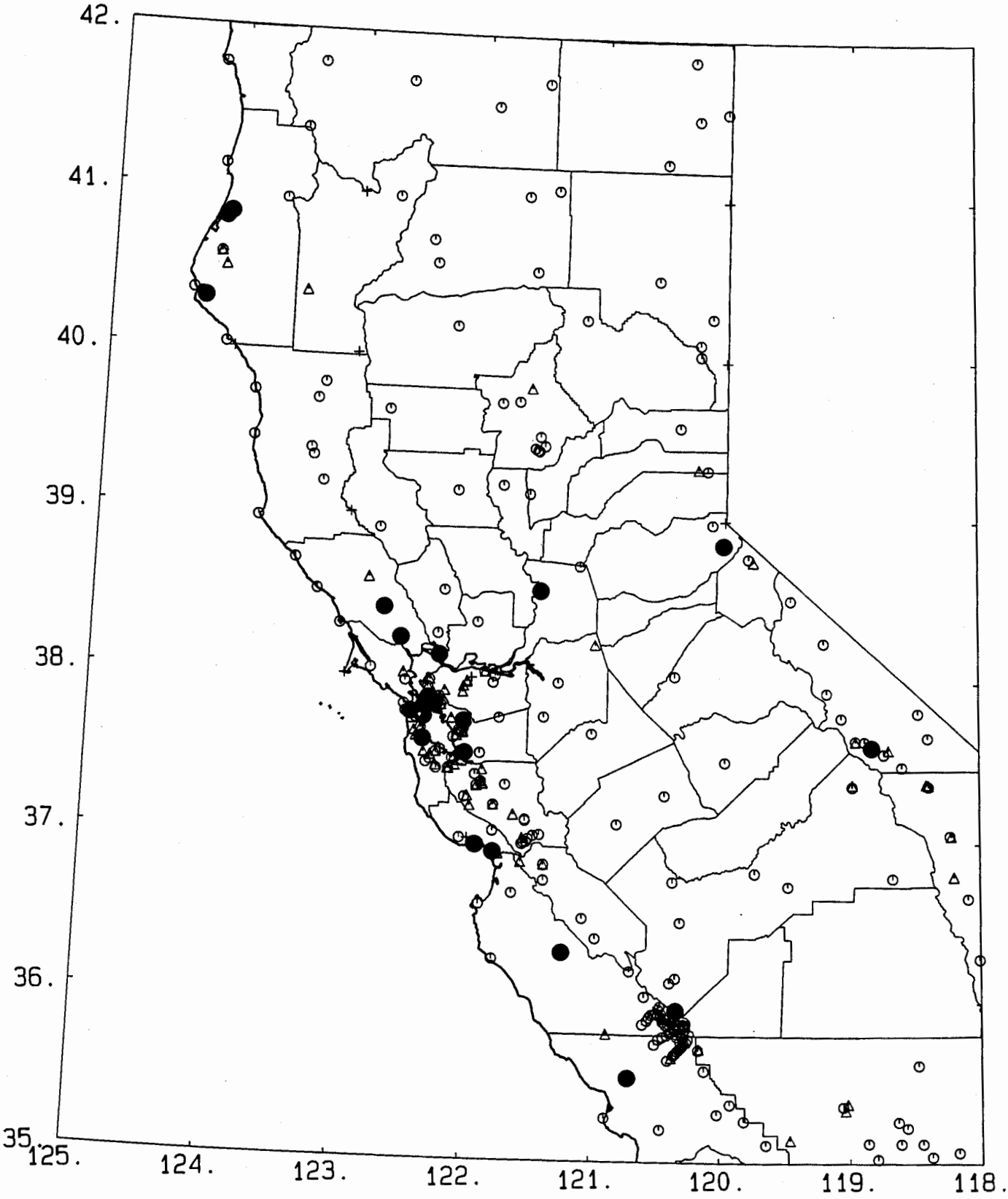

Fig. 2. CSMIP stations in northern California. Stations in the near-real-time network are shown as closed circles. Open circles and triangles are CSMIP ground-response and structure-response stations, respectively.

acceleration, velocity and displacement as well as spectral levels at selected periods to key personnel.

As an example of output of the automated system, Figures 3 and 4 show standard output plots for a record recovered and processed by the near-real-time system. The data are from the magnitude 5 earthquake that occurred about 25 km east of Palm Springs at 4:04 am on May 7 during the final preparation of this paper. Three CSMIP near-real-time stations recorded this event and the data from these stations were transmitted and processed within about 8 minutes after the occurrence of the earthquake. This time includes the delay for one of the field stations, which being remote, has a cellular phone connection running at a much slower baud rate than conventional phone connections.

Figure 3 shows the record recovered from the Desert Hot Springs station, approximately 22 km west of the epicenter. It shows the three components of band-passed acceleration, velocity and displacement. The plotting scale is 1 cm/second, like that of classic analog accelerographs, to expedite the interpretation for individuals accustomed to working with accelerograms. For the same reason, the channels are all plotted with the same vertical scale. The peak ground motions at this station are 0.065 g, 2.3 cm/sec and 0.20 cm. The response and Fourier spectra are also calculated automatically, and the response spectra for 5% damping are shown in Figure 4. Spectral acceleration is plotted up to a period of 4 seconds, and the design curve from the Uniform Building Code (ICBO, 1994) is plotted for convenient comparison.

DATA DISTRIBUTION METHODS

The most effective means of disseminating the near-real-time strong motion data results continue to be developed. Present plans include providing the data parameters to CUBE and REDI within minutes after the earthquake, as part of cooperative data exchange agreements. The data will be provided via automated Internet e-mail message or file transfer, or other electronic means, to target directories on the CUBE, REDI and possibly other computers. Peak strong motion parameters are currently being automatically sent to pagers of key personnel. Automatic data distribution methods will continue to be developed.

To serve cities, counties, state, and local jurisdictions more effectively, a more personnel-oriented approach will be used. The near-real-time information capability will be augmented by automated phoned voice messages to emergency response officials and agency staff members. These prepared messages will report the level of shaking in the community in standardized, easily-understood words. Effectively advising local communities is a central part of these plans.

BENEFITS

The ability to distribute near-real-time strong-motion data provides important benefits to the State. Post-earthquake information provided to the Office of Emergency Services (OES), cities and counties would, for the first time, contain extensive information on strong shaking amplitudes rather than being primarily limited to magnitude and location. Strong-motion instrumentation will be able to handle the largest earthquakes, complimenting the existing weak-motion seismic network instruments which will be off-scale.

Earthquake of Sun May 7, 1995 04:03 PDT
Desert Hot Springs - Fire Station Sta No. 12149
Frequency Band Processed: 5.0 secs to 46.0 Hz
- CSMIP AUTOMATED STRONG MOTION PROCESSING -

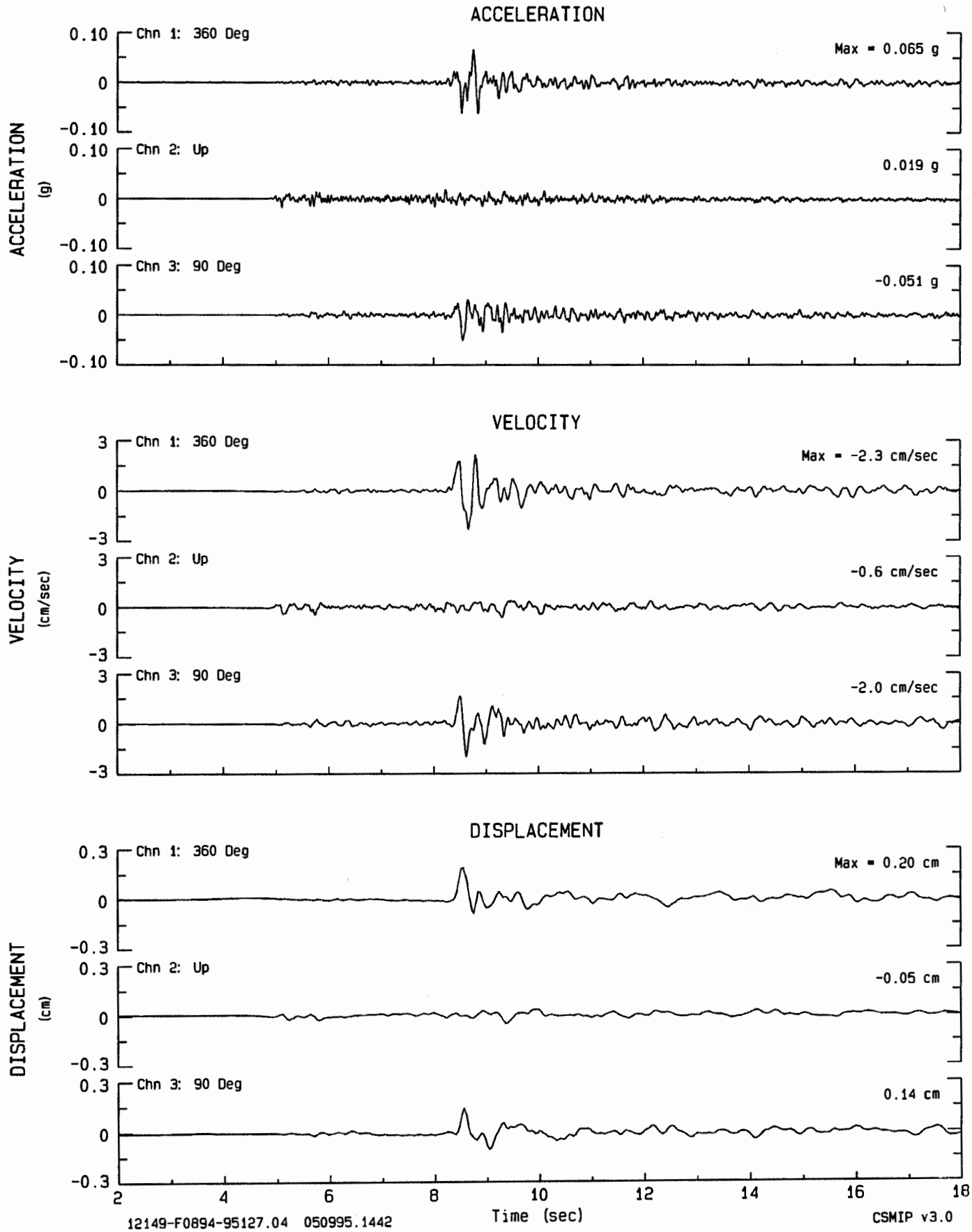

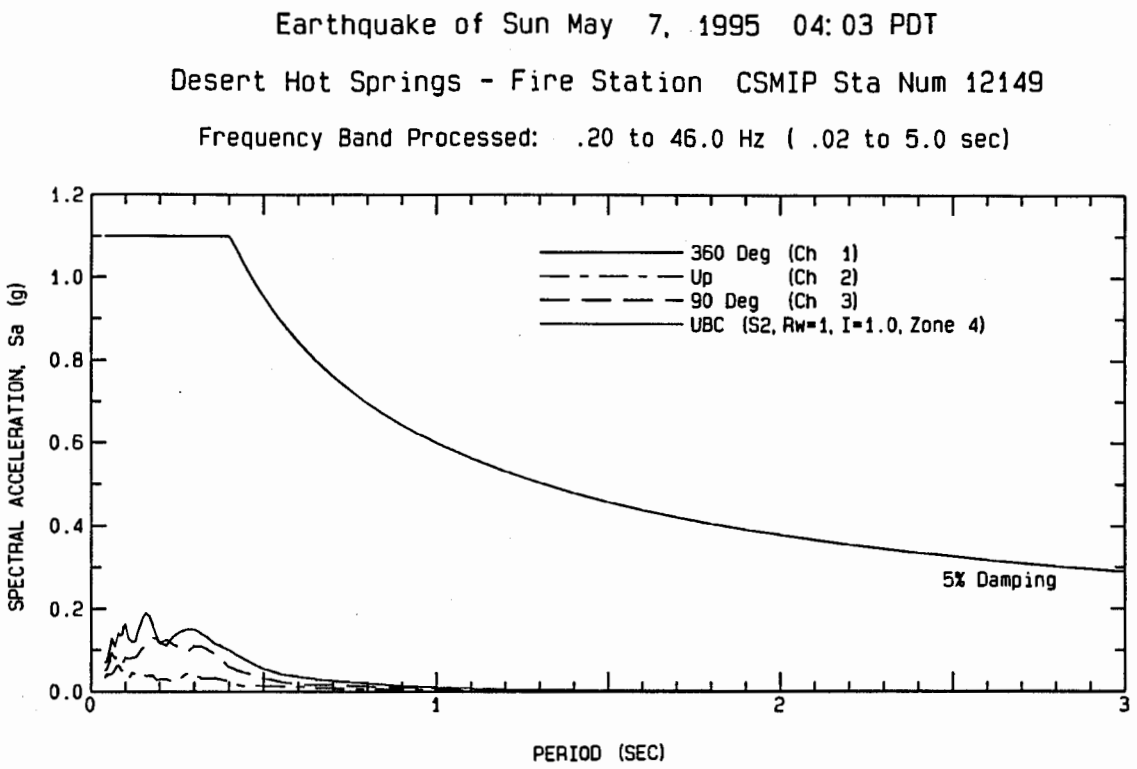

Fig. 4. Three components of band-passed spectral acceleration (5% damping) at Desert Hot Springs for the magnitude 5 earthquake of May 7. The design curve (Rw=1, for an S2 site in Zone 4) from the UBC is plotted for convenient comparison.

Systems like CUBE/REDI can be more effective in locating large earthquakes rapidly with this strong-motion information. For example, the strong-motion signal can be analyzed and the magnitude estimated from the first few tens of seconds of the acceleration. In contrast, the signals from weak-motion instruments may continue at a maximum clipped level for minutes before returning to unclipped levels so that a duration magnitude can be determined.

With the collaboration of CSMIP and CUBE/REDI, California earthquake response information can be significantly improved. More rapid, confident decisions can be made in deploying resources in the early period after an event. For example, this system would mitigate a Santa Monica situation, where unexpected localized damage occurred that unknowingly required focusing of emergency response resources. Finally, CSMIP stations located on dams, bridges, and other lifeline structures will quickly provide data on the shaking of these structures. Responsible public agencies can evaluate the hazard of these structures to the community if the measured data indicates severe shaking. Conversely, if the data indicates light shaking of the structure, that information is also important in guiding post-earthquake prioritization of responsibilities.

Fig. 3. (facing page) Three components of band-passed acceleration, velocity and displacement at Desert Hot Springs for the magnitude 5 earthquake of May 7.

SUMMARY

The CSMIP near-real-time system has successfully recorded and transmitted to Sacramento the strong shaking data from dozens of earthquakes. The largest event was a magnitude 7.2 earthquake on September 1, 1994 that was located 145 km offshore of Eureka, California. This earthquake was recorded at a bridge in the near-real-time network instrumented as part of a California Department of Transportation (Caltrans) - CSMIP statewide bridge instrumentation project currently underway. Peak motions at these stations were less than 0.1 g in acceleration, 8 cm/sec in velocity and 3 cm of displacement. The shaking and spectral information were distributed rapidly to Caltrans emergency response personnel after the earthquake. This information allowed Caltrans engineers to rapidly decide not to send inspectors to the Eureka area, 500 miles from Sacramento, to inspect their bridges in the area.

Near-real-time strong ground motion data is now available from 50 CSMIP stations in California. This expanding network is cost-effective compared to a real-time strong-motion network. Waveform data and processed strong motion (velocity, displacement and spectra) are available within a few minutes after shaking occurs at the station. In addition, both maintenance and post-earthquake data recovery costs are decreased because the station is only visited as required rather than twice per year as had been CSMIP practice. CSMIP plans to increase the number of stations in the near-real-time network both by adding new stations and by upgrading existing stations. Development of the most effective methods of transmitting the processed information to emergency response officials, building officials and the engineering and seismology agencies are underway.

REFERENCES

Darragh, R., T. Cao, V. Graizer and A. Shakal (1995). Processed CSMIP strong-motion data from the Northridge, California earthquake of January 17, 1994: Release No. 11, California Division of Mines and Geology, Office of Strong Motion Studies, Report No. OSMS 95-02, 116 p.

ICBO (1994). Uniform Building Code: Structural engineering and design provisions. International Conference of Building Officials, Whittier, CA, 2.

Kanamori, H., E. Hauksson and T. Heaton (1993). TERRAscope (abstract), *Seismological Research Letters*, **64**, p. 42.

Romanowicz, B., (1993). The Berkeley Digital Seismic Network: Upgrade status (abstract), *Seismological Research Letters*, **64**, p. 42.

Shakal, A., C. Petersen, and A. Cramlet (1995). Near-real-time CSMIP strong motion monitoring and reporting for guiding event response (abstract), *Seismological Research Letters*, **66**, p. 45.

Viksne, A., C. Wood and D. Copeland (1995). Seismic monitoring/strong motion program and notification system, in Water Operation and Maintenance Bulletin, No. 171, Bureau of Reclamation, Denver, CO, 7-12.

GROUND MOTION PREDICTION FOR THRUST EARTHQUAKES

P. SOMERVILLE[1] AND N. ABRAHAMSON[2]
[1]Woodward-Clyde Federal Services, Pasadena, Ca
[2] Consultant, Castro Valley, CA

ABSTRACT

In previous studies, the ground motion for reverse faults has been distinguished from the ground motion from strike-slip faults by a style-of-faulting factor in the attenuation relation. In most studies, this style-of-faulting factor has been assumed to be constant for all magnitudes, distances, and periods; however, some studies have examined these factors but not all together. The empirical ground motions for thrust faults are evaluated by developing a model for the magnitude, distance, and period dependence of the style-of-faulting factor. In developing the distance dependence, we distinguish between sites on the hanging wall from those on the foot wall, and from sites off the edge of the fault rupture. We find that there is a strong magnitude dependence of the style-of-faulting factor with smaller magnitude events producing a larger style-of-faulting factor. A strong distance dependence is found: sites over the hanging wall at distances of 8 to 18 km have an additional increase in ground motion of up to 50%; sites on the foot wall at distances of 12-30 km have a reduction of the ground motion of about 35%. No systematic period dependence is found over the period range of 0.03 to 5 seconds for sites off the ends of the rupture (not over the hanging wall or foot wall), but a strong period dependence is found for sites over the hanging wall and foot wall with smaller style-of-faulting factors at long periods (T> 1 sec).

INTRODUCTION

Recent empirical attenuation relation studies have generally found that peak horizontal accelerations from thrust earthquakes are 20-30% larger than from strike-slip earthquakes for the same magnitude and closest distance (e.g. Campbell 1993; Idriss 1991; Sadigh et al, 1993; Boore et al, 1994). This effect of earthquake mechanism on the ground motion has been called the style-of-faulting factor. For most attenuation relations, the style-of-faulting factor is simply a scale factor that is applied at all magnitudes and distances, and often the style-of-faulting factor derived for peak acceleration is assumed to apply to response spectral values at all periods as well.

Boore et al. (1994) estimated the style-of-faulting factor independently for each period for period of 0.1 to 2.0 seconds (plus PGA). They found that the style-of-faulting factor was not strongly dependent on period but did show a reduction at long periods (Figure 1A). Campbell and Bozorgnia (1994) examined the distance and magnitude dependence of the style-of-faulting factor for peak acceleration. They found that the style-of-faulting factor decreased with increasing magnitude and distance (Figure 1B), but they did not distinguish between sites on the hanging wall from those on the footwall.

Thrust earthquakes typically occur on non-vertically dipping faults. For dipping faults, the ground motion is not expected to be the same on both sides of the fault. Based on simple geometry alone, we expect that sites located above the fault rupture on the hanging wall will have larger ground motions than sites at the same rupture distance located on the foot wall because the hanging wall sites are closer to a larger area of the source than the foot wall sites (Figure 2) . This difference in the proximity of the source to the site is a result in part of using the shortest distance to the rupture plane as the definition of the closest distance. (Note that the distance measure used by Boore et al. accommodates some of the hanging wall and foot wall effects due to its definition.

For fault ruptures that do not reach the surface, we define the separation between the hanging wall and foot wall by the vertical projection of the top of the rupture plane (Figure 2). Using this definition, the hanging wall and foot wall motions must become equal for sites located directly over the top edge of the fault. Therefore, it does not make sense to simple estimate separate hanging wall and foot wall style-of-faulting factors. To do so would create a discontinuity at the surface projection of the top of the rupture. Sites off the edge of the fault rupture are excluded from the hanging wall and foot wall effects for this study (Figure 2).

As part of the CSMIP study, we are examining the magnitude and distance dependence of the style-of-faulting factor using both empirical data analyses and numerical simulations. In this paper, the preliminary results of the empirical data analysis are presented.

APPROACH

The magnitude and distance dependence of the style-of-faulting factor is evaluated by examining the residuals of the ground motion from attenuation relations. The full data set is used to develop the attenuation relations and then the residuals are examined to quantify the systematic differences in the ground motions for reverse and strike-slip events and for hanging wall and foot wall sites.

The data set used in this analysis is from the study of Abrahamson and Silva (1995) and consists of 685 recordings from 56 earthquakes including events up to the 1994 Northridge earthquake. To avoid potentially significant structure effects on the recorded ground motions, recordings from buildings that are greater than two stories in height were excluded from the data set. For all of the ground motion parameters used in this study, the geometric average of the ground motion on the two horizontal components is used.

The regression analysis is performed using the random effects algorithm as described by Abrahamson and Youngs (1992). The random effects model explicitly accounts for the correlations between recordings from the same earthquake. Conceptually, the random effects model finds an optimal weighting scheme (between equal weight to each record and equal weight to each earthquake) based on the given sampling of the data. The random effects model can be interpreted as estimating an event term (random effect) for each earthquake and in this sense it is similar to the two-step procedure used by Boore et al (1994).

PEAK ACCELERATION

An initial reference ground motion attenuation relation (without a distinction between reverse and strike-slip earthquakes) is developed. The residuals of the horizontal peak acceleration from this reference model are shown in Figure 3. These residuals are the mean event residuals including the eta term and the mean residual-eta for each event. This figure shows a magnitude dependence to the style-of-faulting factor similar to that found by Campbell and Bozorgnia (1994). We also found that the reverse oblique events yielded high frequency ground motions between the strike-slip and reverse events, but closer to the reverse events. On average, the style-of-faulting factor for reverse oblique events is about 70% of that of reverse events (at frequencies above 2 Hz). For this study, we will also use a magnitude dependent style-of-faulting factor as given below:

$$f_F(M) = \begin{cases} a_1 & M<5 \\ a_1 - (a_1-a_2)(M-5)/1.5 & 5.0 < M < 6.5 \\ a_2 & M \geq 6.5 \end{cases}$$

After adding the magnitude dependent style-of-faulting factor to the regression equation, the residuals were computed to examine the distance dependence (Figure 4). To distinguish between sites on the hanging wall and sites on the foot wall, the footwall sites are plotted at negative distances and the hanging wall sites are plotted at positive distances. As can be seen in this figure, the peak acceleration residuals on the hanging wall are biased to positive values for the distance range of 10 to 30 km (e.g. the attenuation model under predicts these peak accelerations); the residuals on the foot wall are biased to negative values over the distance range of 10-50 km.

Based on the trends in the residuals (Figure 4), the following piece wise continuous functional form is used for the distance dependence of the style-of-faulting factor on the hanging wall:

$$f_{HW}(r) = \begin{cases} 0 & \text{for } 0 \le r \le x_1 \\ b_1 \dfrac{(r-x_1)}{x_2-x_1} & \text{for } x_1 < r < x_2 \\ b_1 & \text{for } x_2 \le r \le x_3 \\ b_1\left(1 - \dfrac{(r-x_3)}{x_4-x_3}\right) & \text{for } x_3 < r < x_4 \\ 0 & \text{for} \end{cases}$$

where $f_{HW}(r)$ is the hanging wall effect. The boundary distances, x_1, x_2, x_3, and x_4 were estimated by visual inspection of the trends of the residuals. With the boundary distances fixed, the constant coefficient, b_1, was then estimated by regression. A similar model is used for the footwall sites with coefficients b_2, x_5, x_6, x_7, and x_8. The resulting parameter values are listed in Tables 2 and 3.

The resulting model is plotted in Figure 5. The results of the regression show that for sites located at closest distances of 8 to 18 km on the hanging wall the peak acceleration is about 50% larger than at sites off the ends of the fault at the same closest distance.

SPECTRAL CONTENT

The spectral values were also studied to estimate the period dependence on the style-of-faulting factor. The regression analysis was performed on the normalized spectra values (Sa/pga) because this approach helps to constrain the results to give a smooth spectral shape. In this study, we want to model effects that have a smooth and systematic period dependence. An initial regression is performed at each spectral period independently and then the period dependence of the resulting coefficients is examined to determine if the coefficient does vary smoothly and systematically with period.

The period dependence of the coefficients for the magnitude dependence of the style-of-faulting factor is shown in Figure 6. This figure shows that the magnitude dependence does not have a systematic trend with period. Therefore, we adopt a period independent magnitude dependence of the style-of-faulting factor (shown in Figure 5A).

The second effect to examine is the period dependence of the hanging wall and foot wall effects. The period dependence of the coefficients for the distance dependence of the style-of-

faulting factor is shown in Figure 7. This figure indicates that there is a systematic reduction in the Hanging wall / Foot wall effect at long periods. This indicates that the spectral content of reverse earthquakes is different from that of strike-slip earthquakes for sites located over the hanging wall or foot wall.

DISCUSSION

The impact of the distance dependence of the style-of-faulting factor on peak acceleration and 1 Hz spectral acceleration attenuation relations is shown in Figure 8. This figure shows the average rock site attenuation for M=7.0 strike-slip events, reverse events (at sites not over the fault), and reverse events for sites on the hanging wall and foot wall. The flat attenuation from 4 to 8 km on the hanging wall is expected to be a recurring feature of ground motions from reverse events which should be considered in seismic hazard analyses in regions with thrust faults. We expect that a similar effect would be observed for normal faulting events, but there is not enough strong motion data from normal faulting events to test this. The reduction in the footwall motions is not as well determined as the increase on the hanging wall. The 1 Hz attenuation shows a similar hanging wall effect as peak acceleration (but somewhat less) and a larger reduction on the foot wall. The reduction on the footwall should be used with caution until the final results of this study are available, including the numerical simulation results.

ACKNOWLEDGMENTS

This work was supported by grants from the Data Interpretation Project of the CDMG Strong Motion Instrumentation Program.

REFERENCES

Abrahamson, N. A. and W. Silva (1995). A consistent set of attenuation relations, Poster at SSA meeting in El Paso.

Abrahamson, N. A. and R. R. Youngs (1992). A stable algorithm for regression analyses using the random effects model, Bull. Seism. Soc. Am., 82, 505-510.

Boore, Joyner, and Fumal (1994). Ground motion estimates for strike- and reverse-slip faults, personal communication.

Campbell, K. W. (1993). Empirical prediction of near-source ground motion from large earthquakes, Proc. International Workshop on Earthquake Hazard and Large Dams in the Himalaya, January 15-16, 1993, New Delhi, India.

Campbell, K. W. and Y. Bozorgnia (1994). Near-source attenuation of peak horizontal acceleration from workwide accelerograms recorded from 1957 to 1993, Proc. Fifth National Conf. Earthquake Eng., III, 283-192.

Idriss, I. M. (1991). Selection of earthquake ground motions at rock sites, Report prepared for the Structures Div., Building and Fire Research Lab., NIST.

Sadigh, K., C-Y Chang, N. A. Abrahamson, S. J. Chiou, and M. S Power (1993). Specification of long period ground motions: updated attenuation relationships for rock site conditions and adjustment factors for near-fault effects, Proc. ATC 17-1, Seminar on Seismic Isolation, Passive Energy Dissipation, and Active Control, Vol I, 59-70.

Table 1. Events Used Analysis of Hanging Wall / Foot Wall Effects (M>6.0)

				Number of Recordings	
Event	**M**	**Dip**	**Mech**	**Foot**	**Hang**
1952 Kern County	7.4	67	RV	1	0
1971 San Fernando	6.6	53	RV	3	1
1976 Gazli	6.8	38	RV	0	1
1978 Tabas	7.4	30	RV	1	2
1983 Coalinga	6.5	32	RV	0	2
1985 Nahanni	6.8	23	RV	1	2
1989 Loma Prieta	7.0	70	OBL	6	3
1992 Cape Mendocino	7.1	13	RV	0	3
1994 Northridge	6.7	42	RV	7	10

Table 2. Coefficients for Hanging Wall Effects

Parameter	**Value**
x_1	4
x_2	8
x_3	18
x_4	25
x_5	-6
x_6	-12
x_7	-25
x_8	-50

Table 3. Coefficients for Style-of-Faulting Factor

period	**a_1**	**a_2**	**b_1**	**b_2**
0.0	0.58	0.27	0.38	-0.29
0.1	0.58	0.27	0.38	-0.29
0.2	0.58	0.27	0.38	-0.29
0.3	0.58	0.27	0.38	-0.35
0.4	0.58	0.27	0.38	-0.41
0.5	0.58	0.27	0.38	-0.48
0.75	0.58	0.27	0.35	-0.59
1.0	0.58	0.27	0.28	-0.64
2.0	0.58	0.27	0.10	-0.64
3.0	0.58	0.27	0.00	-0.64
4.0	0.58	0.27	0.00	-0.64

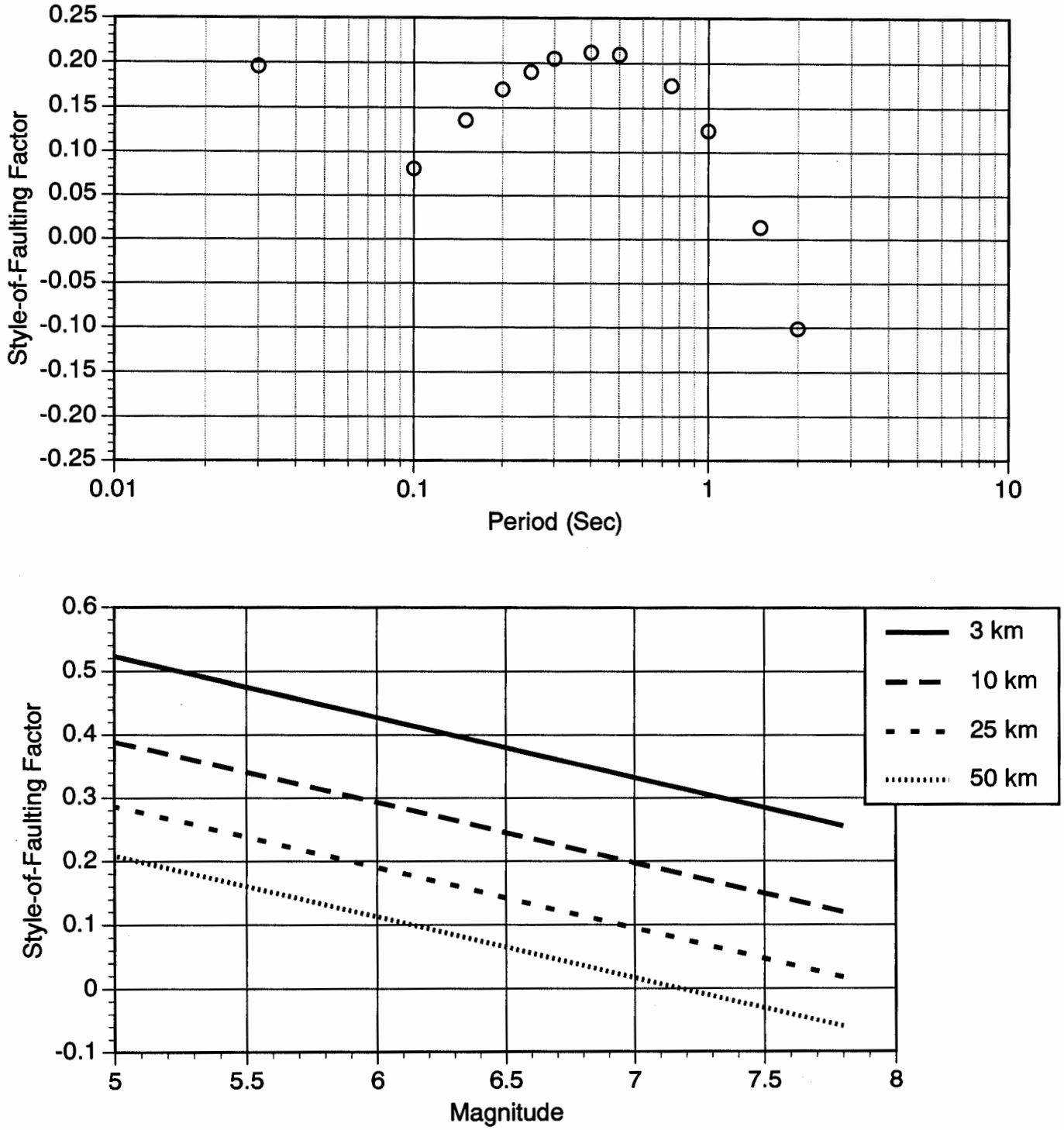

Figure 1. (A) Period dependence of the style-of-faulting factor estimated by Boore et al. (1994). (B) Magnitude and distance dependence of the style-of-faulting factor estimated by Campbell and Bozorgnia (1994).

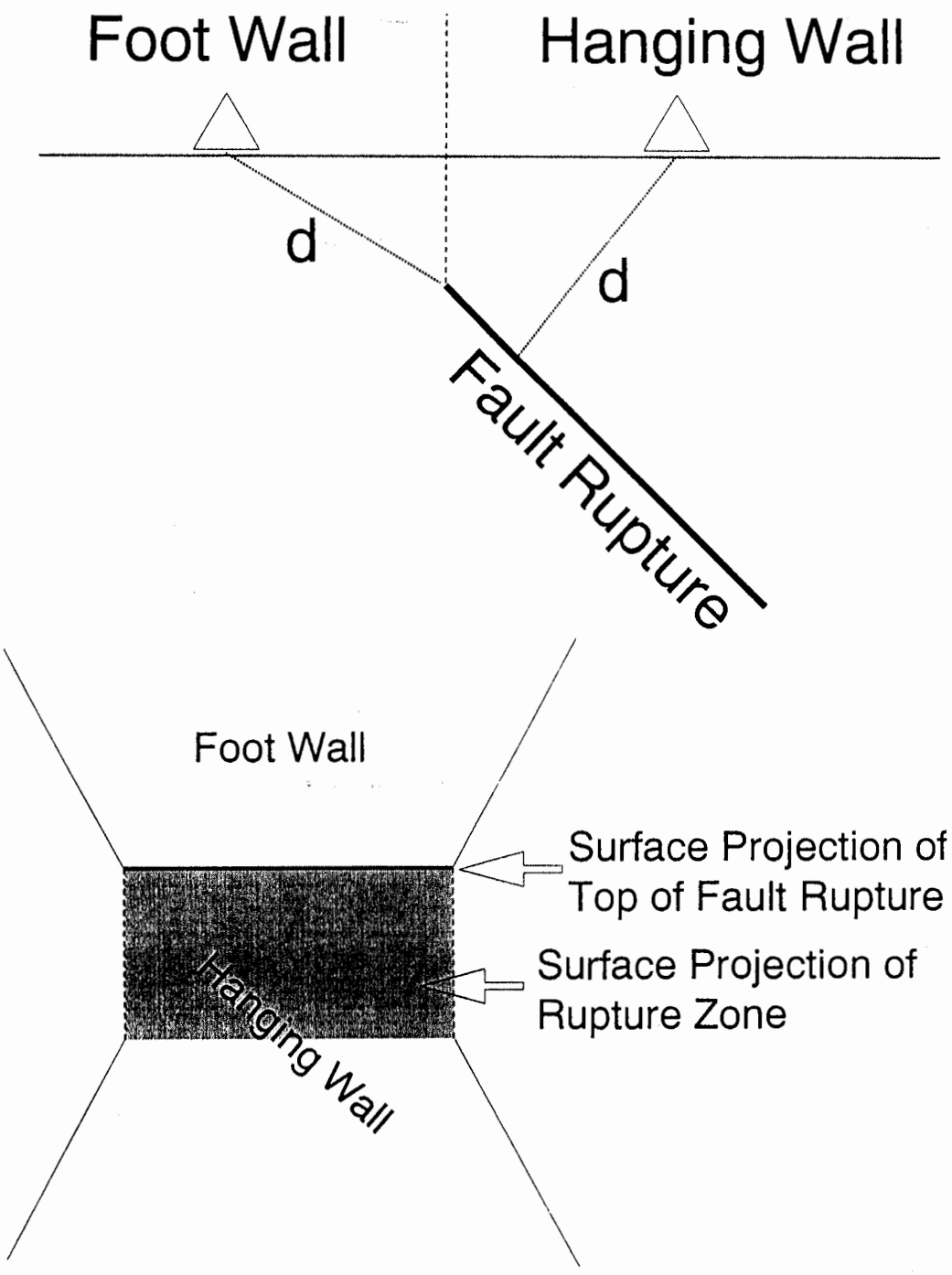

Figure 2. Classification of the stations into hanging wall and foot wall sites is based on the geometry shown above. The dividing line is the vertical projection of the top of the rupture (top frame). Sites off the ends of the fault are not included as either foot wall or hanging wall sites (lower frame).

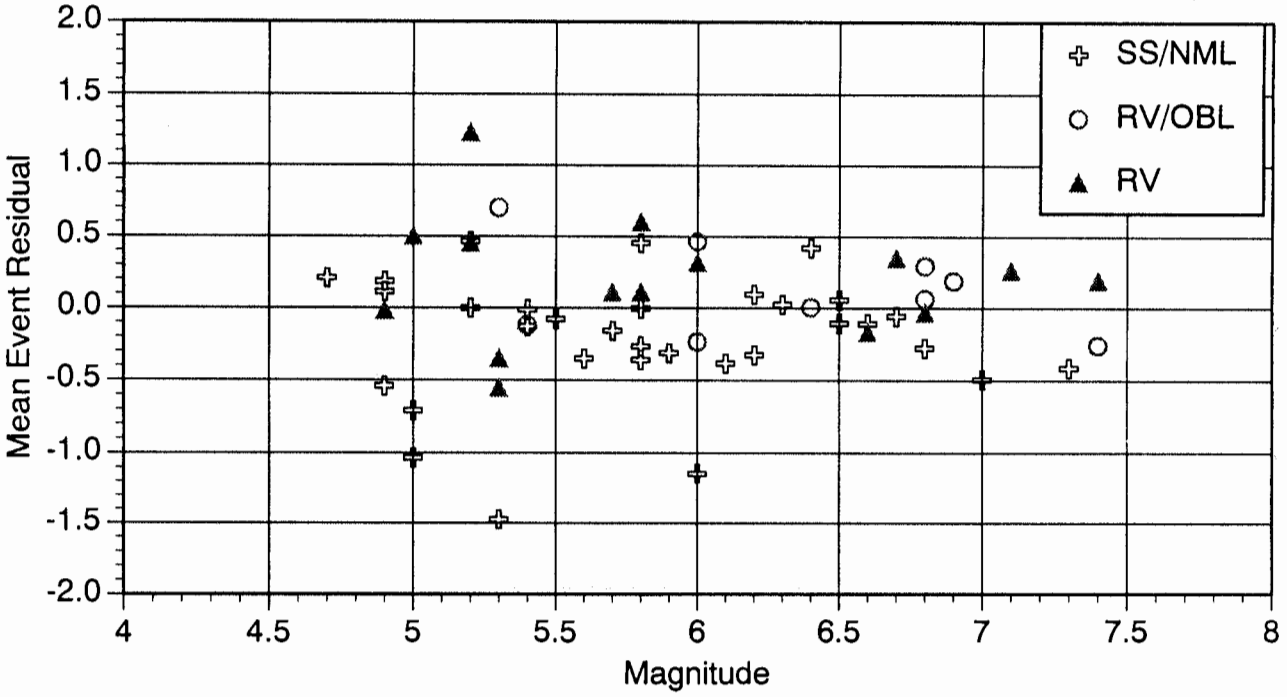

Figure 3. Mean event terms for peak acceleration (without a style-of-faulting factor in the regression).

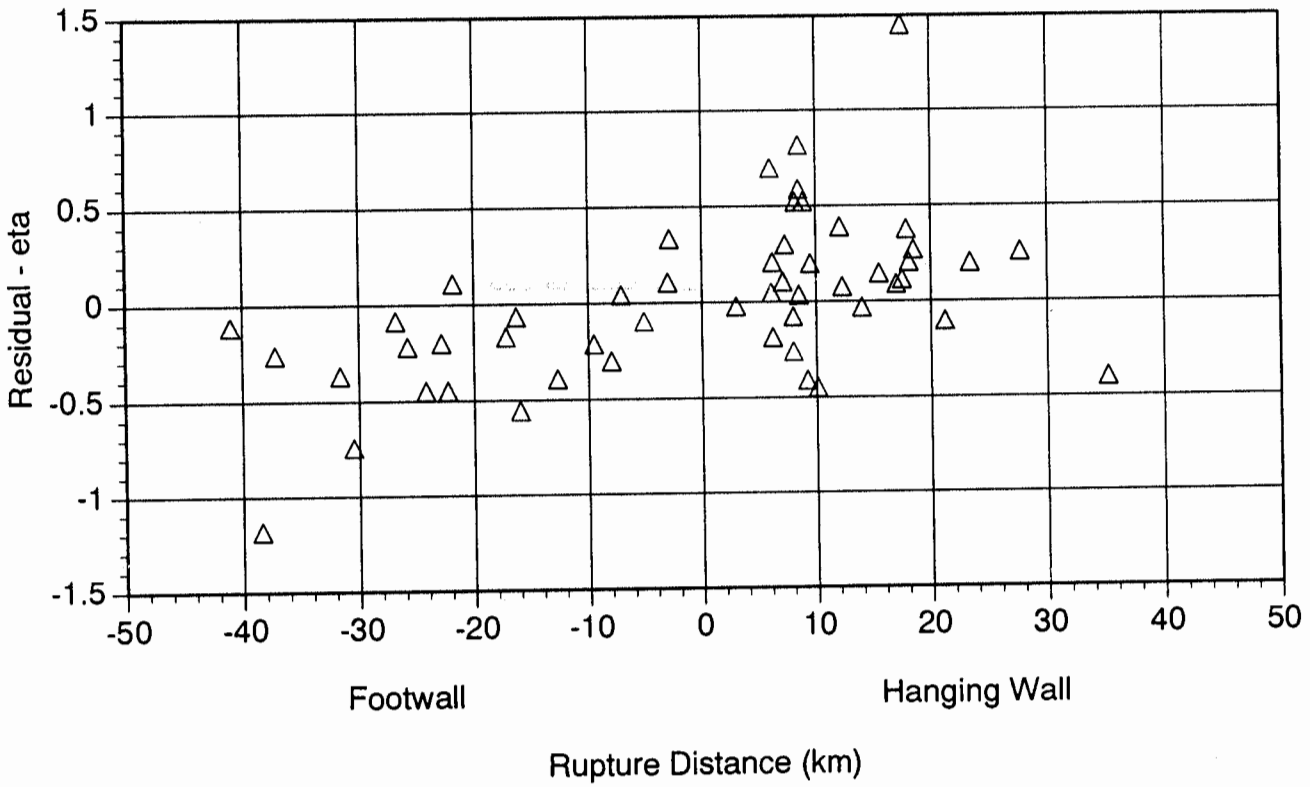

Figure 4. Peak acceleration residuals from a regression with a magnitude dependent style-of-faulting factor but without a distance dependent term.

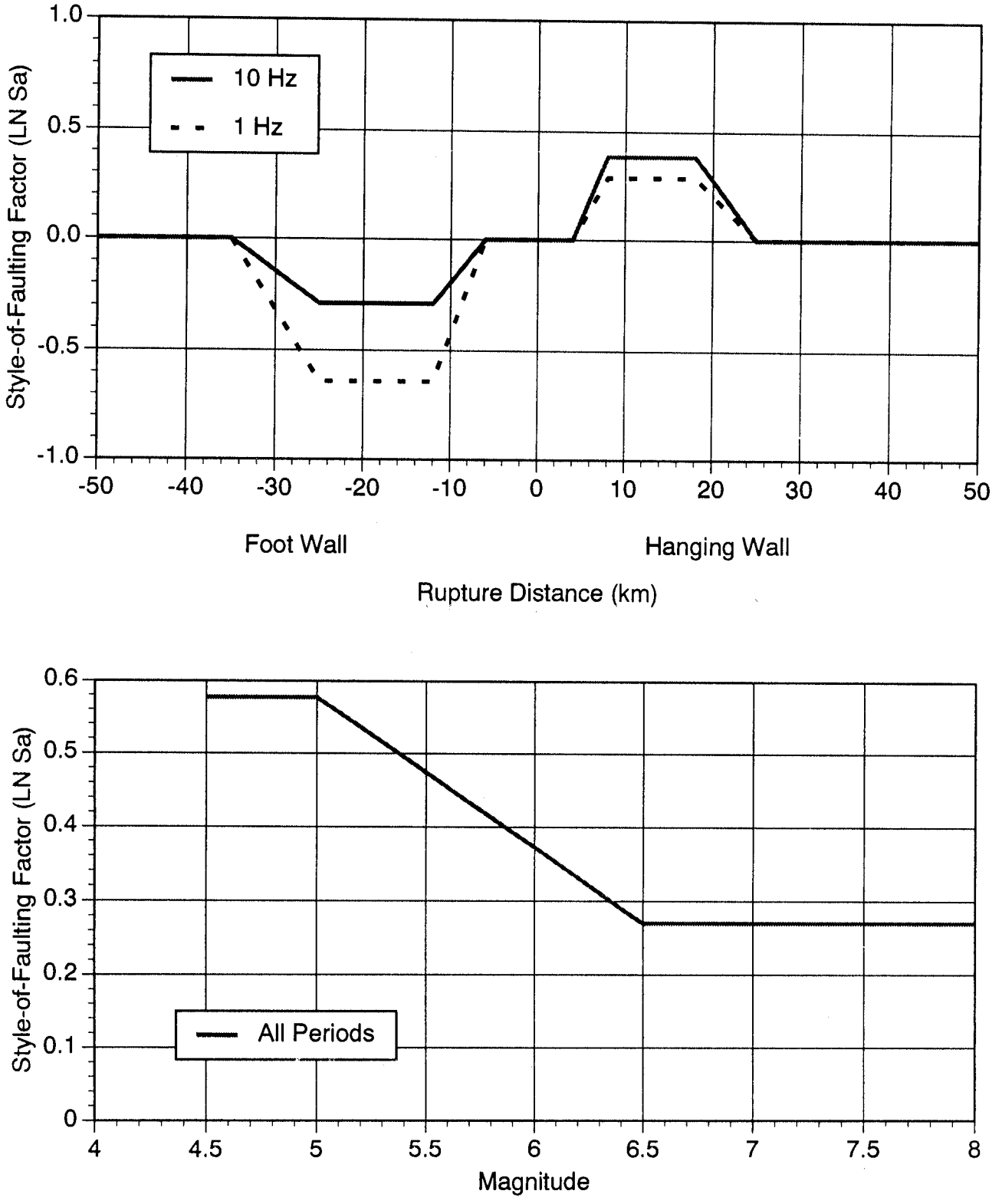

Figure 5. Magnitude dependence of the style-of-faulting factor (lower frame) and effect of the hanging wall and foot wall (top frame). The 10 Hz value for the HW/FW effect also applies to peak acceleration.

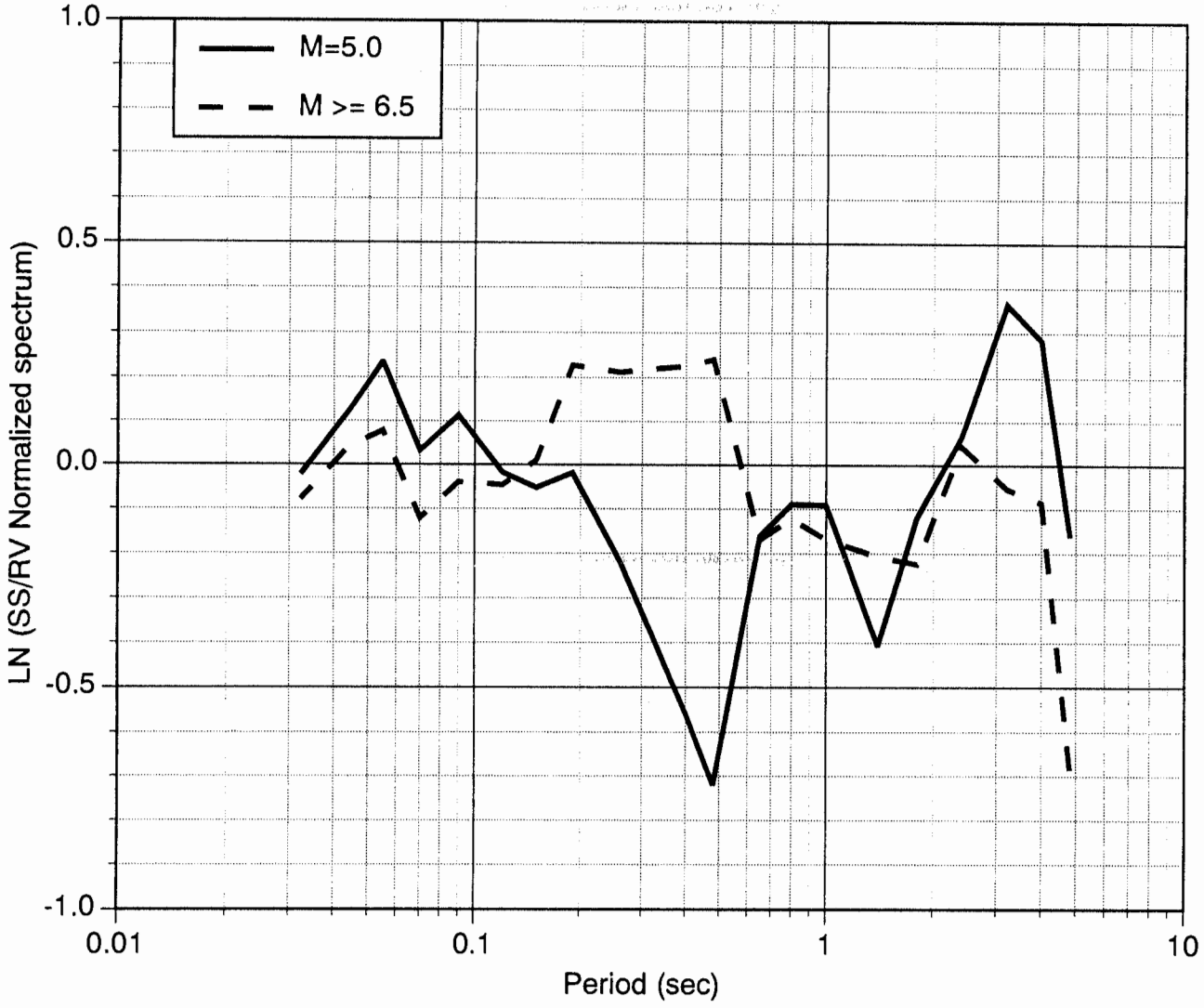

Figure 6. Difference in spectral content between strike-slip and reverse events for all sites characterized by the coefficients a_1 and a_2 derived from normalized spectral shapes. There is not systematic effect that is modeled.

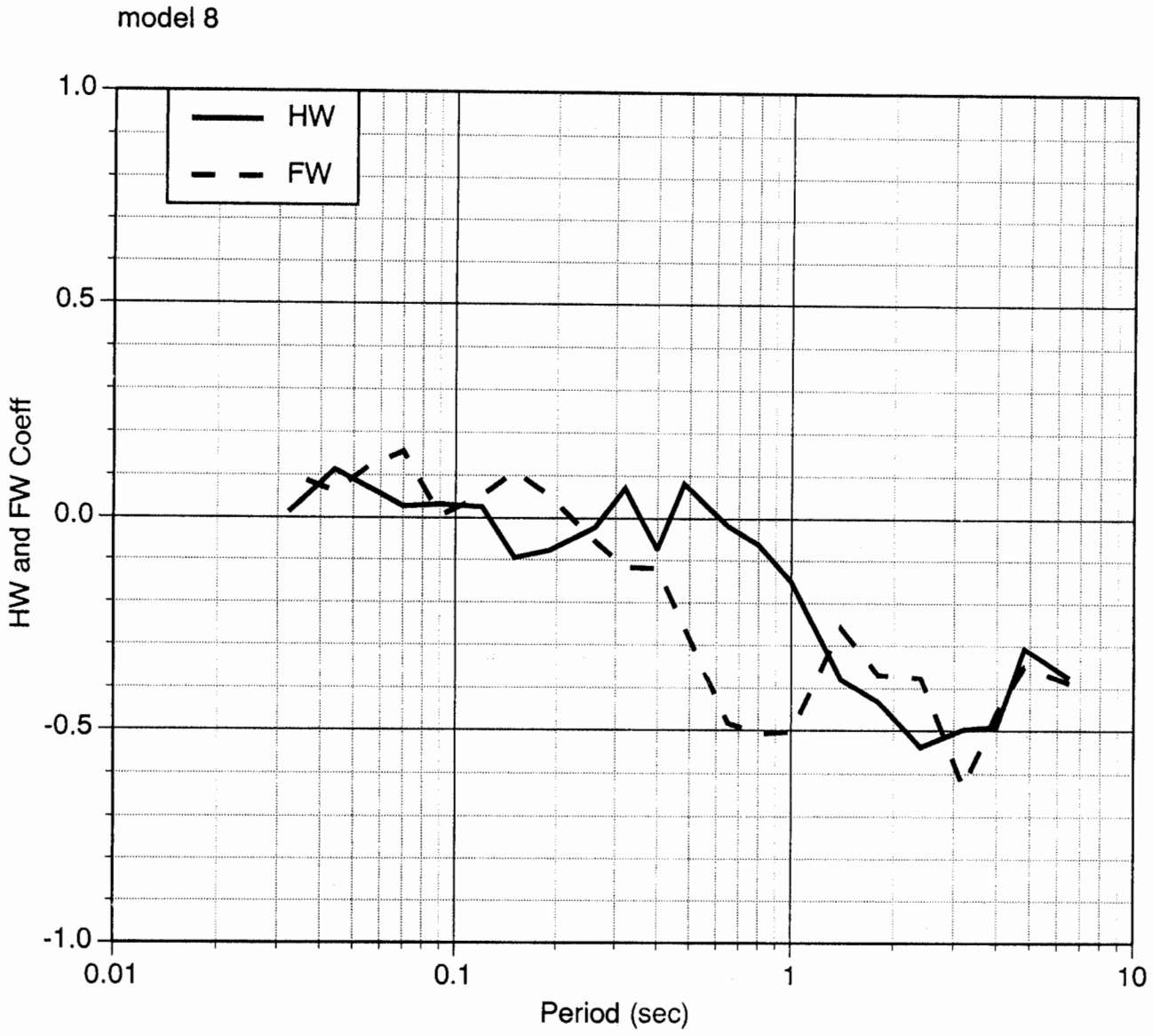

Figure 7. Difference in spectral content between strike-slip and reverse events for sites on the hanging wall and foot wall characterized by the coefficients b_1 and b_2 derived from normalized spectral shapes. This shows a systematic trend of decreasing b_1 and b_2 (HW and FW respectively) at long periods.

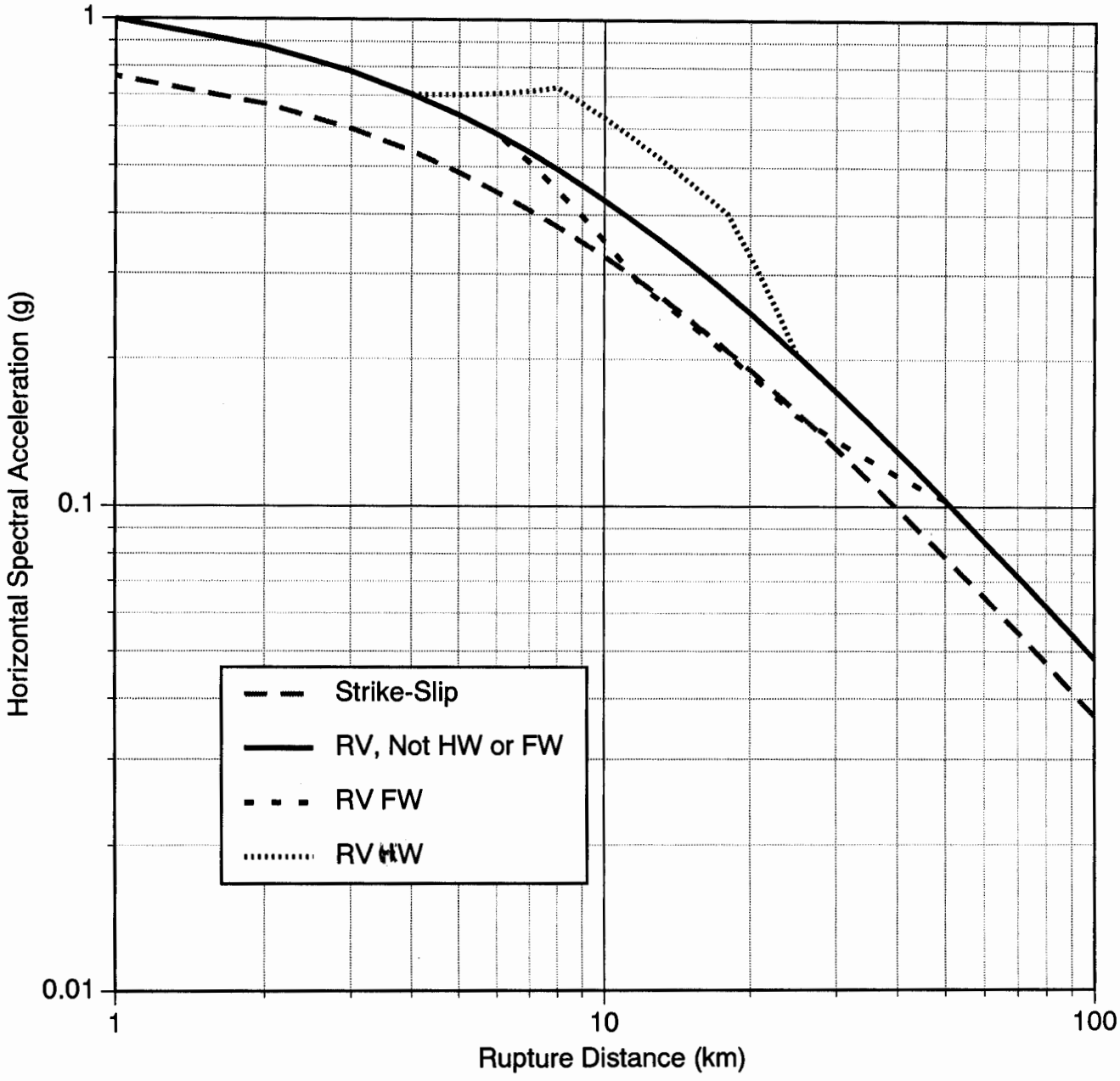

Figure 8A. Median attenuation for peak acceleration for M=7 events.

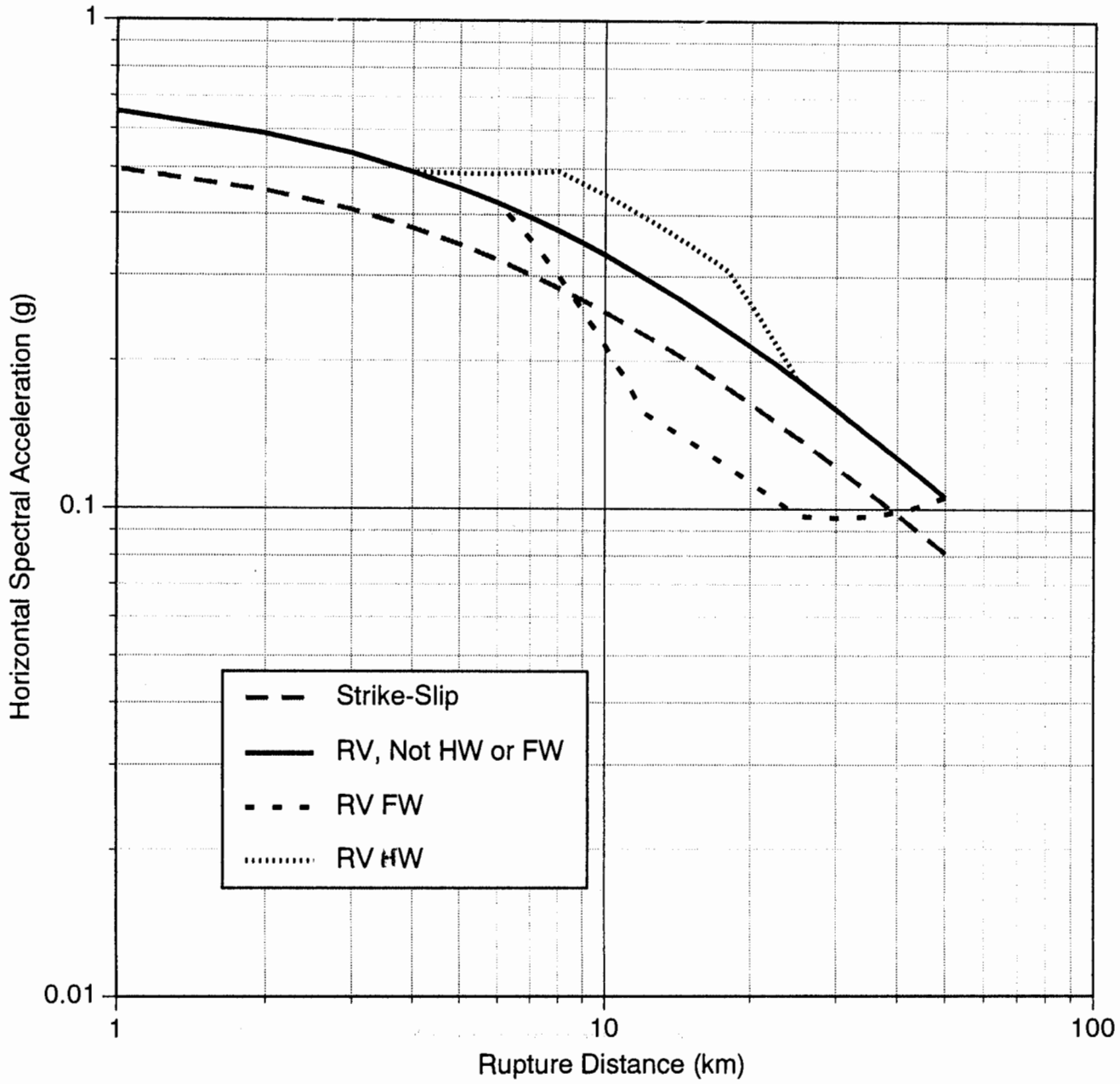

Figure 8. (B) Resulting attenuation relation for 1 Hz spectral acceleration.

EVALUATION OF SEISMIC CODE PROVISIONS USING STRONG-MOTION BUILDING RECORDS FROM THE 1994 NORTHRIDGE EARTHQUAKE

Juan C. De la Llera[1] and Anil K Chopra[2]

ABSTRACT

In this investigation the recorded motions in eight buildings obtained during the 1994 Northridge earthquake are studied and used to evaluate seismic code provisions and conventional building analysis techniques. These motions are first subjected to signal processing techniques to identify important building properties such as vibration periods and story stiffnesses. Then, the recorded ground motion in each building is used, in conjunction with a linear model of the structure, to predict the dynamic response of the building. Such response is then compared with the recorded response in order to assess the uncertainty present in the modeling procedure. Besides, a recently proposed improved inelastic model, based on the use of ultimate story shear and torque surfaces, is used to predict the response of buildings and explain conceptually their seismic behavior. Finally, instrumentation and code issues are discussed in light of the results generated in this research.

INTRODUCTION

The 1994 Northridge earthquake has produced one of the most valuable databases of ground and earthquake building responses in history. A total of 193 stations of the California Strong Motion Instrumentation Program recorded 116 free-field ground motions and 77 structural responses. From the latter, 57 correspond to buildings records obtained in a range of structural configurations.

The purpose of this investigation is to evaluate seismic code provisions using recorded motions in 8 buildings. In particular, the objectives are to: (1) evaluate current procedures for seismic analysis of structures; specifically, the uncertainty present in conventional structural building models; (2) evaluate deficiencies in current code provisions for earthquake analysis and design, and (3) propose improved analysis and design procedures calibrated using "measured" responses.

Because of the comprehensive nature of this study, this investigation has been subdivided into four phases. First, buildings records are studied and analyzed exhaustively to extract useful information of building properties and performance. Second, linear structural models are constructed for each building using conventional techniques. Third, improved, or state-of-the-art, structural models are developed to explain discrepancies in conventional linear models using nominal building properties. And fourth, improved code provisions are developed and calibrated using recorded building motions.

BUILDINGS CONSIDERED

The eight medium rise buildings considered in this study are listed in Table 1. They cover a wide range of typical structural systems in use today, such as R/C frames, precast R/C walls, R/C column-flat-slab frames, steel bracings, steel walls (uncommon), and mixed R/C and steel framing systems. Notice that for all these structures the peak ground accelerations during Northridge exceeded 0.2*g*. A brief description of each building is presented next.

[1] Department of Structural Engineering,, Catholic University of Chile

[2] Department of Civil Engineering, University of California at Berkeley

Building A

The building was designed in 1965, constructed in 1966, and is located 4.5 miles east of the epicenter aproximately. It is a nominally symmetric seven story R/C frame with approximate plan dimensions 62 x 150 feet. Its typical framing consists of columns spaced at 19 and 20 foot centers in the longitudinal and transverse directions, respectively., and spandrel beams run along the perimeter of the structure. The floor system consists of a 10 in. thick R/C slab at the second floor, 8 1/2 in. at the third to seventh floors, and 8 in. at the roof. The cylindrical strength of the concrete varies from 5 ksi and 4 ksi at the first and second stories to 3 ksi in upper stories. After the earthquake, the building was severely damaged on the longitudinal perimeter frames; damage also occurred on the E-W transversal frames but limited to minor flexural cracks in the end bays.

Table 1 Buildings considered

CSMIP Station	Building	Number of Stories	System	PGA x-direction	PGA y-direction
24386	**A**: Van Nuys (hotel)	7	R/C frame	0.44g	0.37g
24514	**B**: Sylmar (hospital)	6	R/C and steel frame and walls	0.52g	0.67g
24231	**C**: UCLA (Math-Science)	7	R/C walls and steel frame	0.25g	0.29g
24332	**D**: LA (commercial)	3/2[3]	Braced frame	0.33g	0.32g
24385	**E**: Burbank (residential)	10	R/C precast walls	0.27g	0.29g
24370	**F**: Burbank (commercial)	6	Steel frame	0.25g	0.29g
24652	**G**: LA (office)	5/1	Braced frame	0.24g	0.20g
24463	**H**: LA (warehouse)	5/1	R/C frame-flat slab	0.20g	0.26g

Building B

The building was designed in 1976 and its construction finished in 1986. Its lower two stories have a rectangular shape of approximate dimensions 302 x 452 feet; the upper four stories are cross-shaped with external dimensions 101 x 302 feet. The lateral force resisting system consists of R/C walls in the lower two stories and steel shear walls stories running along the 12 edges of the cross-shaped configuration in the upper stories. The floor system is composed of a corrugated steel deck and a 6" LWC slab. Only nonstructural damage to roof piping and chillers has been documented after the earthquake. This nonstructural damage is consistent with the high level accelerations (over 2g) recorded at the roof of the structure.

Building C

The building has a rectangular plan with dimensions 48 x 60 feet and was designed in 1969. The lateral resisting system in the first two stories consists of R/C walls, which enclose a nuclear reactor, and steel moment resisting frames in upper stories. The floor system is composed of a 2.5" floor slab over a corrugated steel deck at floors 4 through 8 and a thicker R/C slab on the third floor. No damage was reported in this building after the earthquake.

[3] n/m denotes n and m stories over and under ground level, respectively

Building D

This building was designed in 1974 and its construction finished in 1976. The two underground levels have a rectangular plan of dimensions 227 x 519 feet and a lateral resisting system consisting of 18" thick R/C shear walls running along the perimeter, 24" circular columns in the interior, and a 4.5" waffle slab with 14" beams. In the upper three stories the framing system consists of steel braced frames along the perimeter of the structure. The typical plan dimension for these stories is 219 x 241 feet; the floor system consists of a 3.5" LWC slab over a steel corrugated deck. No damage was reported on this building after the earthquake.

Building E

This ten story building was designed and constructed in 1974. It has a rectangular plan with dimensions 75 x 215 feet. Its lateral resisting system consists of precast concrete walls in both directions. The precast walls were fabricated using normal weight concrete with a cylindrical strength of 5 ksi. A wire mesh ASTM A185-61T of size 4"x4" (#4x#4) was used in all panels. Further, grade 60 reinforcing steel is specified in all drawings. The vertical load carrying system consists of precast and poured in place LWC slabs tied together with prestressing strands and supported by the laterally resisting walls. The foundation system is formed by 202 NWC piles 25' to 35' deep. No damage was reported on the building after the earthquake.

Building F

This six story steel building was designed in 1976 and constructed in 1977. It has a square plan of 120 x 120 feet. The lateral resisting system is formed by a perimeter moment resisting steel frame; the specified structural steel is A-36. All other interior frames are intended to carry only gravity loads. The floor decking system is formed by a corrugated steel deck filled with LWC (3" slab). The foundation system consists of 76 NWC piles 32 feet deep approximately. No damage was reported on the building after the earthquake.

Building G

This steel building was designed in 1988 and constructed in 1989. It has a square plan of 94 x 94 feet with four adjoined rectangular towers in each of the building corners. Each of these towers have Chevron type steel braced frames and moment resisting frames in two of their faces, respectively. A-36 steel is specified for all structural members with the exception of rigid frame columns which are ASTM-572, grade 50. Lateral resistance in the building is provided by these towers since all interior structural elements are intended to carry gravitational loads only. A 1 foot thick mat foundation is used under each tower and spread foundations are used for interior columns. No damage has been reported in the building after the earthquake.

Building H

This building is a five-story plus basement warehouse 280 x 361 feet in plan and was designed in accordance with the 1970 Los Angeles building code. The lateral resisting system consists of a ductile R/C frame along the building perimeter. An interior 6" flat-slab column system was designed to carry vertical loads only. The foundation system is formed by spread footings. No damage was reported after the earthquake.

ANALYSIS OF BUILDING RECORDS

The first task was to use techniques of signal processing, system identification and procedures alike to infer as much building information as possible from records without introducing strong modeling assumptions. Shown in Figure 1 is the flow of the eleven tasks considered for the analysis of building records.

First, the records were transformed into MATLAB [1] readable format in order to be processed within this computational environment. Once in MATLAB, the integrated building displacements were used to

interpolate deformations in those floors where no instruments were present. A cubic spline interpolation procedure was used to preserve not only the values of displacement at recorded floors but also smooth trends in the deformed shape of the building. Given the absolute displacements in the interpolated floors, their absolute accelerations were computed by differentiation of the displacements. These accelerations were then low-passed filtered by using a filter calibrated by recorded accelerations on instrumented floors. By using these accelerations, spectral analysis, time-frequency analysis and parametric identifications were performed to estimate the natural vibration frequencies of the building and possible nonlinearities of the buildings response. Besides, by assuming the building masses as known, story shear and torque plots were constructed (these plots are used later to characterize the behavior of the structure). Finally, empirical force displacement relationships were computed for each building story.

Because of the large amount of information generated in this task, it would be impractical to reproduce all results obtained. Hence, only few typical results are presented as examples of the methodology used. The reader is referred to [2] for more detailed information in all buildings.

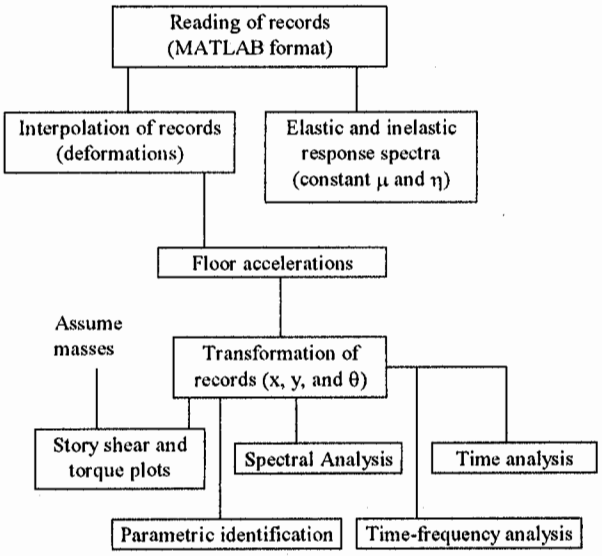

Spectral Analysis

Empirical transfer functions were determined with the purpose of estimating the fundamental building frequencies. These transfer functions were computed using Welch's method for spectral estimation [1]. Shown in Figure 2 is the result of spectral analysis, in this case for the records of Building F. The building frequencies are apparent from this figure; however, such is not always the case for other stiffer buildings. In this case the fundamental periods of the system are fx=0.68 Hz, fy=0.73 Hz, and 1.12 Hz .

Time-frequency analysis

In time frequency analysis a record is divided into overlapping segments and for each the power spectrum of the signal computed. This enables us to observe if the building properties vary in time because of nonlinearities in the structure. As an example consider the time frequency analysis of the records of Building A obtained during the San Fernando, Whittier, Landers, Big Bear, and Northridge earthquakes presented in Figure 3. In this figure the abscissa represents the central time of the segment of record considered and the ordinates the frequency ordering number. It is documented that Building A underwent some minor structural damage during the San Fernando earthquake but no damage until Northridge.

A careful examination of Figure 3 shows that the fundamental frequency of the building in the x-direction was f_x=0.68 Hz at the onset of the San

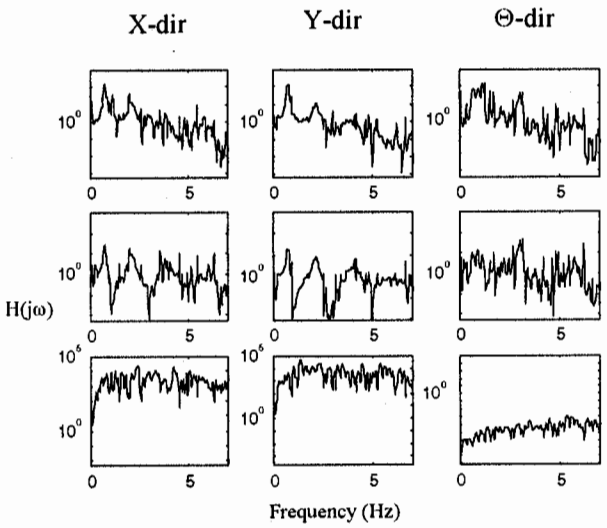

Figure 2 Transfer function of Building F accelerations

Fernando (1971) earthquake; this frequency was reduced to 0.58 Hz at the end of the earthquake, which is consistent with the observed structural damage in the building. Moreover, at the time of the Whittier (1987) earthquake, the building had increased its fundamental frequency to 0.88 Hz, probably because of the retrofit performed in the building after the San Fernando earthquake. During Whittier, the fundamental frequency of the building remained constant, implying elastic behavior of the structure. The same frequency is observed at the onset of the Landers (1991) earthquake; however, during the earthquake the building reduced again its fundamental frequency to 0.68 Hz, which was increased to 0.78 Hz, corresponding to the small amplitude vibration frequency, at the end of the record. This suggests that the building underwent some structural or nonstructural damage (or both) during Landers. Essentially no variation of frequency is observed during the Big Bear earthquake. Finally, at the beginning of Northridge the structure has a fundamental frequency of 0.64 Hz, similar to the minimum frequency obtained during Landers. This frequency is dramatically reduced to 0.44 Hz during the first twenty seconds of response; thus, justifying the damaged observed. Again, a small increase of this frequency to 0.54 Hz is observed toward the end of the record.

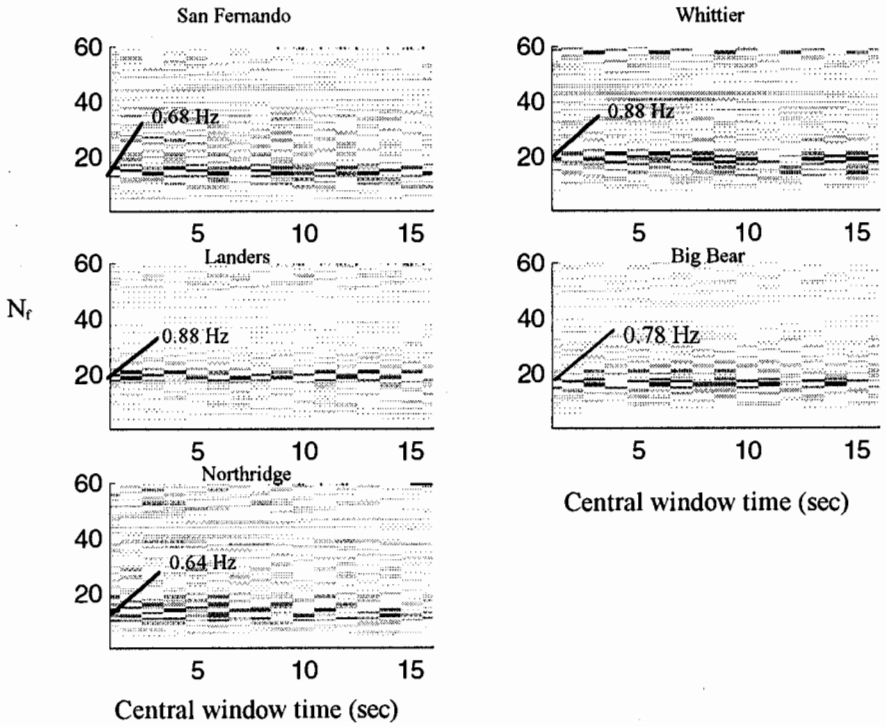

Figure 3 Time frequency analysis Building A

Following similar procedures to the ones already described, the natural periods of the other buildings considered were estimated. The results are summarized in Table 2 for six of the buildings considered. Presented in this table are also the torsional to lateral frequency ratios, $\Omega=f_\theta/f_x$, used later in the evaluation of accidental torsion

Table 2 Measured vibration periods

Building	T_x (sec)	T_y(sec)	T_θ(sec)	Ω_x	Ω_y
A	2.17	1.92	1.45	1.50	1.32
B	0.33	0.41	0.25	1.32	1.64
D	055	0.51	0.28	1.96	1.82
E	0.69	0.58	0.72	0.96	0.81
F	1.46	1.37	0.89	1.64	1.54
H	1.52	1.37	1.11	1.37	1.23

effects. As shown in this table, several of the buildings considered have closely spaced periods in the x and y directions of analysis.

Story Shears and Torques

This investigation uses extensively a recently developed structural building model that considers a single element per building story. The inelastic properties of such model are defined in the space defined by the story shears and torque. Consequently, the study of the building response in this space is of primary importance. Shown in Figure 4, for instance, are the story shears and torques generated in Building A during Northridge; these values have been computed assuming nominal values for the floor masses. For simplicity, results are presented only in the two dimensions defined by the x-direction story shear V_x and torque T. Each cross symbol plotted in this figure corresponds to a combination of story shear and torque for a different instant of time.

It is apparent from the figure, especially in the third, fourth, and fifth stories, that several story shear and torque combinations reach the same maximum value of shear, implying that there must be a surface (or region) beyond which these combinations cannot go. Such region is denoted as the story shear and torque surface and will be introduced later. Such surface will provide an interpretation to the story shear and torque combinations in terms of the behavior of the system.

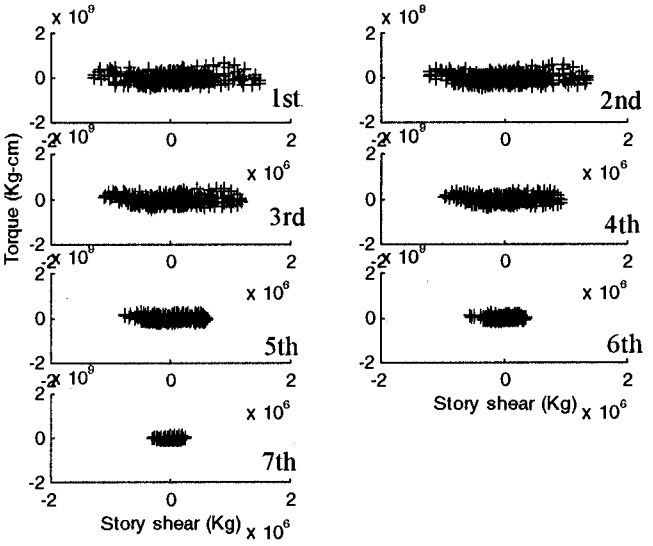

Figure 4 Story shears and torque (Building A)

Building deformations and story force-deformation relations

Because of the direct correlation between building damage and building deformations, the latter as well as the interstory drifts were computed for all buildings. Shown in Figure 5 are the deformations of the roof of Building E relative to the ground. Note that these deformations were computed subtracting the "true" absolute roof displacements from the ground displacements.

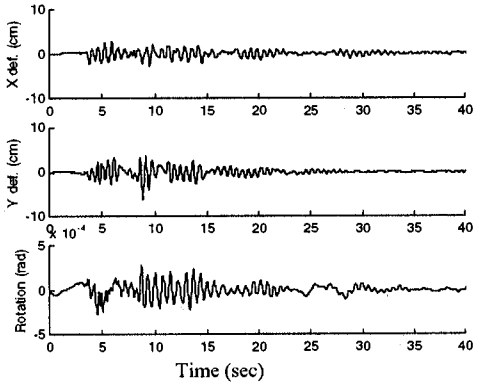

Figure 5 Roof deformations (Building E)

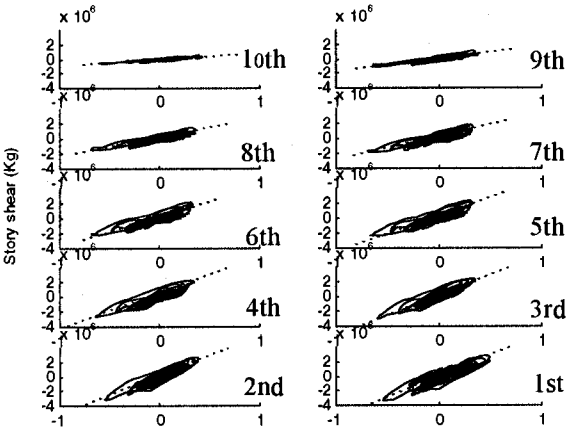

Figure 6 Story shear vs. deformation (Building E)

Using the story shears and torques computed in the previous section together with the interstory deformations of the building, the force deformation relations for each building story were computed. They are presented in Figure 6 for the longitudinal direction of the building. These curves assume, among other things, that the interstory deformations are due primarily to shearing of the story rather than rotation of the building underneath the story considered; an assumption that seems appropriate only for squat structures. Hence, strictly, they are only rough estimators of the true force-deformation characteristics of the building. In spite of this, we will see they provide a good insight on the relative story stiffnesses.

BUILDING MODELS

The objective of this phase is to assess the uncertainty present in building models as used in practice. For that purpose, the dynamic response of full three dimensional finite element models of the buildings considered are computed and compared against the measured response in them during the earthquake. The building responses are obtained assuming in-plane rigid floor diaphragms and three degrees of freedom at the center of mass (CM) of each floor, where all the story masses are lumped. Next, a brief description of the building models is presented together with the most important considerations and assumptions in their development.

Building A

Shown in Figure 7 is the structural model constructed for Building A. The model has 295 nodes and 665 elements and has been assumed fixed at the base level. Because of possible R/C cracking due to gravitational loads, the flexural stiffness of spandrel and interior beams has been reduced by half; this reduction has been considered in the model by ignoring the contribution of the slab in the flexural stiffness of beams.

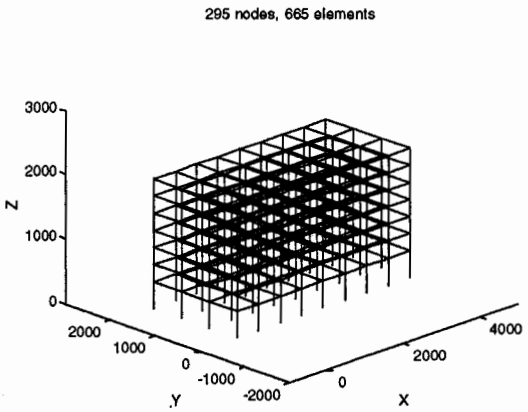

Figure 7 Structural model of Building A

Shown in Figure 8 is the estimated deformation (relative to the base) of the building roof when subjected to the true excitations at the base. For comparison, the true roof deformation is also presented in the figure. It is apparent that the estimated roof deformation using the linear model is substantially different from the true response. A probable explanation for this is the nonlinear behavior of the structure which is not accounted for in the linear model. This can be easily checked by noting that the estimated traces of the roof deformation are similar to the true deformations during the first four and eight seconds of the record in the x- and y-directions, respectively, and then become substantially different. Linear models are common practice in building analysis today in spite of the well known fact that buildings behave inelastically during strong earthquakes.

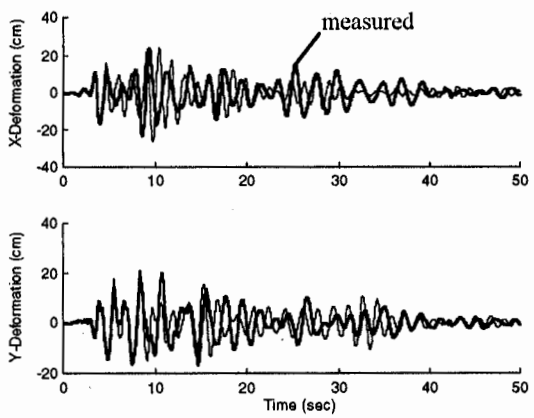

Figure 8 Estimated and 'true' deformations, Building A

Building B

Shown in Figure 9 is the structural model of the upper three stories of Building B. The

lower two stories were modeled using and empirical linear model obtained from the force-deformation story laws shown earlier (e.g.,Figure 6, for Building E). The purpose of this was to isolate the uncertainty in the modeling of the steel shear walls of the structure. The properties of these walls were computed discretizing in layers the walls in height to include the openings in them and then restoring, using basic beam theory, kinematic compatibility at the interface of each layer. This was done for shear as well as flexural deformations. In total, the model considers 730 nodes and 964 elements.

The comparison between estimated and 'true' deformations is presented in Figure 10. Although the estimated building frequencies are closed to those of the real building, the traces show important differences, especially in the x-direction. These discrepancies cannot be attributed to nonlinear behavior of the structure as for Building A since we know the building performed elastically. Rather, they probably come, in great proportion, from stiffness modeling uncertainty. Note, however, that the traces of 'true' deformation show trends at certain instants that are not physical (see, for instance, the linear trend at the initial four seconds of response). Therefore, it would incorrect to attribute all errors to structural modeling.

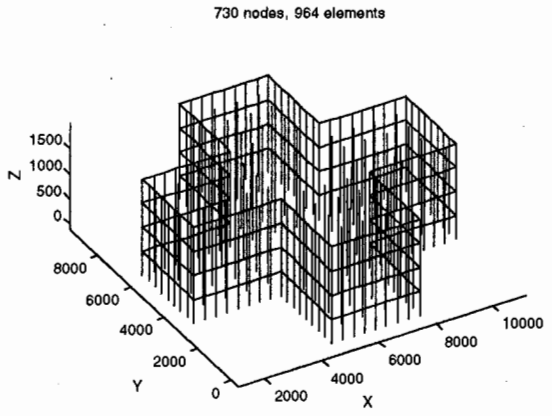

Figure 9 Structural model of Building B

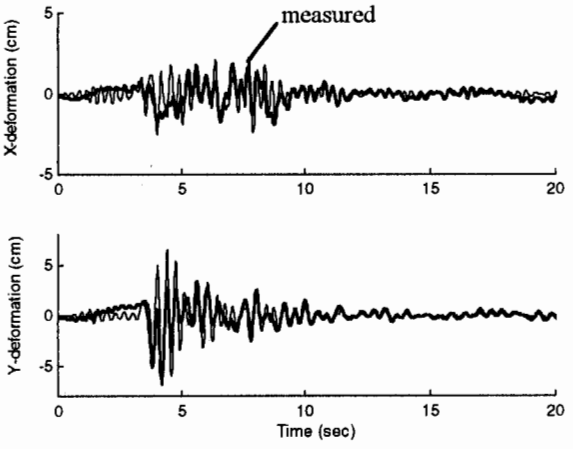

Figure 10 Estimated and 'true' deformations, Building B

Building D

The structural model of this building considers 805 nodes and 1675 elements (Figure 11). Both, the steel bracing structure and framing system of the upper three stories as well as the R/C column-flat-slab system of the lower two stories are included in the model. Such is the case because two other buildings rest on the same column-flat slab system and, hence, interaction with the neighbor structures occurs through the lower two stories. Besides, interstory secondary bracing elements, intended to reduce the effective length of the principal braces, were also included in the model.

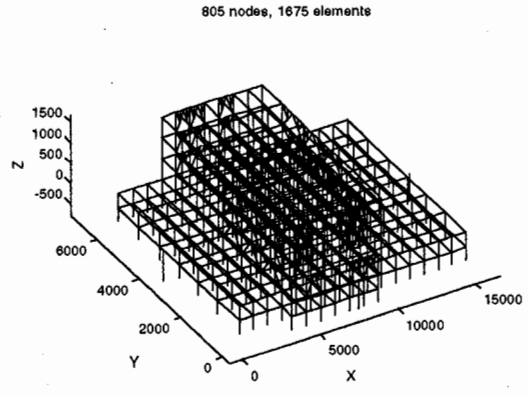

Figure 11 Structural model of Building D

Shown in Figure 12 are the roof deformations estimated using the building model and the actual deformations of the roof computed from building records. The responses have certain similarity in their frequency content but otherwise the response histories are different. Indeed, they are relatively similar only in the first few seconds in spite of the

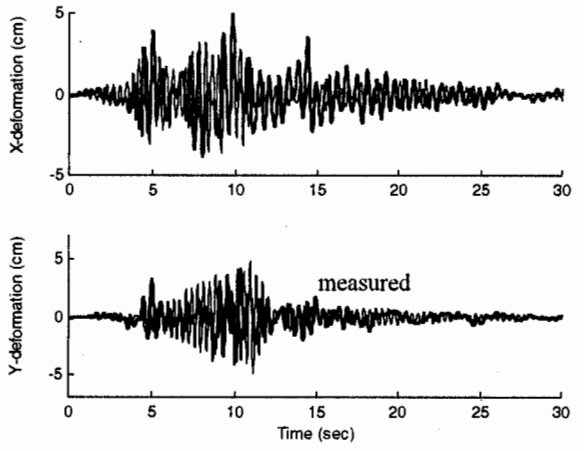

Figure 12 Estimated and 'true' roof deformation, Building D

tremendous effort done to model this structure accurately.

Building E

The model of this building is shown in Figure 13. It considers 1242 nodes and 2090 elements. Spring-like connection elements are used among R/C precast walls with the purpose of modeling the uncertain stiffness of these connections and their effect on the building response. The model presented herein, however, considers connections with zero stiffness as suggested by the details presented in the structural plans. Cracked properties, associated to the building dead loads, have been considered in defining the flexural stiffness of walls. Finally, the building model was considered fixed at the base of the first story.

The estimated and 'true' building deformations at the roof are presented in Figure 14. The figure shows that the estimated response contains slightly higher frequencies than the measured response. Moreover, the estimated deformations are consistently smaller than the measured ones. Such smaller vibration period could be due to soil structure interaction, as have been suggested by an earlier study on the building [3].

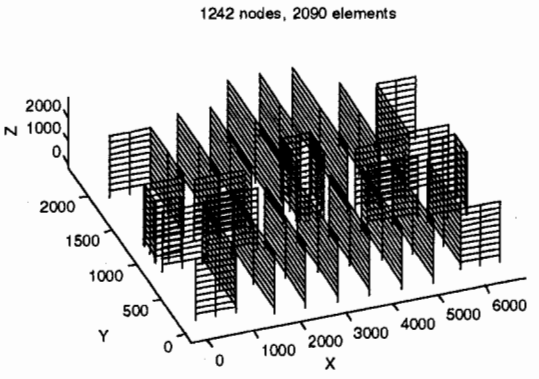

Figure 14 Structural model Building E

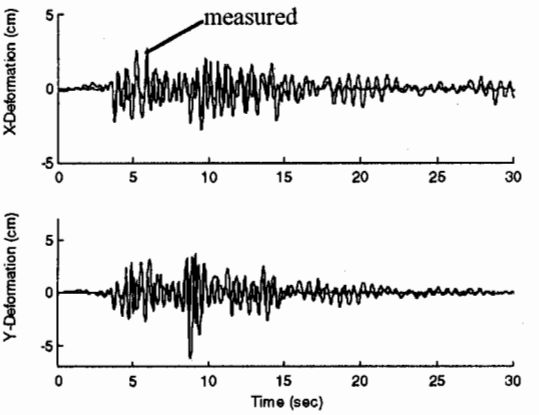

Figure 13 Estimated and 'true' roof deformation, Building E

Building F

The model for this six-story building is presented in Figure 15 and considers 349 nodes and 288 elements. The lateral resisting elements along the perimeter of the structure as well as all internal columns, intended to carry gravitational loads only, are considered in the structural model.

A comparison between the estimated and 'true' roof deformations is presented in Figure 16. The estimated response presents a predominant frequency that is slightly higher than that present in the 'true' building response. Apart from this difference both traces have amplitudes that differ considerably at certain instants and become closer at others, for instance, during the first ten seconds and trail of the record.

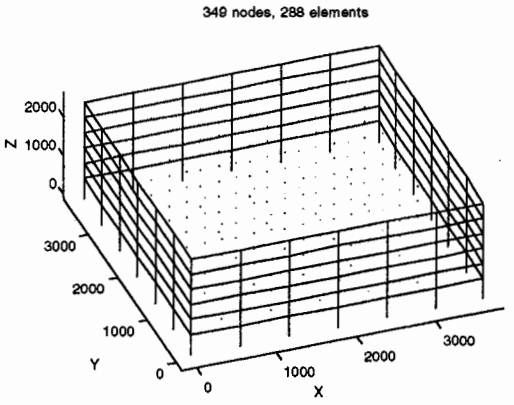

Figure 15 Structural model, Building F

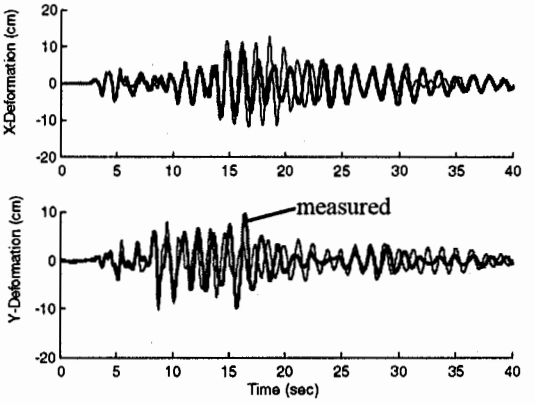

Figure 16 Estimated and 'true' roof deformations, Building F

It is important to note that any of the models presented could have been "touched up", even with physical considerations, to provide much closer estimates of the measured responses. However, as they are, they provide a good measure of the real model uncertainty that is present during the analysis process. In general, the estimated building responses using conventional modeling and analysis techniques provide trends that bear some resemblance with the measured responses. However, if the comparison is made in terms of peak responses they may differ typically in 30% to 50%.

IMPROVED ANALYSIS PROCEDURES

In this section a new procedure for building analysis that has been recently proposed by the authors is evaluated and tested using recorded building responses. For the sake of brevity, only the analysis of Building A will be presented in detail.

In the three-dimensional model developed, each story is represented by a single super-element (SEM) capable of representing accurately the elastic and inelastic properties of the story. The formulation of this model is described in [4] where its accuracy was tested using *theoretical* single and multistory systems. Besides, the model is based in the theory of plasticity and, hence, it assumes that the building develops plastic behavior (as opposed to sudden brittle behavior). Because Building A shows a brittle type failure in its columns along the perimeter, the use of the single-element model in this case goes a bit beyond its own scope. However, it will still provide good insight of the behavior of Building A during Northridge.

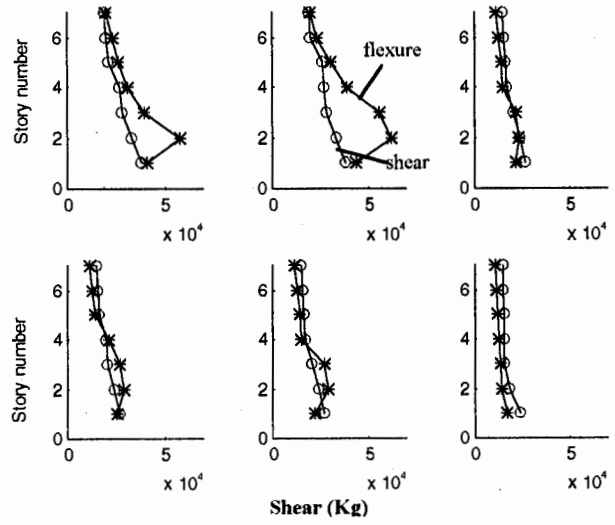

Figure 17a Column capacities in x-dir, Building A

The first step in computing the SEM for Building A requires to estimate the capacities of each story. This is done by first computing the lateral capacity of each building column corresponding to a meaningful axial load in the column. These loads were assumed in this case to be equal to the gravity loads. Shown in Figure 17 are the heightwise distribution of lateral capacities of the different types

of building columns.

The values identified with circles and stars correspond to lateral capacities associated to shear and flexural failure mechanisms in the column, respectively. It is interesting to note that for essentially all columns shear failure mechanisms control over flexural mechanisms in stories two through four, which were exactly those most severely damaged with shear-type mechanisms during the earthquake.

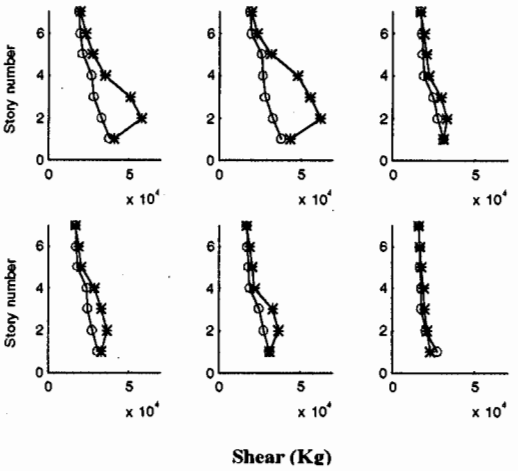

Figure 17b Column capacities y-dir, Building A

Using the column capacities presented above it is possible to construct a surface, denoted hereafter as story-shear and torque surface (SST), which bounds the dynamic response of each story of the building in the shear and torque space. Each point of this surface represents a static combination of story shear and torque that produces collapse of the story. Moreover, the different regions of this surface are associated to different story mechanisms. Recalling Figure 4, where the story shear and torque histories were introduced, it is possible to superimpose the theoretical SST on this plot as shown in Figure 18. Because the SST response histories must be bounded by the SST surface, it is apparent that we have underestimated the strength of the system in stories 1 through 5 (the upper two stories we cannot know since they are elastic).

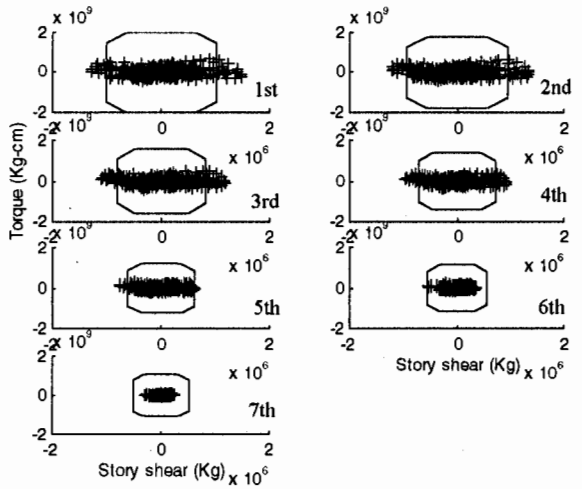

Figure 18 SST surfaces and histories

Therefore, two physically motivated corrections are applied to these surfaces. First, they are corrected for *overstrength,* defined as the ratio between the maximum measured story shear and the maximum estimated story shear capacity. Second, they are corrected for the effect of the orthogonal component of ground motion as proposed in [4]. Shown in Figure 19 is the result of these two corrections.

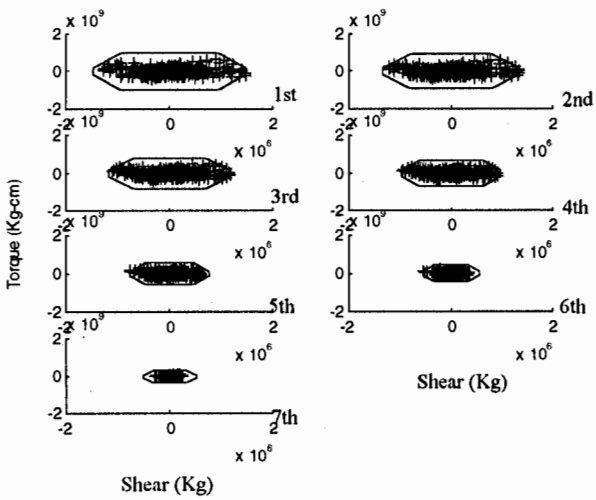

Figure 19a Corrected SST surfaces

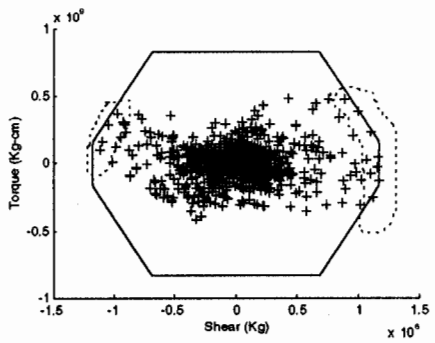

Figure 19b SST surface of third story, Building A

Several interesting observations are obtained from Figure 19. First, it is apparent that all the response shear and torque combinations lie inside the boundaries of the theoretically computed SST. This is important because the only adjustment done to the results of Figure 18 was the overstrength scaling based only on the peak story shear at each story. Second, Figure 19b is remarkable in showing that there is a number of story shear and torque combinations that lie exactly on the SST; these combinations have been circled in the figure. This implies, unless a very unlikely coincidence, that the actual story shear and torque combinations associated to inelastic behavior of the story belong to the SST surface as assumed theoretically. This observation proves that the SST model is in agreement with the actual behavior of buildings. Moreover, the story shear and torque combinations lying on the inclined branches of the surface indicate that the building underwent inelastic torsional behavior in spite of its nominal symmetry. Indeed, this will be the case in most buildings with perimeter frames as the only lateral resisting system. Finally, it is important to note that since there is only few points that reach the SST surface, i.e., few inelastic excursions of the story, the damage of the structure can be justified only if the ductility capacity of the system was small.

To verify this, shown in Figure 20 is the inelastic response spectra of the x-component of ground motion in Building A. According to the results presented earlier, this building has a capacity parameter $\eta=R_y/M$ a_{max} = 0.94, where R_y is the yield capacity of the building (in this case computed at the base), M the mass of the structure, and a_{max} the peak ground acceleration. Recognizing that the undamaged vibration period of the system is about 1.5 sec, the global ductility demand on this structure is slightly less than 1.1. This implies that although the structure was probably designed for target ductilities of, say, 6, its actual ductility capacity was close to one.

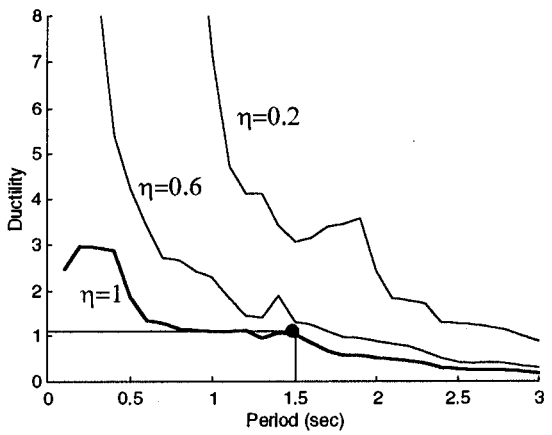

Figure 20 Inelastic response spectra, Building A

Finally, knowing the SST surfaces for each story, the SEM can be constructed an the inelastic response of the building predicted. Such response is presented in Figure 21. Although differences still exist between model and 'measured' responses they have been reduced relative to the elastic prediction shown earlier in Figure 8. It is also possible to show that since yielding in the structure is not substantial, an elastic model with stiffness reduced fits well the response. This confirms once again that Building A had a brittle behavior that could be modeled accurately by simply reducing the stiffness of the structure.

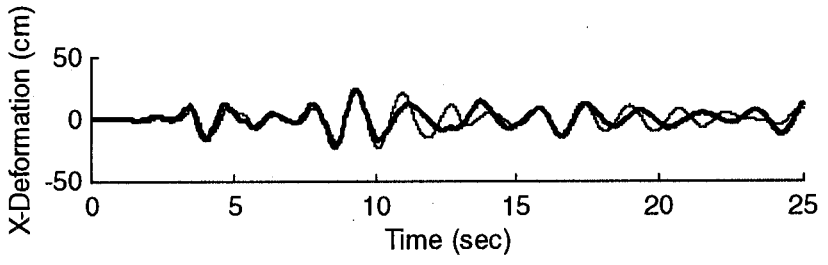

Figure 21 Estimated inelastic and 'true' building responses, Building A

INSTRUMENTATION AND BUILDING CODE IMPLICATIONS

In this section the results presented in the previous sections are used to address a number of instrumentation and code issues. The issues addressed are classified in the following groups: (1) instrumentation and record processing, (2) building modeling, (3) ductility of structures, (4) perimeter frame structural configurations, and (5) accidental torsion. For the sake of brevity, a full treatment of the ideas is not presented herein; rather, they are introduced briefly by showing examples and stating their implications for building analysis and design.

Instrumentation and record processing

A fundamental aspect of the investigation presented is to use recorded motions in buildings to the maximum extent possible without introducing strong modeling assumptions. However, is it possible to test fully our building codes and analysis procedures using only the recorded building information? Strictly speaking, the answer is no, unless all floor have been completely instrumented with at least three independent components; in such case we would be able to compute, for instance, the "true" interstory deformations, story shears and torques (if the masses are known), accidental torsion effects, etc. Such alternative, however, is not economically feasible except for very special buildings. This implies that the current "sparse" records in buildings must be somehow used to predict the motions of uninstrumented floors. Two alternative procedures can be used to do so: (1) system identification, and (2) record interpolation.

Record interpolation has two features that make it attractive. First, it is not restricted to a model structure as any identification procedure. For instance, if the building is linear and nonlinear at intermittent intervals the procedure is still valid. Second, it is simple to use and calibrate.

The interpolation procedure proposed considers first interpolation of the building deformations using cubic splines---cubic splines are truncated polynomials that possess continuity of slopes at interpolated points, and differentiation of the total interpolated displacements to estimate floor accelerations. A low-pass filter is designed, based on the recorded displacements and accelerations, to filter the resulting floor accelerations. Because building deformations are smoother functions they are preferable to accelerations for the interpolation procedure. An illustration of such procedure is presented in Figure 22, in which the recorded motions of Building A are used to estimate the displacements and recorded accelerations of the 6th floor. These predicted motions are compared against the recorded motions at the East end of the structure. The results show that the procedure can be quite accurate even for Building A which has a strong nonlinear behavior.

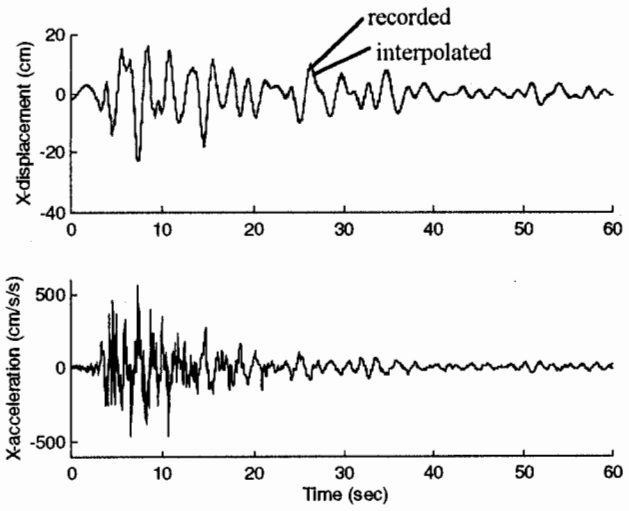

Figure 22 Exact and interpolated motions, Building A

Building modeling

In conventional studies of building records a model of the building is developed and subjected to the recorded ground motions. Frequently, such building model is then identified and adjusted in order to reproduce closely the recorded responses. It is an important question, however, how close was the response of the first model attempted relative to the recorded motions in the structure. That discrepancy or model uncertainty would have existed in the design of the structure in the absence of recorded information.

The results presented in Figures 8, 10, 12, 13 and 16 partially answer the question of model uncertainty. It is extremely hard to achieve better accuracy in practice using these conventional building models. It is apparent from these figures, however, that model uncertainty is highly correlated with the complexity of the structural system. Thus, the dynamic response predicted for Building F (Figure 16), which is essentially a clean perimeter frame, is much closer to the actual response than is for the complex structural plan of Building D (Figure 12).

Another important issue regarding structural modeling is the use of elastic models for building analysis and design. Although Building A (Figure 8) did not have substantial inelastic behavior, it seems inappropriate to use an elastic model to design this structure knowing, a priori, that the building is designed to experience substantial inelastic behavior during an earthquake like Northridge. This point is demonstrated by comparison of the elastic and inelastic building responses shown in Figures 8 and 21; indeed, the differences would be much more striking if the ductility demand on the building would have been larger.

A fundamental result of this investigation is the experimental verification (Figure 19) of the SEM (single element model) used for elastic and inelastic building analysis. This simplified model enables the engineer to compute the inelastic response of a building at a cost that is considerably smaller to that incurred in a full elastic three-dimensional analysis, with the advantage of capturing better the actual building response. Moreover, the use of the SST (story shear and torque surfaces) forces the engineer to understand the properties of the structure that control its inelastic behavior, thus, revealing any gross deficiencies in the planwise distribution of strength.

Ductility of structures

It is a widely accepted philosophy for earthquake resistant design that the capacity of a structure may be reduced if the system is able to accommodate in a *stable manner* larger deformations that surely imply damage in the structural elements. This philosophy is built in the reduction factor R_w present in most building codes; however, how can the engineer guarantee that the target design ductility values are achievable in the structure as built. Generally, it is argued that this is obtained through a good detailing but it should also be added a conceptually healthy structural configuration.

A good example of the lack of consistency between the assumed R_w in building analysis and the 'true' ductility capacity of a building is provided by Building A. According to current building codes a R/C ductile moment resisting frame could be designed for an R_w of 8 (up to 12), i.e., μ=6 (8), approximately. The ductility demand on Building A did not exceed 1.1 and, yet, the building collapsed. This is only possible if the building had a brittle behavior; thus, contradicting the initial design assumption of large deformation capacity.

Perimeter frame

Intimately related to the discussion above of building ductility is the issue of a conceptually healthy structural configuration. Several conditions characterize a good structural configuration: redundancy, capacity to generate uniform deformation demands in structural elements (regularity), and insensitivity to changes in the ground motion characteristics. A good example of redundancy is Building E in which damage of one element does not imply collapse of the system. In turn, a nominally symmetric systems, such as Building F, is a good example of a structure that generates (in theory) uniform displacement demands. Finally, insensitivity to ground motion characteristics is achieved by structures which confine the response in specific regions of the SST space.

The perimeter frame, as a structural concept, violates almost automatically the redundancy condition. Redundancy is violated because all columns at a given story and one edge of the building undergo simultaneously similar deformations and, hence, failure of one column signals, almost always, failure of all the other columns in the same resisting plane. A good example of such behavior is Building A, in which essentially all columns on the south perimeter resisting frame collapsed. This is because similar displacements are imposed by the rigid floor to all columns---a phenomenon similar to the one occurring

in piers supporting a rigid freeway deck. In general, plan redundancy is achieved primarily by more resisting planes and not by more structural elements on a resisting plane.

Besides the redundancy problem of perimeter frame configurations, they also have a serious deficiency in their inelastic behavior that can be visualized using the story shear and torque plots (e.g., Figure 19a and b). From this figure we observe that the building surfaces have three well defined slopes, one associated to constant story shear, one with a finite slope, and the last with constant story torque. The story shear and torques associated to the constant shear region correspond to story mechanisms that involve primarily translation and yielding of all resisting planes; the inclined branches are associated to mechanisms that leave the same perimeter frame elastic; and the constant torque regions involve mechanisms that are essentially torsional. As shown in Figure 19, most of the shear and torque combinations that touch the surface do it on the inclined branches. This implies that Building A, in spite of its nominal symmetry, develops mechanisms that involve important torsion, which in turn implies that one perimeter frame yields and damages while the other remains essentially elastic. This is exactly what happened in Building A where damage was localized more in the south resisting plane than in the north frame. The important observation is that perimeter frame systems will always tend to fail by predominantly torsional mechanisms which use inefficiently the capacity of both frames in the same direction localizing damage in one of them.

Accidental torsion

A new procedure to account for the increase in response due to accidental torsion has been recently proposed [4]. This procedure defines the increase in edge deformations due to different sources of accidental torsion such as stiffness and mass uncertainty and base rotational motion. Such procedure had been tested only with three nominally symmetric structures; however, four new cases: Buildings B, E, F and H can be added to this list. The results are presented in Figure 23, where Ω represents the ratio between uncoupled torsional and lateral frequencies, and the ordinates represent the ratio between the edge story deformation including rotation of the plan and without it. These deformation ratios have been computed using the SMIP displacement data and the interpolated displacement data for uninstrumented floors.

It is important to note that the envelopes presented are statistical estimates---associated to a 30% exceedance probability approximately, and cannot be checked with a single building point. A sufficiently large number of buildings would be necessary to describe the probability distribution for each Ω. However,

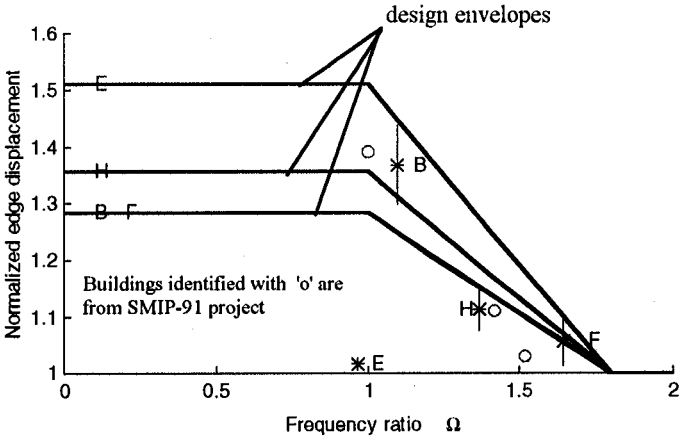

Figure 23 Increase in edge displacements, X-direction

Several observations can be obtained from these results. First, buildings with larger frequency ratios Ω present a smaller increase in displacements as predicted theoretically. It might seem contradictory that Building E presents such a small effect; however, recalling that the actual shape of the envelopes (not the simplified ones presented here) has a dip about Ω=1, this result actually agrees with theoretical predictions. Second, Building B and one of the old SMIP-91 buildings have the larger increase in edge displacements due to accidental torsion. This increase occurs for values of Ω slightly larger than one as expected analytically. It is because this sensitivity of the response around Ω=1 that the proposed design envelopes are flat at the maximum value up to this frequency ratio. Third, the vertical bars associated to each building studied denotes the heightwise variation of the increase in edge deformation. Such variability is zero only in buildings that have resisting planes with proportional stiffnesses.

ACKNOWLEDGMENTS

This investigation has been funded by the Strong Motion Instrumentation Program, California Division of Mines and Geology. The authors are grateful for this support and to Dr. Moh Huang and Dr. Gustavo Maldonado for helping in gathering all building information required during the project . Thanks are also extended to all members of the SMIP project committee for their very useful comments on the progress reports of the project.

REFERENCES

1. MATLAB, 1994. The Mathworks, Inc., Natick, Massachusetts, 1994.

2. De la Llera, J.C., and Chopra, A.K.,"Evaluation of seismic code provisions using strong-motion building records from the 1994 Northridge earthquake", CSMIP report, 1995.

3. Moehle, J., Wallace, J., and Martinez-Cruzado, J., "Implications of strong motion data for design of reinforced concrete bearing wall buildings", CSMIP Final Report, June 1990.

4. De la Llera, J.C., and Chopra, A.K., "Accidental and natural torsion in earthquake response and design of buildings", UCB/EERC-94/07, University of California, Berkeley, June 1994.

RESPONSE OF BASE ISOLATED BUILDINGS DURING THE 1994 NORTHRIDGE EARTHQUAKE

By
Satish Nagarajaiah, Assistant Professor,
and Sun Xiahong, Graduate Research Assistant

Dept. of Civil Engineering, University of Missouri - Columbia, MO 65211

ABSTRACT

The objectives of this study are (1) to evaluate the seismic performance of base isolated USC hospital building and Fire Command Control building, in Los Angeles, during the 1994 Northridge earthquake, and (2) to evaluate the analysis techniques and design criteria used in base isolated structures. USC hospital base isolated building is a 8 story steel braced frame; the seismic isolation system consists of 68 lead-rubber isolators and 81 elastomeric isolators. Fire Command Control (FCC) base isolated building is a two story steel braced frame with 32 high damping rubber isolators. Both the USC hospital building and Fire Command Control building experienced strong motion during the Northridge earthquake. The approach adopted in this study is (1) system identification, (2) nonlinear analytical modeling, (3) interpretation of structural behavior during the Northridge earthquake, and (4) evaluation of the effectiveness of seismic isolation. It is shown that (1) USC hospital performed well, deamplified the accelerations, and reduced the overall response, (2) FCC building performed to expectations; however, accidental pounding reduced the effectiveness of seismic isolation, and (3) the analysis techniques used in base isolated structures are accurate and can reliably predict the response.

INTRODUCTION

Post earthquake evaluation studies play a very important role in (1) evaluation of the effectiveness of seismic isolation, and (2) assessment of the analysis techniques and design criteria used in base isolated structures (Buckle et al. 1990, Huang, et al. 1993, Kelly 1990, Kircher et al. 1989, Mayes 1990). California Strong Motion Instrumentation Program records (Shakal et al. 1994) of the response of the base isolated USC hospital and the FCC building in Northridge Earthquake provide a wealth of data for such a performance evaluation.

The objectives of this study are (1) to evaluate the seismic performance of base isolated USC hospital building and FCC building during the 1994 Northridge earthquake, and (2) to evaluate the analysis techniques and design criteria used in base isolated structures. The approach adopted in this study is (1) system identification of the USC hospital building from the recorded response (to verify the dynamic characteristics obtained from detailed analytical modeling of the base isolated building), (2) nonlinear analytical modeling of 8 - story USC hospital building based on as built structural details and prototype bearing test results, (3) simplified modeling of FCC building including accidental pounding, (4) comparison of computed response with recorded response of the USC hospital and FCC building in Northridge Earthquake, (5) interpretation of structural behavior and effectiveness of seismic isolation during Northridge

Earthquake, (6) examination of modeling techniques used in base isolated structures, and (7) development of simplified models to predict structural behavior.

The seismic performance evaluations comparing response of the base isolated buildings with probable response if the buildings were to be fixed-base are presented. The isolation system of the USC hospital was activated beyond its yield level and responded in the inelastic range with the superstructure being elastic. Recorded/computed response which support the fact that the base isolated USC hospital building performed to expectations and reduced the response as compared to a fixed base structure are presented. The isolation system of the FCC building was activated beyond its yield level; however, accidental pounding in portions of the base caused sharp acceleration spikes. The effects of accidental pounding on the structural response are presented. Evaluations of analytical modeling techniques, used in base isolated structures, and their validity are presented.

ANALYSIS TECHNIQUES

The computer program 3D-BASIS [Nagarajaiah, et al. 1990, 1991] is used for analyzing both USC hospital and FCC building. Computer program 3D-BASIS has been used for analysis and design of several base isolated buildings in California and else where. Nonlinear analytical modeling using 3D-BASIS consists of (1) linear condensed superstructure model with 3 degrees of freedom per floor, and (2) isolation system modeled explicitly using nonlinear force-displacement relationships of individual isolators.

A detailed model of the superstructure is developed using ETABS (Wilson et al. 1975) with rigid floor slab assumption. ETABS uses 6 degrees of freedom (DOF) per node with 3 degrees of freedom per node slaved to the master node at the center of mass of the floor; hence, in the condensed model only 24 DOF (8x3 DOF per floor) and 6 DOF (2x3 DOF per floor) are retained for modeling USC hospital and FCC building, respectively. Eigenvalues and eigenvectors of the condensed model from ETABS are used in modeling the superstructure in 3D-BASIS. Elastomeric isolators are modeled in 3D-BASIS using nonlinear force-displacement relationship based on prototype bearing test results for USC hospital and FCC building. Response to Northridge earthquake is computed using 3D-BASIS.

BASE ISOLATED USC HOSPITAL BUILDING

Superstructure and Isolation System Details

USC hospital base isolated building (Asher et al. 1990) is a 8-story (7 stories above ground and basement) steel braced frame building as shown in Fig. 1. The floor plan is asymmetric with two wings which are connected by a necked down region of the floor/base. The building has setbacks after the 5th floor. The steel superstructure is supported on a reinforced concrete base slab, integral with reinforced concrete beams below, and drop panels below each column location. The isolators are connected in between these drop panels and footings below. The footings also support reinforced concrete pedestal provided for back up safety. The seismic isolation system consists of 68 lead-rubber isolators and 81 elastomeric isolators as shown in Fig.

1. The building has been extensively instrumented by CSMIP (Shakal et al. 1994); the sensor locations are shown in Fig. 1.

System Identification

Frequency domain system identification technique (Ljung 1987) is used to identify the frequencies and damping ratios of the base isolated building from recorded response. The identified frequencies and damping ratios are average dynamic characteristics of an equivalent linear system based on the entire measuring period. Transfer functions are estimated using cross spectrum and power spectrum. Complex-curve fitting is performed and complex poles are extracted. Frequencies and damping ratios are calculated from the poles (Nagarajaiah 1996). Fig. 2 shows the recorded and identified transfer functions in the East-West (EW) and North-South (NS) directions in magnitude and phase angle form. It is to be noted that the transfer function peak at 4.3 Hz in the EW direction is not a mode, but, the effect of interference/noise; this is inferred from examination of coherence function which has a value of 0.13 (Nagarajaiah 1996). Table 1 shows the identified frequencies and damping ratios for the first four modes in the EW and NS directions.

Analytical Modeling

The superstructure properties --such as beam, column, bracing, floor slab details- used for analytical modeling are computed from building drawings provided by CSMIP. Detailed modeling of the superstructure is performed using ETABS both in fixed-base condition (used for modeling the superstructure in 3D-BASIS) and base isolated condition with equivalent linear isolation system (only for comparison with system identification results). The computed periods for the first nine modes, and the damping ratios, in the fixed-base condition, shown in Table 2, are used for modeling the superstructure in 3D-BASIS. The isolation system properties are extracted from prototype test results provided by CSMIP. The test results of both lead-rubber bearings and elastomeric bearings recorded in the form of nonlinear force-displacement loops are used for explicitly modeling all 68 lead-rubber bearings and 81 elastomeric bearings in 3D-BASIS. The properties of the bearings, used in modeling, extracted from test results are: (1) the properties of the lead-rubber bearings at 1.1 inch (2.8 cm) displacement --average displacement experienced by the isolators in Northridge earthquake-- shown in Fig. 3 and Table 3; and (2) the properties of elastomeric isolators at 1.1 inch (2.8 cm) displacement is 17 kip/in and an estimated damping of 3%.

The computed periods and damping ratios for the first four modes in the EW and NS directions, in the base isolated condition with equivalent linear isolation system (based on bearing properties at 1.1 inch maximum displacement), are shown in Table 1. A comparison between computed frequencies and damping ratios obtained from detailed analytical model of the base isolated building with equivalent linear isolation system and the corresponding identified frequencies and damping ratios obtained from system identification is presented in Table 1. It is evident from Table 1 that the dynamic characteristics obtained from detailed analytical modeling are satisfactory.

Response during Northridge Earthquake

The response of USC hospital to Northridge earthquake (foundation level acceleration CHN 5 and CHN 7 --see Fig. 1) is computed using the nonlinear analytical model developed. Fig. 4 shows a comparison of the recorded and computed response in the EW and NS directions; absolute accelerations and relative displacements at sensor locations shown in Fig. 1 are compared. Comparison shows that the correlation between the computed and recorded response is good --both is phase and amplitude (excepting for the roof acceleration in the NS direction in one peak cycle of motion). Fig. 5 shows the recorded and computed displacement and acceleration profiles at instants of occurrence of the peak base displacement, peak acceleration, peak structure base shear (above base), and peak drift. The accuracy with which the analytical model captures the displacement response --as in Fig. 5-- is notable; however, differences in acceleration response occur --given the complexity of the analytical model. The correlation of recorded and computed time histories and profiles demonstrate the accuracy of the analysis techniques used and nonlinear models used in 3D-BASIS.

Fig.6 shows the floor response spectra at the roof, 6th floor, 4th floor, and base for three cases (1) recorded, (2) computed response with bilinear hysteretic model for 68 lead-rubber isolator and linear model for 81 elastomeric isolators, and (3) computed response with the entire isolation system being modeled by global equivalent linear springs, with appropriate effective stiffnesses, and global equivalent damping elements at the center of mass of the base. It is evident that the floor response spectra of the recorded and computed cases --case 2 bilinear-- compare well over most regions of the period range. This shows the appropriateness of modeling the lead-rubber bearings using bilinear hysteretic elements.

The time history of response shown in Fig. 4 indicates that the isolators yield (the yield displacement is 0.34 inch or 0.86 cm) and the isolation system responds in the inelastic range for significant portion of the time history with a period of ~ 1.3 to 1.5 secs. The peak ground acceleration in the EW direction is 0.163 g and 0.37g in the NS direction. The peak acceleration at the base is 0.073g in the EW direction and 0.13g in the NS direction. The peak acceleration at the roof is 0.158g in the EW direction and 0.205g in the NS direction. The accelerations were deamplified because the fundamental periods of the base isolated building in the EW and NS directions are higher than the corresponding fixed-base fundamental periods and predominant periods of the ground motion. Furthermore, this deamplification stems from the dynamic characteristics of the base isolated structure shown in Table 1. The fundamental periods in the EW and NS directions are ~ 1.3 secs with a damping of ~ 11% --essentially similar to the case if the structure were to be rigid. The structural modes or the second modes in the EW and NS directions, however, are reduced to ~ 0.55 secs (reduced from fundamental modes of ~ 0.9 secs in the fixed-base case --see Table 2) with a damping of ~ 16% (increased from 5% in the fixed-base case --see Table 2-- because of high damping in the lead-rubber isolators). An examination of the transfer function in the EW direction reveals that the structural mode at 1.83 Hz or 0.55 secs has large damping ~ 16%; hence, the suppressed transfer function peak. Similar observation holds for the NS direction. The Northridge earthquake which has energy in the structural mode range cannot transmit the energy effectively because of this dynamic characteristic of the base isolated structure; this is the main reason for the effectiveness of the isolation system (Kelly 1990).

Fig. 7 shows a comparison between the computed peak response envelops of base isolated USC hospital and probable response if the building were to be fixed-base. The benefits of seismic isolation become clear by examining the peak story shear and peak story drift envelops, in both cases, in the EW and NS directions. The superstructure remains elastic in the base isolated case; however, the fixed-base structure will yield. Furthermore, the higher mode effects are dominant in the fixed base case; whereas, in the base isolated case the higher mode effects are not as dominant. The changes in stiffness after the fifth floor, because of setbacks, are the cause for these higher mode effects; this is clear in the displacement and acceleration profiles in NS direction, presented in Fig. 7. The profiles in Fig. 7 are at instants of occurrence of the peak acceleration, peak structure base shear (above base), and peak drift, in the base isolated and fixed-base case. In Fig. 7 examination of the displacement profile reveals that when the peak structure base shear occurs, in the base isolated building, the isolation mode is dominant.

The maximum flexible floor diaphragm displacements inferred from the records are of the order of 0.5 inch or 1 cm, which is negligible compared to the length of the building of 303 ft (3636 inch or 9235 cm); hence, no significant flexible diaphragm effects occurred during the earthquake (Nagarajaiah et al. 1995). Examination of the records for torsional response revealed that nominal torsional response occurred (Nagarajaiah et al. 1995). The corner displacements at different floors/base were approximately 25% more than the displacement at the center of mass.

Simplified Modeling

In Fig. 7, as described earlier, floor response spectra of three cases are examined. The last case is intended to examine the effectiveness of simplified linear modeling of such a complex structure. In the simplified model only nine modes shown in Table 2 are used for modeling the superstructure with the isolation system being represented by global springs and damping elements at the center of mass of the base. The floor response spectra using the simplified linear model do not match the recorded case as well as the bilinear case. It is, however, found (Nagarajaiah et al. 1995) that the simplified model yields satisfactory peak response values -- provided proper effective stiffness and damping properties are used for the isolators-- making it useful for design.

BASE ISOLATED FIRE COMMAND BUILDING

The FCC is a 2-story steel frame base isolated building with 32 high damping rubber bearings as shown in Fig. 1. The superstructure of FCC is modeled using ETABS and building drawings provided by CSMIP. The isolation system properties are extracted from prototype test results (Bachman et al. 1990, 1995). Equivalent linear analytical model is developed in 3D-BASIS using 6 modes from ETABS analysis and equivalent properties of the isolation system. The period of the fundamental mode in the base isolated condition with equivalent linear isolation system in both the EW and NS directions is 1.56 secs (Nagarajaiah et al. 1995). The equivalent linear isolation system is based on bearing properties at 1.38 inch (3.5 cm) maximum displacement experienced by the isolators in Northridge earthquake. Estimated level of damping at this amplitude is 15%.

The building has been extensively instrumented by CSMIP (Shakal et al. 1994); the sensor locations are shown in Fig. 1. An examination of the records indicates sharp acceleration

spikes. The cause for these acceleration spikes is accidental pounding against entry bridge -- repaired incorrectly after the Landers earthquake-- across the isolation gap at the North-East corner of the building (Bachman 1995). As described earlier a simplified model is used to study the effect of accidental pounding. The simplified model has two floors and base, with three DOF per floor/base, as shown in Fig. 8. The isolation system is modeled by equivalent global linear springs and damping elements at the center of mass of the base. The accidental pounding is modeled by a nonlinear gap element with a contact spring at the North-East corner of the building as shown in Fig. 8. It is evident from the recorded response (see Fig. 8) that the building pounded upto approximately 16 secs into the time history response and then moved freely and behaved as a typical base isolated building --acceleration spikes cease after approximately 16secs. Hence, the contact spring is moved back to equal the isolation gap at approximately 16 secs into time history response. Fig. 8 shows a comparison of the recorded and computed response in the EW direction; absolute accelerations and relative displacements at sensor locations shown in Fig. 1 are compared. Comparison shows that the correlation between the computed and recorded response is good --both is phase and amplitude. Simplified model yields good results provided proper effective stiffness and damping properties are used for the isolators.

The effects of pounding are examined in Fig. 9 by comparing the case of the base isolated building with and without pounding and the fixed-base case without pounding. The floor response spectra are shown in Fig. 9. The peak story shear and peak drift envelopes are shown in Fig. 9. It is evident from the results in Fig. 9 that pounding causes (1) an increase in high frequency/low period response, and (2) an increase in peak story shear and drift. The effectiveness of base isolation is thus reduced; however, even with pounding, response of the base isolated building is less than that of the fixed-base case. As described before the reason for this is the dynamic characteristics of the base isolated building.

CONCLUSIONS

The seismic response and performance evaluation of base isolated USC hospital and FCC building has been presented. It is evident from the evaluation that (1) the USC hospital performed very well and the seismic isolation is effective in reducing the response and providing earthquake protection, (2) the FCC building performed as a base isolated structure should, excepting for the accidental pounding, (3) accidental pounding should be avoided by ensuring free movement at the seismic isolation gap, and (4) the analysis techniques, such as 3D-BASIS, used in base isolated structures are accurate and can reliably predict the response of base isolated structures.

ACKNOWLEDGEMENT

This research is supported by a grant from the Strong Motion Instrumentation Program of the California Department of Conservation (Contract No. 1093-556). The authors are grateful for this support. The authors wish to thank Drs. Huang, M. J., Maldonado, G., Darragh, R. B. and Shakal, A. F of CSMIP for providing building drawings, bearing test results, and strong motion records. Thanks are due to Bachman, R. E. of Fluor Daniel for providing bearing test data for FCC building. 3D-BASIS and portions of the analysis capabilities used in this study are supported by the National Center for Earthquake Engineering Research (NCEER grants 93-5003,

94-5001B). This support is gratefully acknowledged. In particular the first author wishes to thank Profs. Buckle, I. G., Lee, G. C., Shinozuka, M., and Soong, T. T. for continued support and encouragement. The assistance of graduate student Anupama Dochibotla in making computer runs and plotting is appreciated.

REFERENCES

Asher, J. W. , Van Volkinburg, D. R., Mayes, R., Kelly, R. L., and Sveinsson, B. I. and Hussain, S., "Seismic isolation design of the USC university hospital ," *Proc. Fourth US National Conf. on Earthquake Engrg.*, Palm Springs, CA, 534-538.

Bachman, R. E., Gomez, M. J., and Chang, K. C. (1990). "Verification analysis of the base isolated Los Angeles Fire Command and Control Facility," *Proc. Fourth US National Conf. on Earthquake Engrg.*, Palm Springs, CA, 539-548.

Bachman, R. E., (1995). Personal communication.

Buckle, I. G. and Mayes, R. L. (1990). "Seismic isolation: history, application, and performance - A world view," *Earthquake Spectra*, Vol. 6, No. 2, 161-201.

Huang, M. J., Malhotra, P. K. and Shakal, A. F. "Analysis of records from four base isolated buildings during low levels of ground shaking," *Proc. ATC-17-1 Seminar of Base Isolation and Active Control*, San Francisco, California, 319-330 (March 1993).

Kelly, J. M. (1990). "Base isolation: Linear theory and design," *Earthquake Spectra,* Vol. 6, No. 2, 223- 244.

Kircher, C. A., and Lashkari, B., "Statistical evaluation of nonlinear response of seismic isolation systems," *JBA Tech. Report 109-070*, June 30, 1989.

Ljung, Lennart, (1987). *System Identification,* Prentice Hall, Englewood Cliffs, N. J.

Mayes, R. L. "Response of isolated structures to recent California earthquakes," *Proc. Structures Congress '93,* editors- Ang, A. H. S. and Villaverde, R., 169-174 (1993).

Nagarajaiah, S., Reinhorn, A. M. and Constantinou, M. C. "3D-BASIS: Nonlinear dynamic analysis of three dimensional base isolated structures - Part II," *Report No. NCEER-91-0005, National Center for Earthquake Engrg. Res.*, SUNY, Buffalo, New York, (1991a).

Nagarajaiah, S., Reinhorn, A. M. and Constantinou, M. C. "Nonlinear dynamic analysis of 3D-base isolated structures," *J. of Struct. Engrg.*, ASCE, Vol. 117, No. 7, 2035-2054, (1991b).

Nagarajaiah, S. and Sun, X. (1995). "Response of base isolated buildings to moderate earthquakes: a post earthquake evaluation," Report on Project No. 1093-556 to the California Department of Conservation, Division of Mines and Geology, SMIP, in preparation.

Nagarajaiah, S., (1996). "System identification of base isolated USC hospital building using recorded response from Northridge Earthquake," *Structures Congress '96,* ASCE, Chicago, accepted for presentation.

Shakal, A., Huang, M. Darragh, R. et al. (1994). *CSMIP strong motion records from the Northridge earthquake of 17 January 1994*, Report No. OSMS. 94-07, California Strong Motion Instrumentation Program, California Department of Conservation, Division of Mines and Geology, California.

UBC - Uniform Building Code (1994), *International Conference of Building Officials,* Whittier, CA.

Wilson, E. L., Hollings, J.P., and Dovey, H H. (1975). "ETABS - Three dimensional analysis of building systems," Report No. UCB/EERC - 75/13, Earthquake Engineering Research Center, University of California, Berkeley.

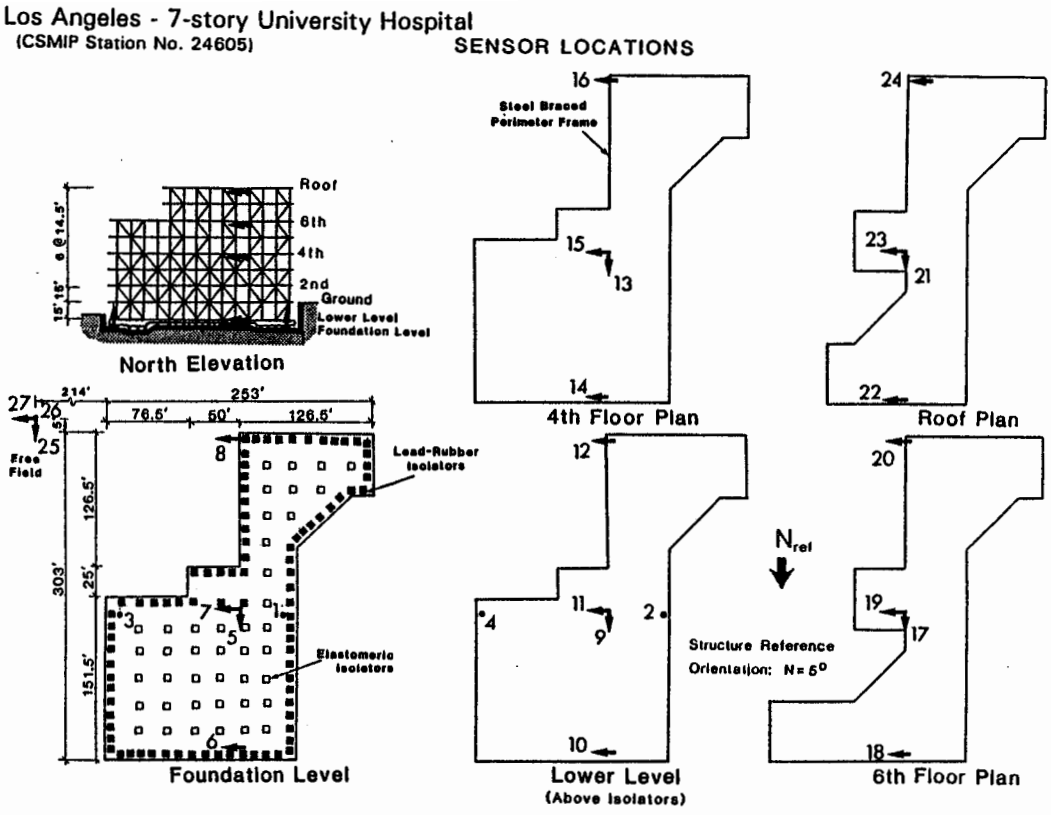

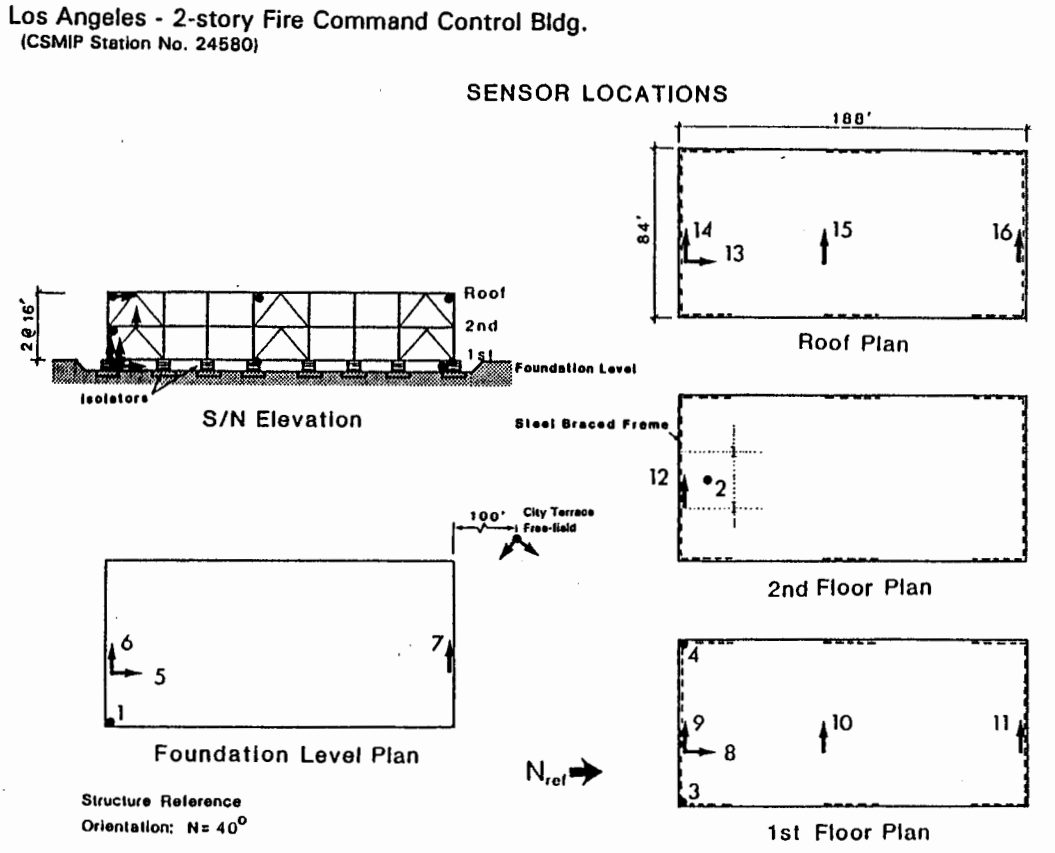

Fig. 1. USC Hospital and FCC Building: Superstructure and Isolation System Details, Sensor Locations.

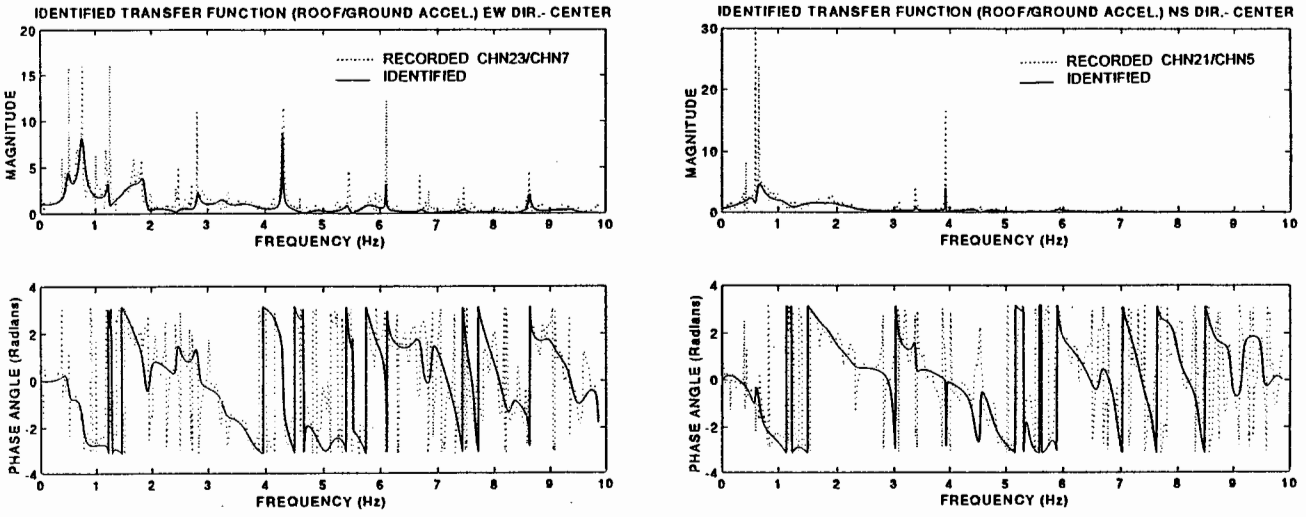

Fig. 2. USC Hospital: Recorded and Identified Transfer Functions -- Northridge Earthquake.

TABLE 1 Computed and Identified Periods and Damping Ratios of Base Isolated USC Hospital Building

Mode	Computed Period				Identified Period			
	EW - Dir		NS - Dir		EW - Dir		NS - Dir	
	Period(s)	Damping Ratio	Period(s)	Damping Ratio	Period(s)	Damping Ratio	Period(s)	Damping Ratio
1	1.250	0.110	1.370	0.110	1.320	0.100	1.560	0.100
2	0.546	0.160	0.514	0.160	0.546	0.150	0.549	0.150
3	0.262	0.050	0.245	0.050	0.262	0.050	0.256	0.050
4	0.163	0.050	0.152	0.050	0.164	0.070	0.145	0.070

TABLE 2 Fixed Base Periods and Damping Ratios of USC Hospital Building

Mode	1	2	3	4	5	6	7	8	9
Period	0.92	0.82	0.62	0.37	0.35	0.28	0.20	0.18	0.16
Damping Ratio	0.05	0.05	0.05	0.05	0.05	0.05	0.05	0.05	0.05

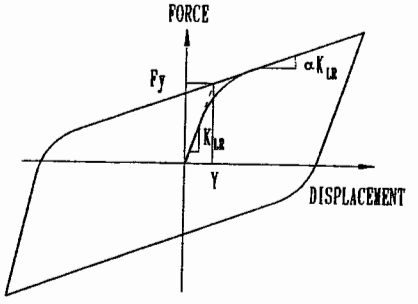

Fig. 3. Bilinear Model for Lead-rubber Isolators.

TABLE 3. PROPERTIES OF LEAD - RUBBER ISOLATOR (AT 1.1 INCH DISP.)

Qd - Characteristic strength	13.9 kips
F_Y - Yield force	18.0 kips
αK_{LR} - Post-yield stiffness	12.0 kip/in
K_{LR} - Elastic stiffness	53.0 kip/in
K_{eff} - Effective stiffness	24.7 kip/in

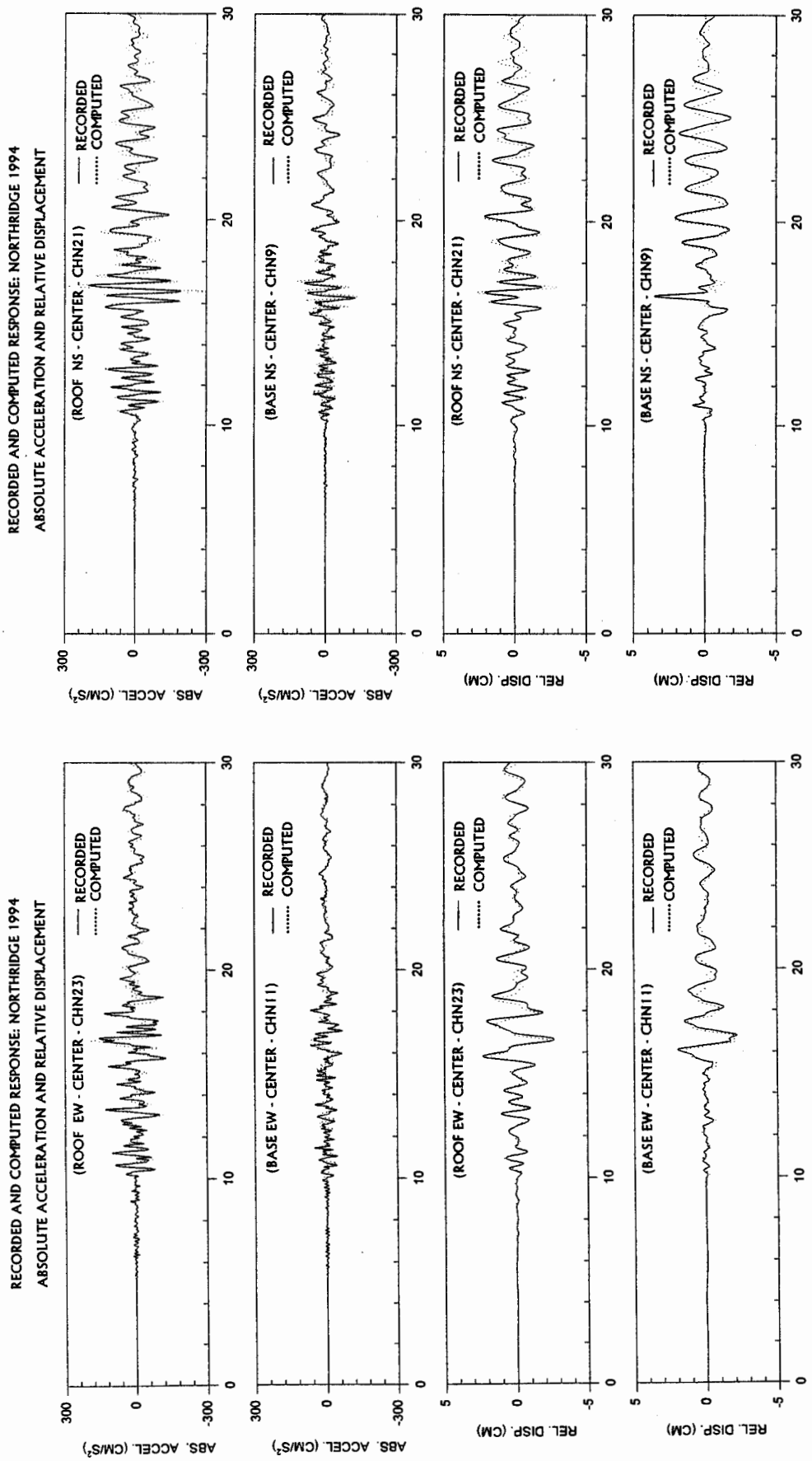

Fig. 4. USC Hospital: Recorded and Computed Response in the EW and NS directions at Sensor Locations shown in Fig. 1.

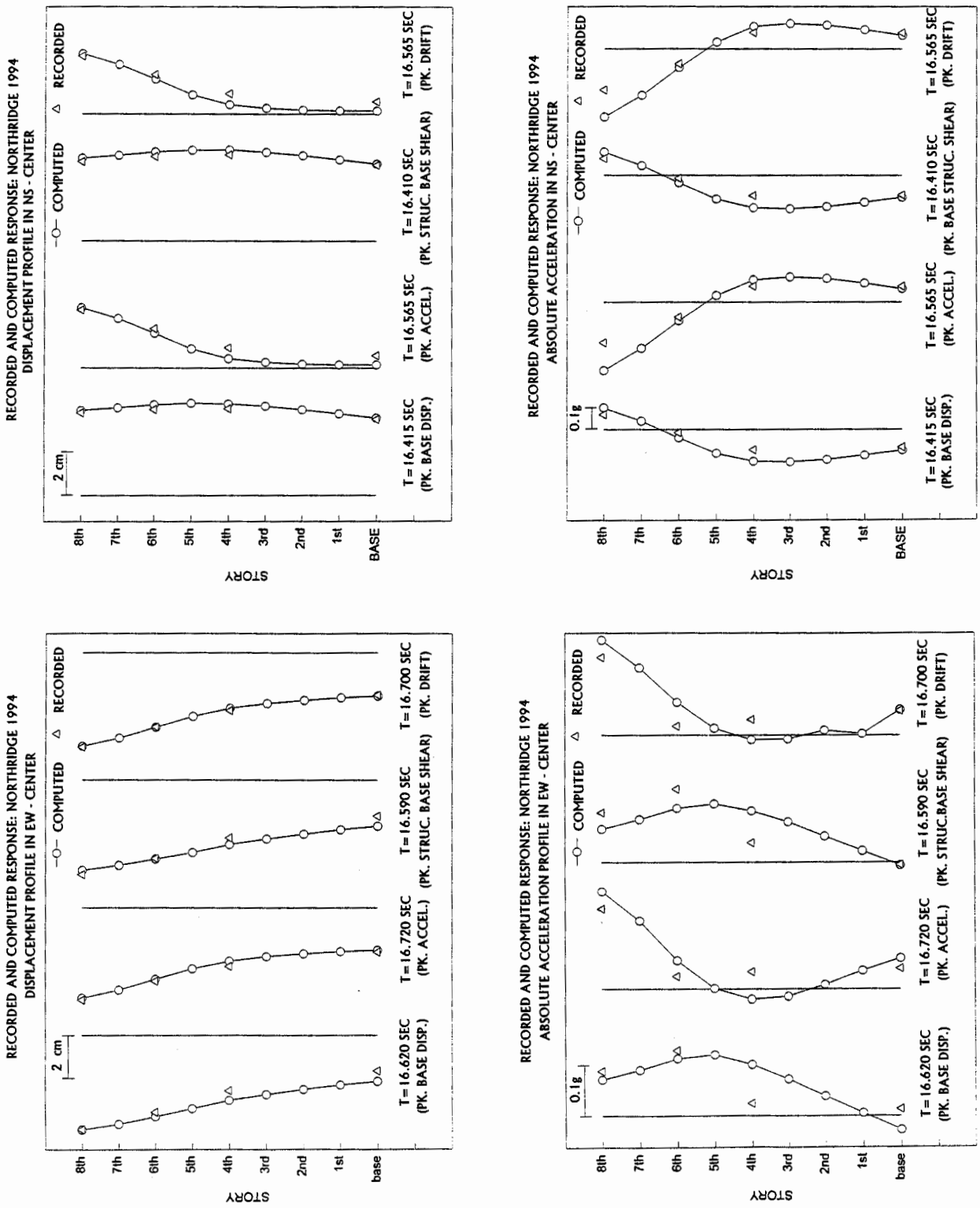

Fig. 5. USC Hospital: Recorded and Computed Displacement and Acceleration Profiles at Instants of Occurrence of the Peak Base Displacement, Peak Acceleration, Peak Structure Base Shear (above base), and Peak Drift --in the EW and NS Directions.

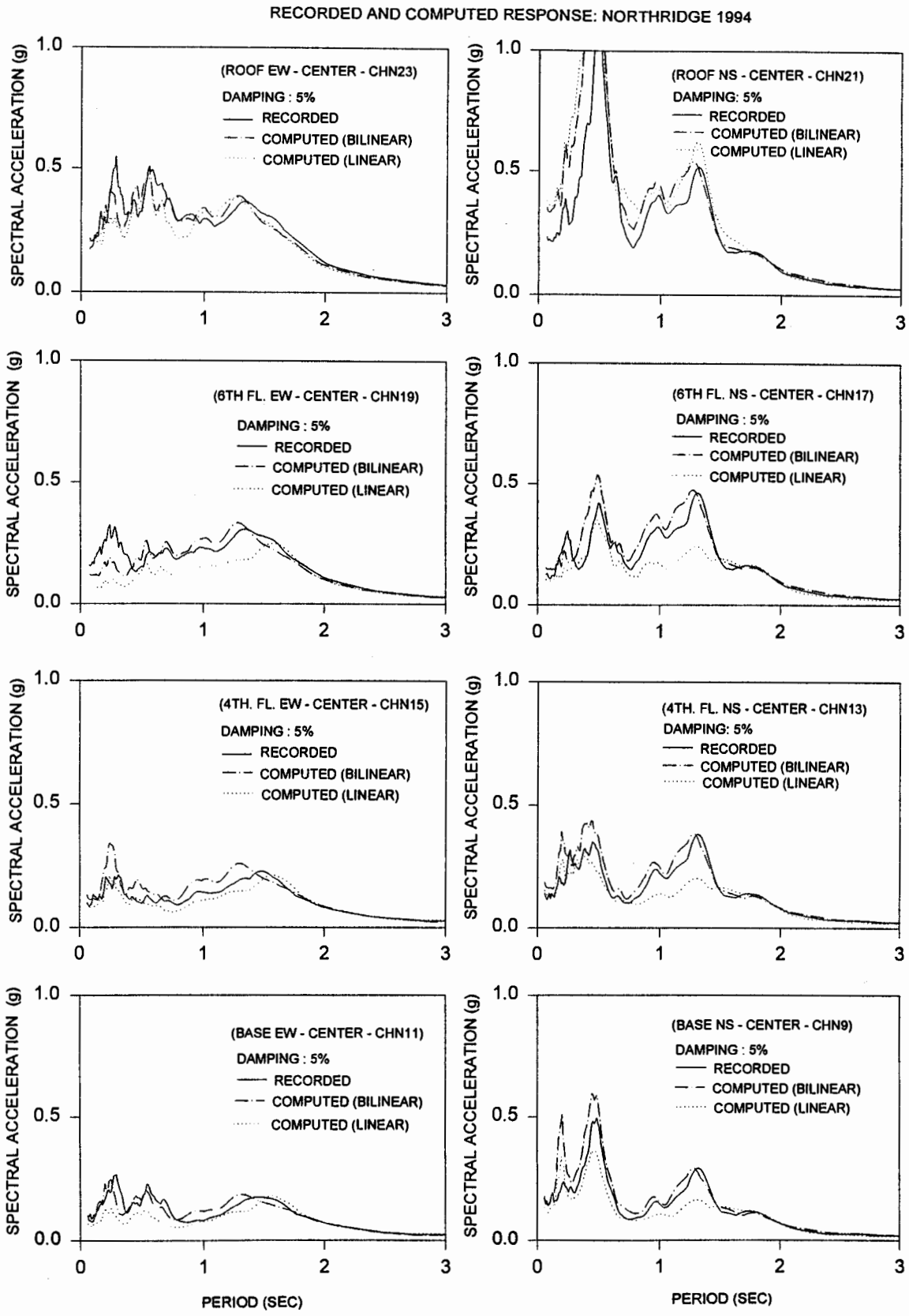

Fig. 6. USC Hospital: Floor Response Spectra for Three Cases (1) Recorded, (2) Computed Response with Bilinear Model for 68 Lead-rubber Isolators and Linear Model for 81 Elastomeric Isolators, (3) Computed Response with Linear Equivalent Global Springs and Damping Elements for Modeling the Isolation System --in the EW and NS Directions at Sensor Locations shown in Fig. 1.

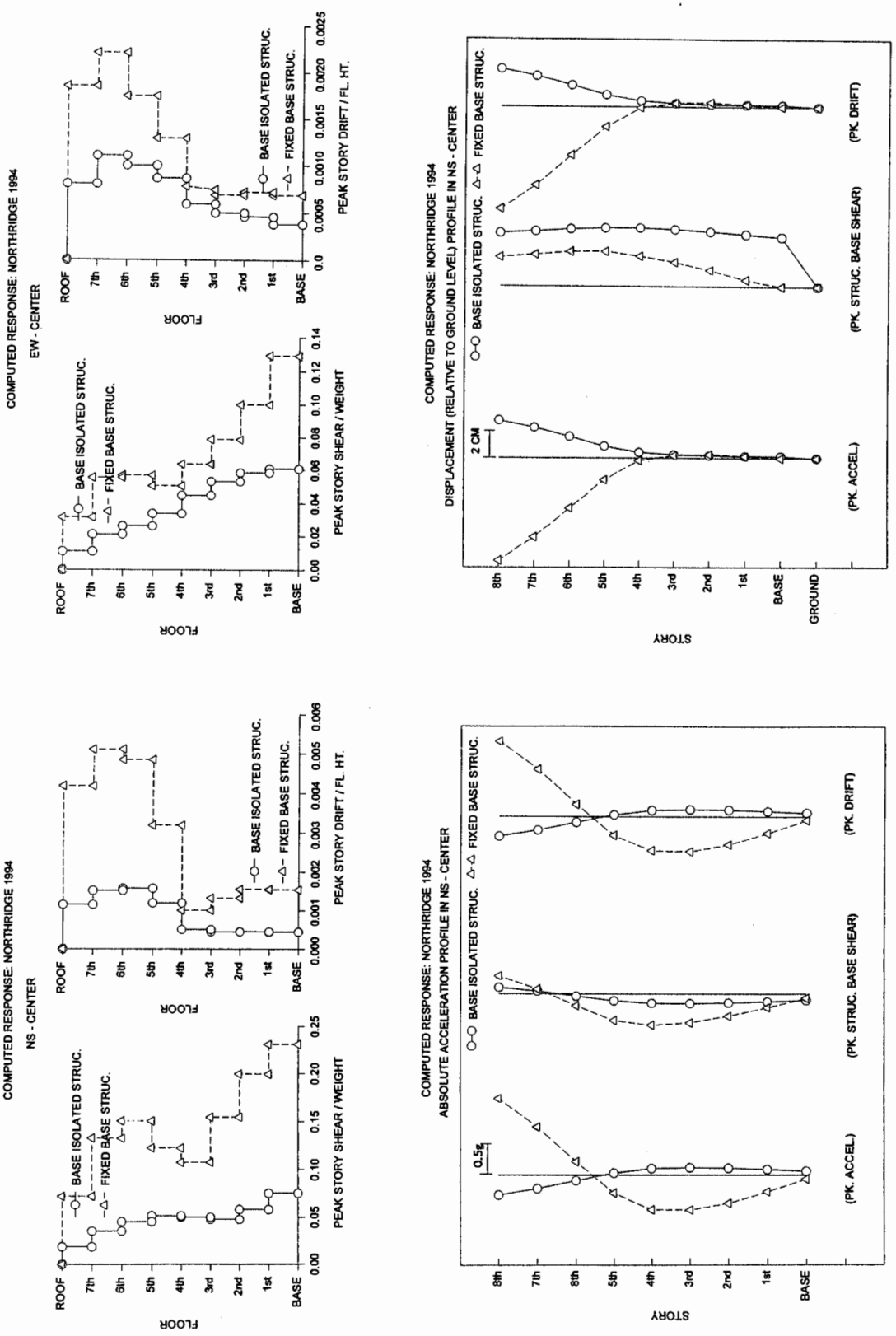

Fig. 7. USC Hospital: Comparison Between Base Isolated and Fixed-base Case (1) Normalized Peak Story Shear and Drift Envelopes in NS and EW Directions, (2) Displacement and Acceleration Profiles at Instants of Occurrence of the Peak Acceleration, Peak Structure Base Shear (above base), and Peak Drift in the NS Direction.

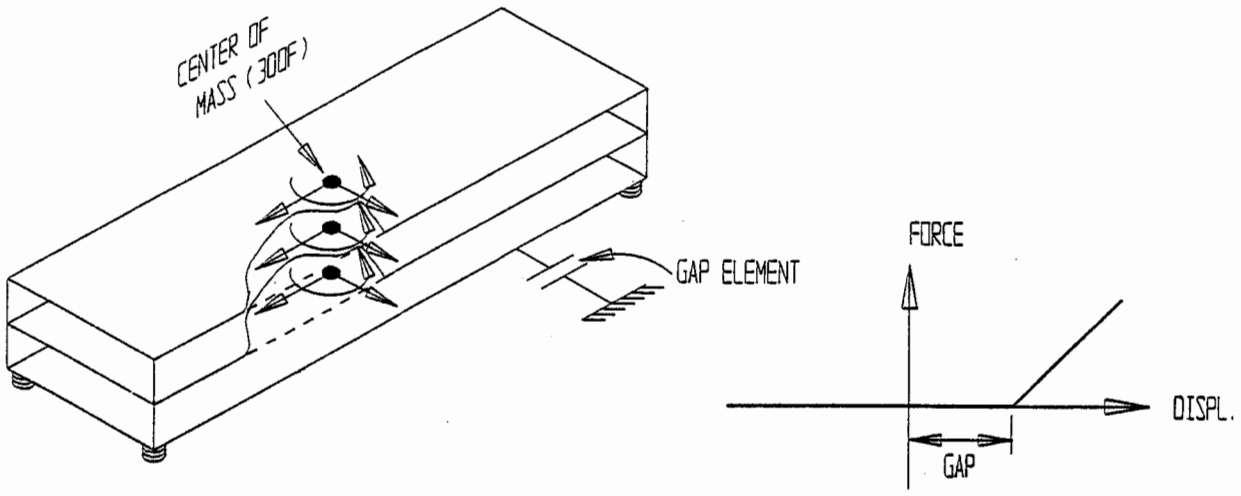

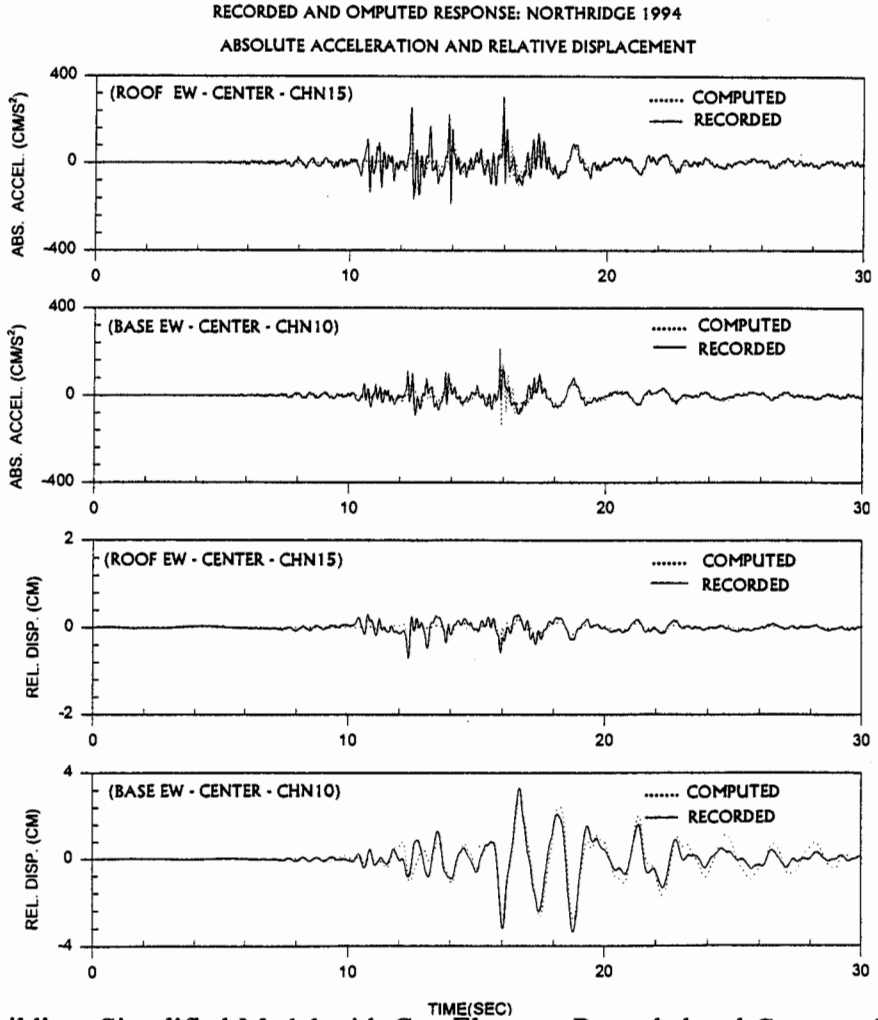

Fig. 8. FCC Building: Simplified Model with Gap Element; Recorded and Computed Response in the EW direction at Sensor Locations shown in Fig. 1.

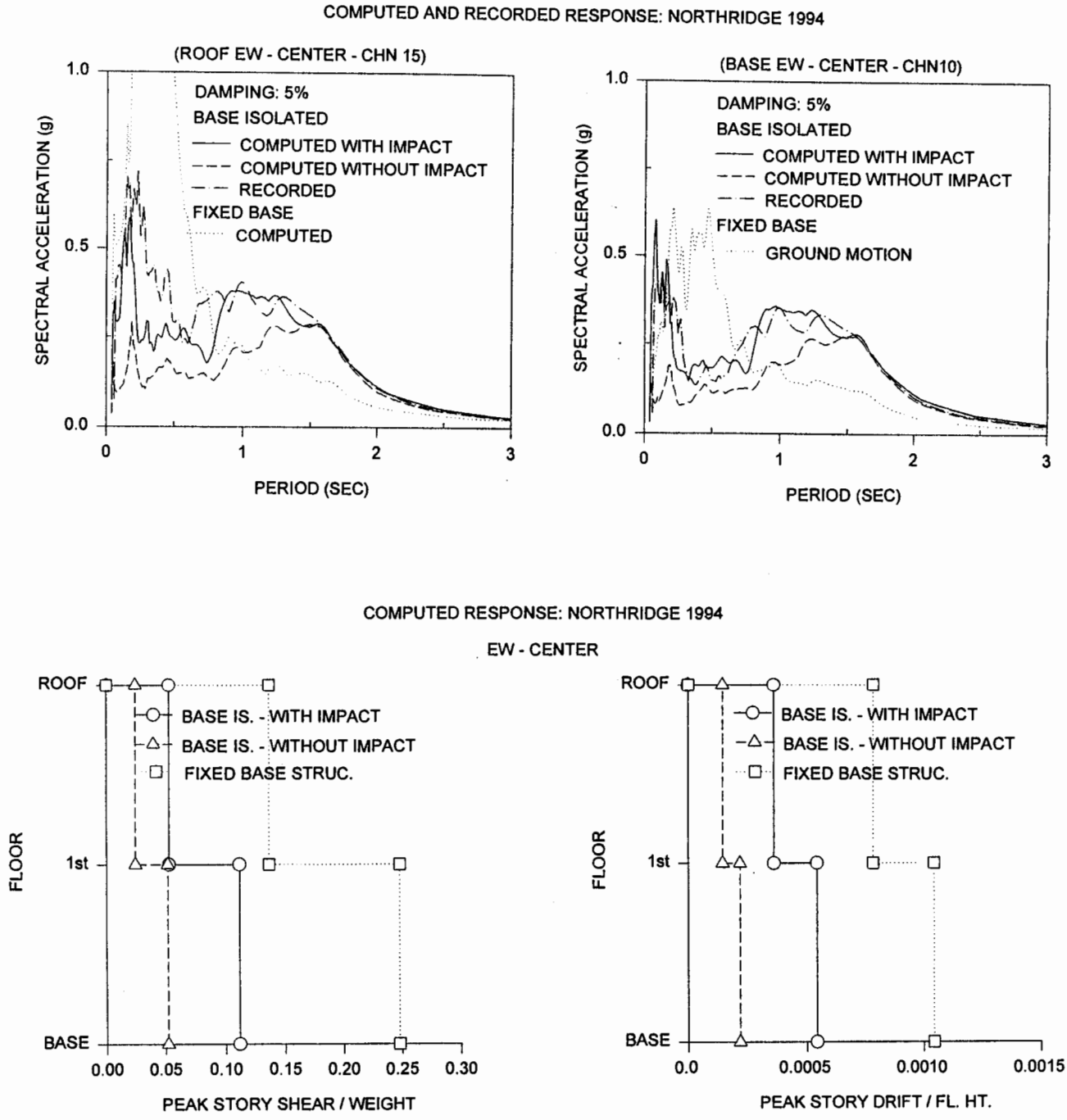

Fig. 9. FCC Building: Comparison between Base Isolated and Fixed-base Case (1) Floor Response Spectra in the EW Direction at Sensor Locations shown in Fig. 1, (2) Normalized Peak Story Shear and Drift Envelopes in the EW Direction.

EFFECT OF CONTRACTION JOINT OPENING ON PACOMIA DAM IN THE 1994 NORTHRIDGE EARTHQUAKE

G. L. Fenves and S. Mojtahedi

Earthquake Engineering Research Center
University of California, Berkeley

ABSTRACT

Pacoima Dam is constructed as cantilever monoliths separated by vertical contraction joints. A seismic safety evaluation of an arch dam often relies on a linear dynamic analysis assuming the dam is a monolithic structure. The CDMG network of strong motion accelerometers recorded the canyon and dam response in the 1994 Northridge earthquake. An analysis of dam models for the earthquake shows that joint opening occurrs and that it redistributes the stresses in the dam. The effects of non–uniform free–field motion were found to be important on the stresses and joint opening displacements.

INTRODUCTION

Concrete arch dams, such as Pacoima Dam in Los Angeles County, are constructed as cantilever monoliths separated by contraction joints. Since the joints cannot transfer substantial tensile stresses in the arch direction, the joints may open as the dam vibrates in response to earthquake ground motion. The earthquake response of arch dams is further complicated by the effects of dam–water interaction, dam–foundation rock interaction, and the spatial variation of the input motion along the interface between the dam and canyon.

A seismic safety evaluation of an arch dam often relies on a linear dynamic analysis assuming the dam is a monolithic structure and uses uniform free–field ground motion. The joint opening behavior is not represented, and hence a linear analysis can show unrealistically large tensile stresses in the arch direction. Design criteria have been developed to interpret arch dam behavior from stresses obtained from linear earthquake analysis. Although the effect of contraction joints has been recognized analytically and from shaking table tests of arch dam models, there has not been evidence of contraction joints opening during an earthquake. This situation changed on January 17, 1994, when Pacoima Dam was subjected to the Northridge earthquake. The contraction joints opened during the strong vibration. Some cracking and block offset occurred in parts of the dam body. The contraction joints closed under static forces after the earthquake, except for the left–most joint which had a permanent opening of two inches because the abutment thrust block slid downstream. The left abutment was damaged in

a similar manner in the 1971 San Fernando earthquake, although the permanent opening was only 3/8–inch after that earthquake. The abutment was repaired after 1971 by post–tensioning the thrust block.

The strong motion response of Pacoima Dam in the 1994 Northridge earthquake was recorded by a network of California Division of Mines and Geology (CDMG) accelerometers (CSMIP, 1994). This data offers a unique opportunity to evaluate the contraction joint behavior in an arch dam subjected to a strong earthquake. The objective of this study is to examine the response of Pacoima Dam in the Northridge earthquake using the computer program ADAP–88 which has been developed at the University of California, Berkeley, for nonlinear analysis of arch dams considering joint opening effects (Fenves, Mojtahedi et al., 1992a; Fenves, Mojtahedi et al., 1992b). Seismic analyses of the Pacoima Dam are performed with the joints assumed closed as well as allowed to open. In view of the importance of the ground motion variation along the abutment of the dam, seismic analyses were performed considering non–uniform seismic input (based on simplifying assumptions) and the results were compared with seismic response which would have been obtained using uniform seismic input.

RESPONSE OF DAM IN THE NORTHRIDGE EARTHQUAKE

Pacoima Dam is a flood control structure constructed in the San Gabriel mountains in 1929 by Los Angeles County. The concrete arch dam is 365 ft high and has a crest length of 589 ft. The thickness of the dam at crown section varies from 10.4 ft at crest to 99 ft at base. A plan and profile of the dam are shown in Fig. 1. The water level was about two–thirds full at the time of the Northridge earthquake (234 ft above the base compared with the full operating water level of 300 ft above the base). Consequently, dam–water interaction is not particularly important because there is no hydrostatic pressure inducing compression in the upper arches, and the added mass of the water is important for reservoirs more than two–thirds full.

The epicenter of the 1994 Northridge earthquake (M_s=6.8) was approximately 11 miles southwest of the dam. Figure 2 shows the CDMG accelerometer locations on the dam and the images of the film records (CSMIP, 1994). The motion at a downstream location had a peak acceleration of 0.44 g. The accelerometer above the left abutment recorded a peak acceleration of 1.53 g, illustrating the topographic amplification of ground motion. At the base of the dam, the peak acceleration was 0.54 g in the radial direction and 0.43 g in the vertical direction. At the crest of the dam, peak acceleration in the radial direction reached 2.3 g at the left quarter point. The peak acceleration at 80% of the height was also 2.3 g. The motion of the dam shows higher frequency components than the downstream and base records, possibly because of higher mode contributions of the dam or impact caused by open contraction joints pounding closed. It was not possible for CDMG to digitize and process all the strong motion records

because the traces became intertwined with the large acceleration peaks that exceeded the range of the instruments. Processed records are available for Channels 8 – 11 on the dam, the downstream site, and the left abutment site (see CSMIP Report Nos. 94–12A, 94–13, and 94–15A). Partial unprocessed records for Channel 1 – 6, 12, 13, and 15 – 17 are available in CSMIP Report 95–05.

In the 1971 San Fernando earthquake, the dam experienced strong motion close to the epicenter. The left abutment was damaged and several rockslides had to be repaired. An accelerometer above the abutment recorded a peak acceleration of 1.25 g, one of the largest recorded accelerations at the time. The topographic amplification in a canyon and the non–uniform support motion for an arch dam were recognized over twenty years ago in a study of Pacoima Dam in the San Fernando earthquake (Reimer, 1973). The computed base rock and dam accelerations from that study were remarkably similar to those in Northridge.

Examining the response of the dam in the 1994 Northridge earthquake, Fig. 3 shows the transmissibility function between radial motion at the base (Channel 9) and radial motion of the dam at 80% height (Channel 8). The transmissibility function is computed from estimates of the power spectral density functions. It indicates response peaks below 15 Hz at 4.0, 6.25, 8.25, 10.1, and 14.5 Hz. More analysis is required to identify vibration mode shapes from the limited processed strong motion data.

FINITE ELEMENT MODEL OF DAM

The finite element modeling concepts of ADAP–88 program are described in Fenves (1989). For the present study, the modeling was improved in three ways: (i) 3–D solid elements can now be used for the dam body instead of thick shell elements; (ii) nonlinear joint elements can be used for opening of lift joints and at the dam–foundation interface; and (iii) non–uniform free–field motion can be specified instead of the previous restriction to uniform ground motion (Mojtahedi and Tseng, 1994).

The finite element model used in the analysis of the Pacoima Dam is shown in Fig. 4. A total of 564 eight–node 3–D elements are used for modeling of the dam body. Four contraction joints are included in the model (the dam has eleven joints); three are located at the quarter points along the crest and the fourth joint represents the interface of the dam with its thrust block at left abutment. The four joints included in the model is adequate for representation of joint opening effects for uniform free–field ground motion; peak stresses can be expected to remain unchanged with increasing of the number of joints in the model. Three joint elements through the thickness are used for simulating opening–closing at the contraction joints and at the dam–foundation interface. This paper does not address opening of lift joints or cracking of the concrete, nor does it consider slippage at the contraction joints or dam–foundation interface. The material properties of the dam concrete were obtained from previous evaluations of the

dam (based on core samples). The elastic modulus is 2400 ksi and Poisson's ratio is 0.20. The unit weight is 150 lb/ft^3, as used in a previous study of the dam (County, 1983).

For analysis with uniform free–field motion, a foundation rock region of depth equal to the height of the dam is included in the model to account for dam–foundation interaction effects. To suppress stresses caused by propagation of seismic waves, the foundation rock is assumed to be massless and ground motion is specified at the rigid base of the foundation model. For analyses with non–uniform motion, free–field ground motions are specified for nodes along the dam–foundation interface and the same foundation model which is included in the analysis for uniform seismic input, is used to determine the impedance matrix of the foundation rock domain. In view of complexity of the foundation geometry and uncertainty in the foundation material properties, a prismatic shape is assumed for the canyon and a coarse mesh is used for finite element modeling of the foundation. A total of 220 3–D solid elements are used in discretization of the foundation rock domain. The material properties used for foundation rock are: modulus of elasticity = 2000 ksi, Poisson's ratio = 0.20, again based on previous investigations.

The hydrodynamic pressure of the impounded water acting on the dam is represented by an added mass matrix neglecting compressibility of water (Kuo, 1982). Compressibility of water in a full reservoir can have an important effect on the earthquake response of arch dams (Fok and Chopra, 1987). However, the frequency analysis required to include compressibility cannot be combined with the time domain analysis required to account for the nonlinear joint opening effects. For computing the added mass for all analyses, the water is assumed to be bounded by a cylindrical surface obtained by translating the dam–reservoir interface in the upstream direction. A total of 280 8–node 3–D elements is used for computing the added mass of the partially full reservoir.

The first ten free vibration frequencies of the Pacoima Dam, considering dam–reservoir–foundation interaction effects, are: 4.3, 4.4, 6.2, 7.5, 7.8, 8.5, 9.1, 9.8, 10.4, and 11.3 Hz. The first two analytical modes appear to have a slightly higher frequency with the broad peak in Fig. 3 at 4.0 Hz. The analytical model also shows more distinct modes which are not separated in the transmissibility function in Fig. 3. Considering the uncertainties in the material properties, the correspondence is judged to be adequate. The limited processed data may make it difficult to obtain a closer correspondence between the identified and model vibration properties.

Rayleigh damping was assumed for the dam–foundation system with the parameters selected to produce 10% damping at 5 Hz and 20 Hz. The damping was selected after several trial solutions. It is an acceptable value considering that energy dissipation in not modeled in the foundation, there was slight damage to the dam body, and the broad peaks in the transmissibility function (Fig. 3).

DAM RESPONSE ASSUMING CLOSED JOINTS

Three cases are considered to examine the response of the dam with the contraction joints prevented from opening. This is the typical assumption used in the seismic safety evaluation of arch dams. For Cases 1 and 2 uniform free–field motion is specified for three components of the ground motion. Case 3 uses an assumed spatial variation of the ground motion to account for the topographic amplification. Case 1 uses the recorded acceleration from the downstream instrument (in the canyon). Case 2 uses the acceleration from the upper left abutment, reduced by one–third to represent the motion of the canyon. The free–field motion for the two cases is very different because of the topographic amplification of the canyon, but they have been proposed as bounds for the response of the dam to the actual spatially varying ground motion.

The problem of determining the spatial variation of the free–field motion in the canyon is difficult because it depends on complicated wave propagation effects for seismic waves emanating from the extended source and scattering on the canyon. The instrumentation for the dam is not sufficient to define the spatial variation of input motion, and even if it were sufficient, the recorded motion of the abutments would include dam–foundation interaction effects. Since the principal objective of this study was to examine the contraction joint behavior, a very simple assumption for the non–uniform motion is made. For Case 3, the free–field motion is based on an interpolation of the recorded motion at the dam base and the recorded motion at the left abutment. The interpolation function should represent the dynamic characteristics of the canyon. In this study a linear interpolation function is selected in lieu of a detailed model of wave propagation effects. Consequently, each component of the free–field motion at an elevation is a linear interpolation between the toe and left abutment recorded motions.

Figure 5 shows a comparison of the acceleration for Channel 8, the radial motion at about the 80% height in the left quarter of the dam (see Fig. 2 for the location). For Cases 1 to 3, the computed peak acceleration is reasonably close to the corresponding measured value. The computed histories for Case 3, however, differ in phase with the recorded motion.

Figure 6 shows the envelopes of maximum arch and cantilever stresses for Case 2 (positive is tension). All stress contour plots are viewed looking in the downstream direction. For Case 1 (not shown) with the uniform downstream motion the peak tensile stresses are 450 psi in the arch direction and 150 psi in the cantilever direction. For Case 2 with uniform motion based on the upper left abutment record, reduced by one–third, Fig. 6 shows that the peak tensile stresses more than double: 1100 psi in the arch direction (upstream) and 400 psi in the cantilever direction (downstream).

The stress distributions for the assumed non–uniform free–field motion Case 3 in Fig. 7 are very different than the stresses for the uniform free–field cases. The largest arch and cantilever stresses develop near the abutments, in contrast with Cases 1 and 2

for which the greatest stresses are at the center of the dam. The stress contours also have a very different pattern than the uniform ground motion cases. Very large tensile arch stresses, exceeding 3000 psi, are obtained at the upper right abutment. The cantilever stresses reach 1200 psi tension in the lower portion of the dam. The large stresses near the abutments are caused by the relative displacements of the non–uniform free–field motion at the interface; they tend to reduce towards the center of the dam where vibration contributes more to the stresses. From these results, the two uniform ground motion cases do not represent the response of the dam considering the assumed non–uniform ground motion.

DAM RESPONSE INCLUDING JOINT OPENING

As shown in Fig. 7, maximum tensile arch stresses of up to 1800 psi develop away from the abutment for Case 3 with the non–uniform free–field ground motion. Tensile stresses cannot be transmitted by the contraction joints, so it is expected that the joints will open during the earthquake preventing such tensile stresses from developing. To examine this issue, Case 4 allows the joints to open with the non–uniform free–field ground acceleration.

A comparison of the Channel 8 histories for Cases 3 and 4 (Fig. 5) shows that the agreement between the computed and recorded acceleration further improves when the joints are allowed to open. The main pulse in the recorded response is captured by the model with joint opening effects and non–uniform ground motion. After the main pulse, however, the analysis shows larger amplitude vibration than recorded. The overestimate of vibration is most likely caused by the lack of radiation damping in the foundation model.

As shown by the stress contours in Fig. 8 the maximum arch stresses in the dam body reduce to about 200 psi and there is a small increase in the cantilever stresses as seismic forces are transferred from arch action to cantilever action when the joints open. However, near the abutments the arch stresses are still large because of the pseudo–static effects of the relative input motion displacements. Figure 9 plots the joint opening history at the crest of each joint. The opening at the upstream and downstream faces are in–phase indicating complete separation of the joints. Also shown are the joint history plots for the pseudo–static joint displacements: the joint opening that would occur due to slow application of the free–field ground motion. Joint 1, near the right abutment, has the largest opening of 4 in., but most of that is due to the pseudo–static response. The vibration produces about 1 in. of the opening. Joints 3 and 4, the latter near the left abutment, have mostly pseudo–static opening. Joint 2 at the crown opens because of vibration, reaching a maximum opening of 3.5 in during the strong vibration response. Figure 10 shows the contours of maximum joint opening in each of the joints.

CONCLUSIONS

Examination of the limited CDMG processed records of Pacoima Dam in 1994 Northridge earthquake and comparison with analytical models indicates the following conclusions: (i) The contraction joints opened during the earthquake, and the effect of the joint opening is an important factor in the response, (ii) the non–uniform free–field ground motion caused by topographic amplification has a significant effect on the dam response; (iii) the computed response using uniform free–field ground motion does not provide an adequate representation of dam performance; (iv) damping due to foundation rock radiation appears to be important. The pseudo–static effects of the non–uniform ground motion cause high stresses. It is necessary to use more than three or four joints in the model to represent the effect of joint opening on the stresses, particularly near the abutments.

ACKNOWLEDGMENTS

This study was supported by the California Department of Conservation, Division of Mines and Geology, Strong Motion Instrumentation Program, Contract 1093–558. Drs. Moh Huang and Robert Darragh of that organization provided valuable assistance. The authors thank Mr. Robert Kroll of the Los Angeles County Department of Public Works for his assistance and willingness to provide information about the dam.

REFERENCES

County, L. A. (1983). "Stability Reanalysis of Pacoima Dam," *Final Report*, MK International Engineering.

CSMIP (1994). "Strong Motion Records from the Northridge, California Earthquake of January 17, 1994," *Report No. OSMS 94–07*, California Department of Conservation, Strong Motion Instrumentation Program.

Fenves, G. L., S. Mojtahedi, et al. (1989). "ADAP–88: A Computer Program for Nonlinear Earthquake Analysis of Concrete Arch Dams," *Report No. UCB/EERC–89/12*, Earthquake Engineering Research Center, University of California at Berkeley.

Fenves, G. L., S. Mojtahedi, et al. (1992a). "Effect of Contraction Joints on Earthquake Response of an Arch Dam," *J. Struct. Eng.*, AS CE, Vol. 118, No. No. 4, pp. 1039–1055.

Fenves, G. L., S. Mojtahedi, et al. (1992b). "Nonlinear Earthquake Analysis of Arch Dam/Reservoir," Tenth World Conference on Earthquake Engineering, Vol. 8, Madrid, Spain, pp. 4595–4600.

Fok, K.-L. and A. K. Chopra (1987). "Water Compressibility in Earthquake Response of Arch Dams," *J. of Struct. Engr.*, ASCE, Vol. 113, No. 5, pp. 958–975.

Kuo, J. (1982). "Fluid–Structure Interactions: Added Mass Computations for Incompressible Fluid," *Report No. UCB/EERC–82/09*, Earthquake Engineering Research Center, University of California at Berkeley.

Mojtahedi, S. and W. S. Tseng (1994). "ADAP–NF, A Computer Program for Nonlinear Analysis of Arch Dams Considering Non–uniform Seismic Input," International Civil Engineering Consultants, Inc.

Reimer, R. B. (1973). "Deconvolution of Seismic Response for Linear Systems," *Report No. EERC 73–10*, Earthquake Engineering Research Center, University of California at Berkeley.

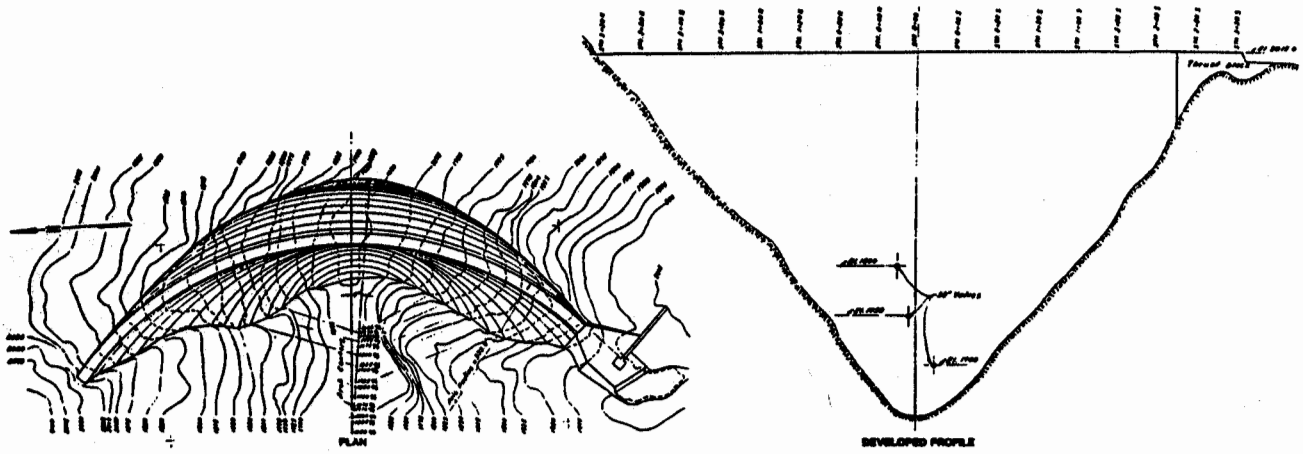

Fig. 1. Plan and Profile of Pacoima Dam (County, 1983).

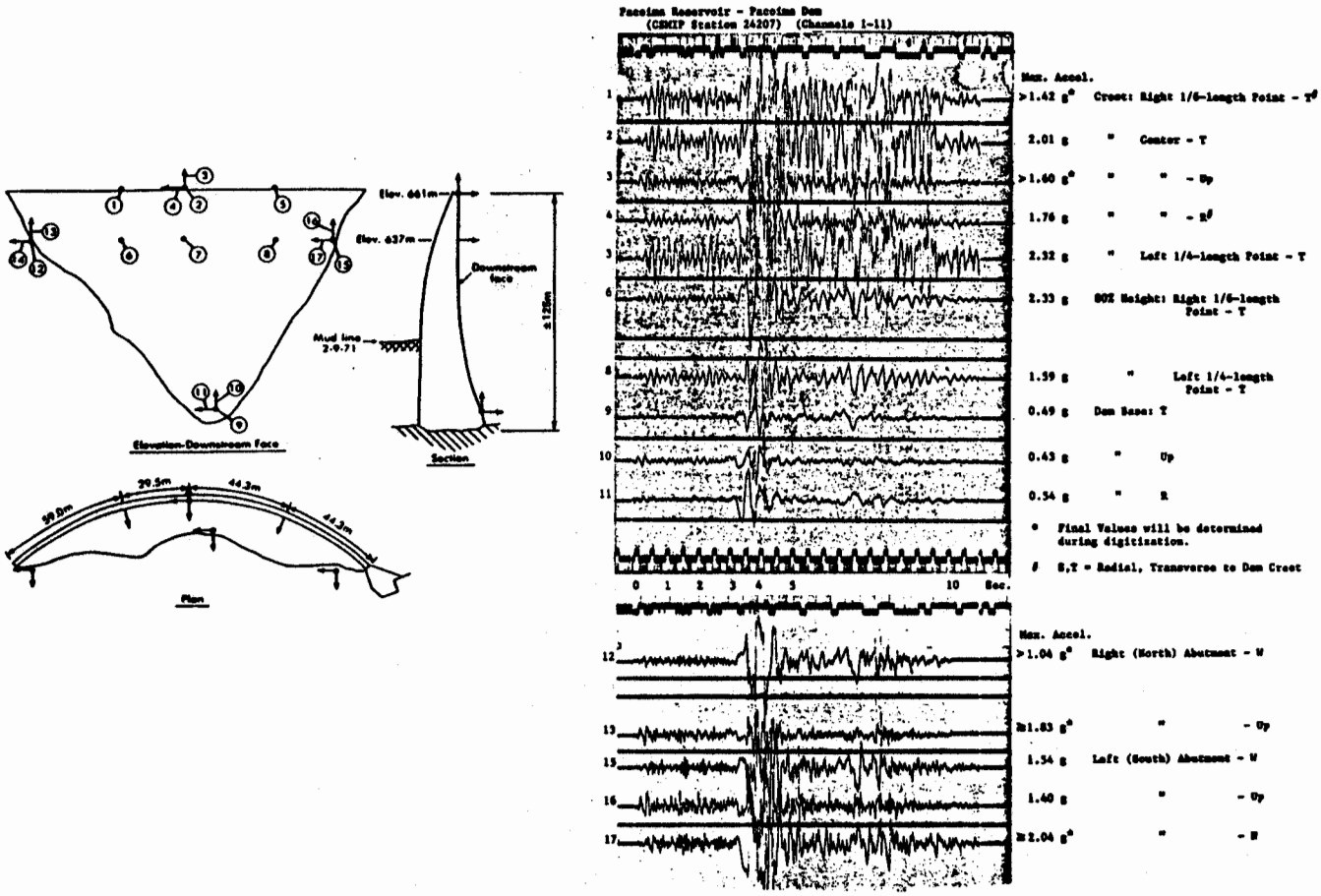

Fig. 2 CDMG Strong Motion Instrumentation for Pacoima Dam and Records from 1994 Northridge Earthquake (CSMIP, 1994).

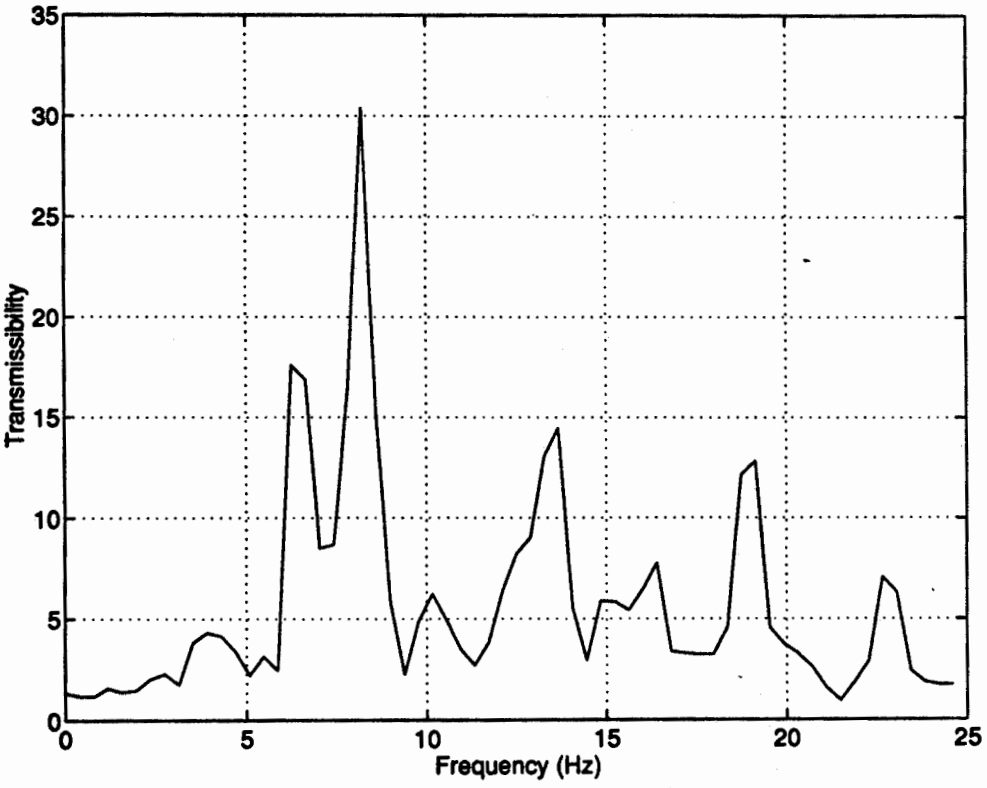

Fig. 3 Transmissibility for Radial Response of Pacoima Dam.

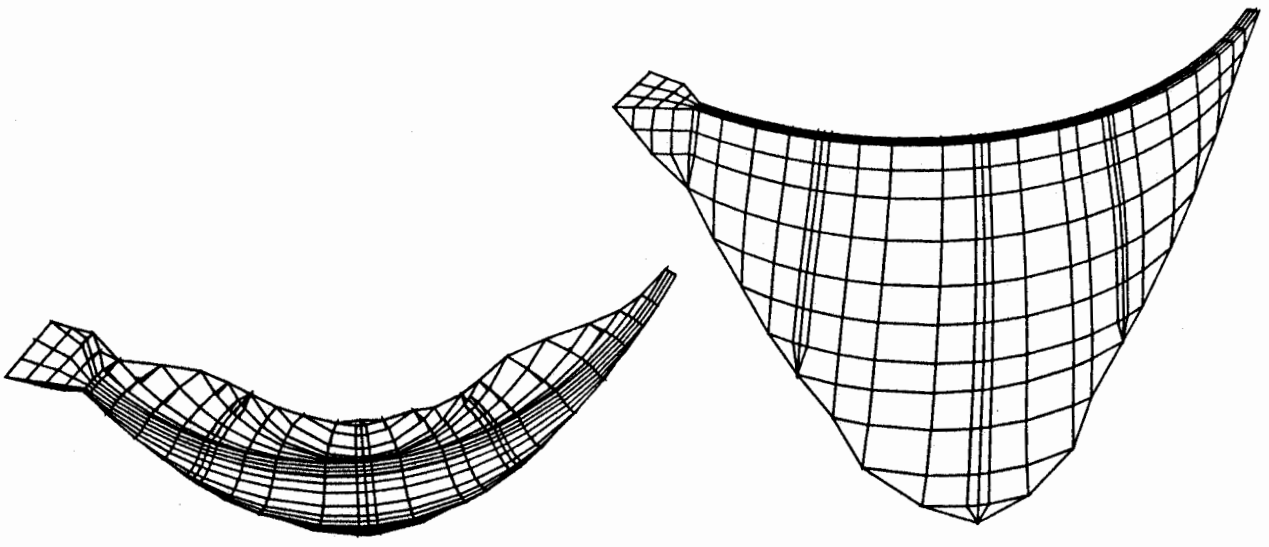

Fig. 4 Finite Element Model of Pacoima Dam Including Vertical Contraction Joints.

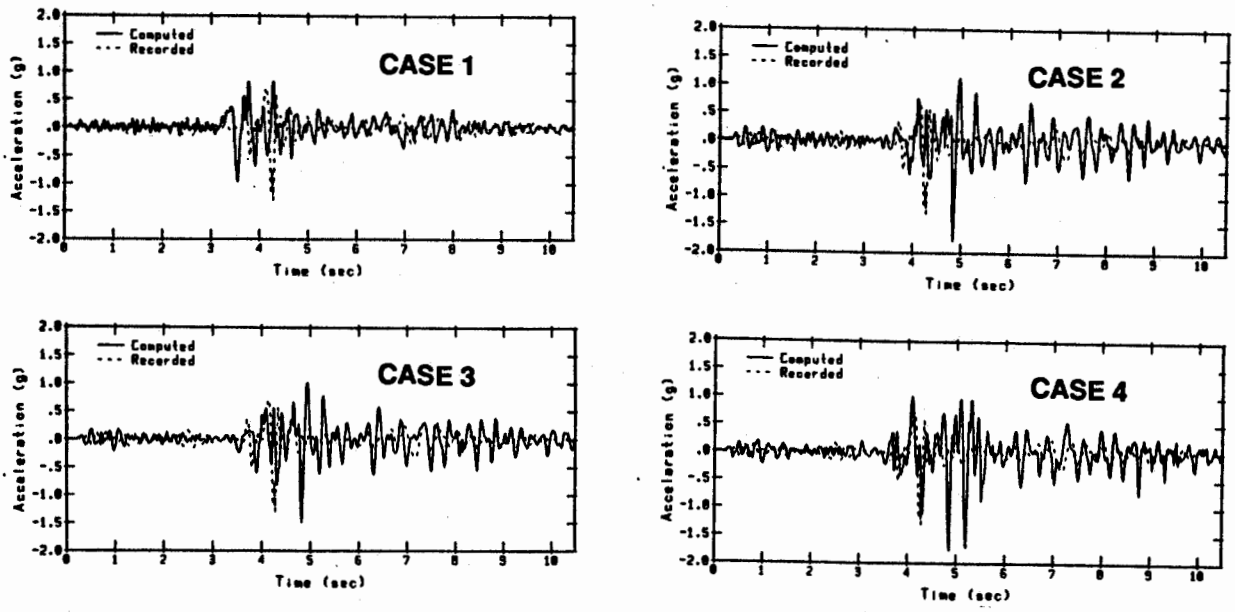

Fig. 5 Computed Acceleration for Channel 8 for Case 1 (Uniform Downstream, Closed Joint), Case 2 (Uniform 2/3 Upper Left Abutment, Closed Joint), Case 3 (Non–uniform, Closed Joint), and Case 4 (Non–uniform, Open Joint), Compared with Recorded Acceleration.

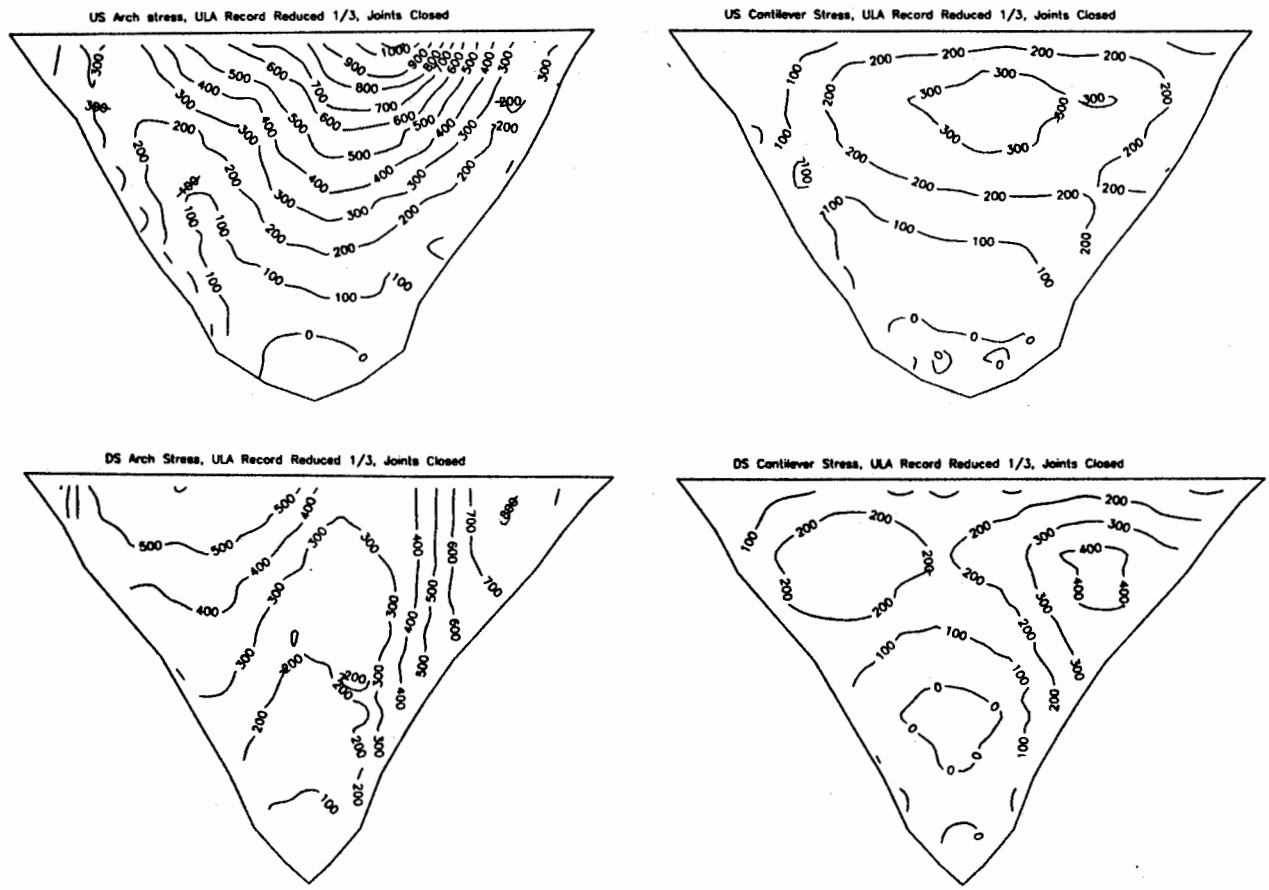

Fig. 6 Contours of Maximum Principal Stress (in psi) for Closed Joint Model of Pacoima Dam. Case 2: Uniform Upper Left Abutment Free–field Ground Motion Reduced by One–Third.

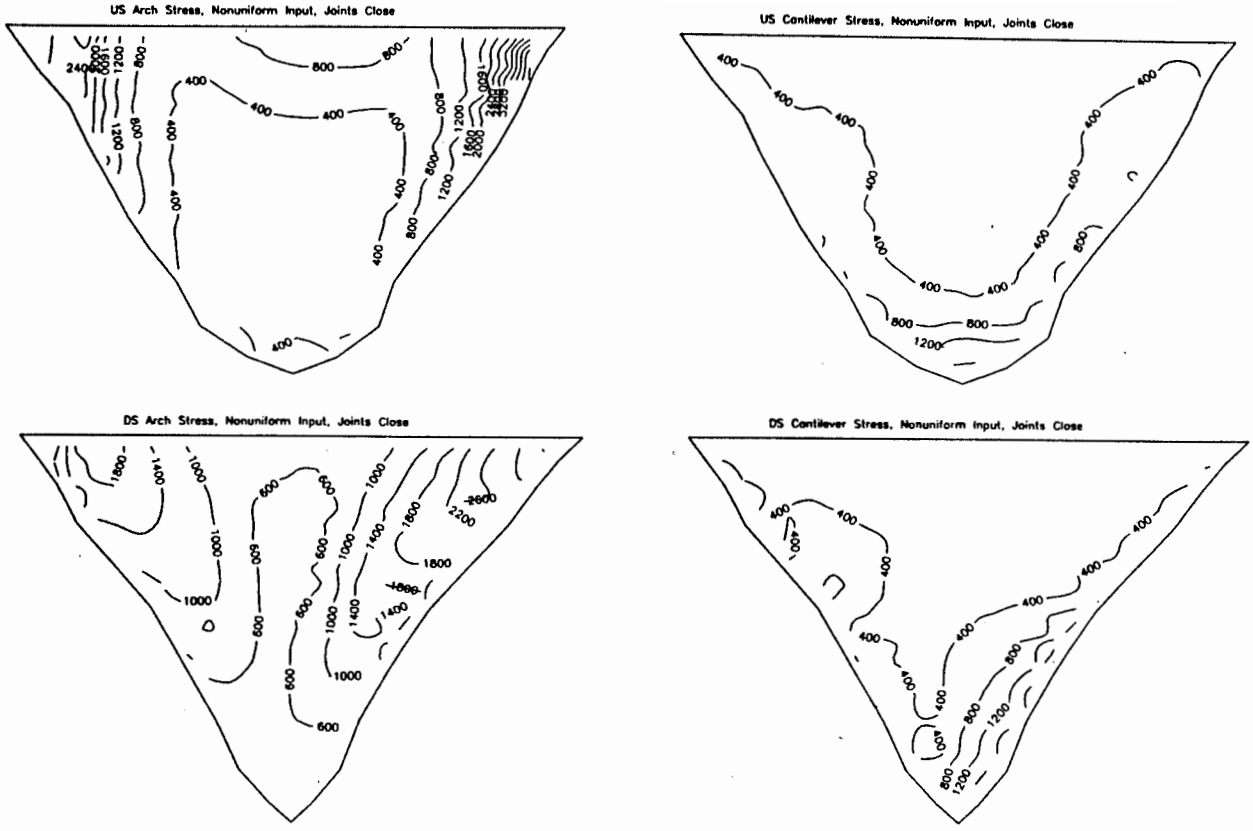

Fig. 7 Contours of Maximum Principal Stress (in psi) for Closed Joint Model of Pacoima Dam. Case 3: Non-uniform Free-field Ground Motion.

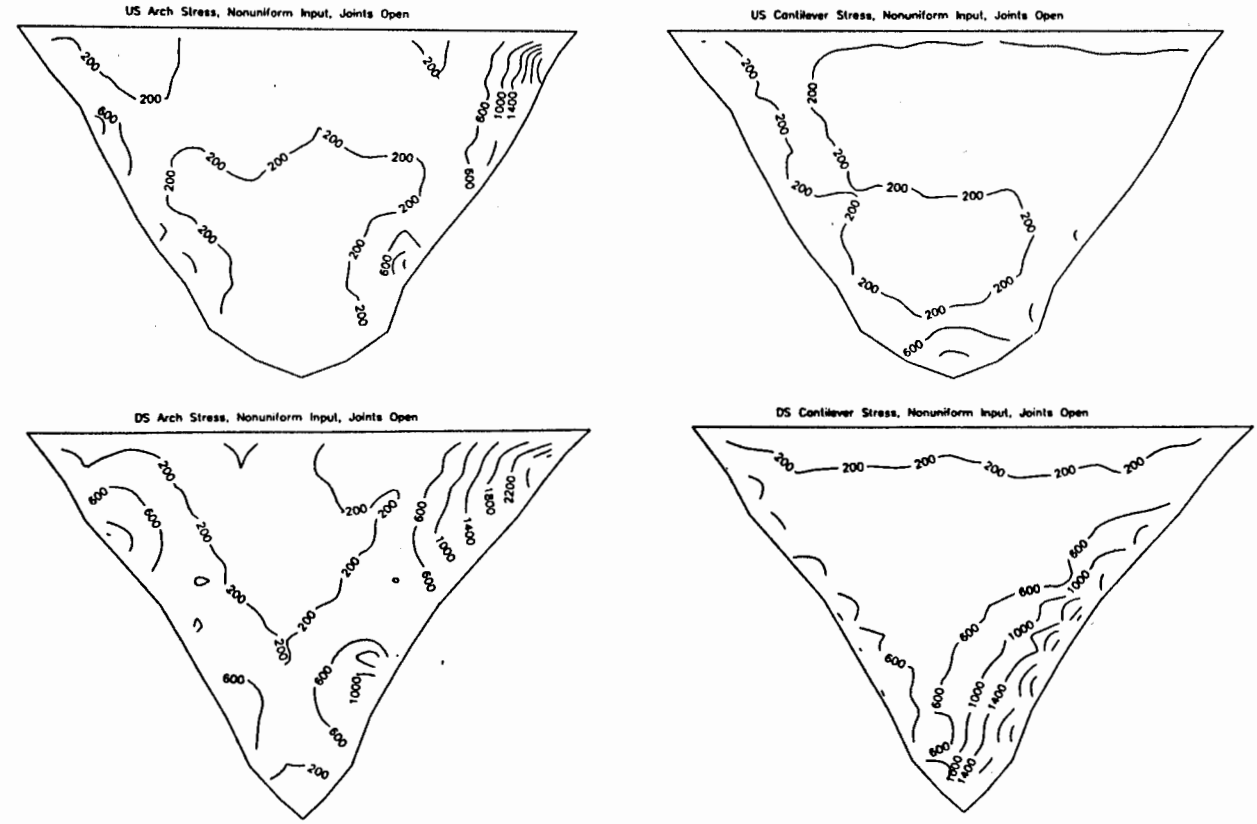

Fig. 8 Contours of Maximum Principal Stress (in psi) for Open Joint Model of Pacoima Dam. Case 4: Non-uniform Free-field Ground Motion.

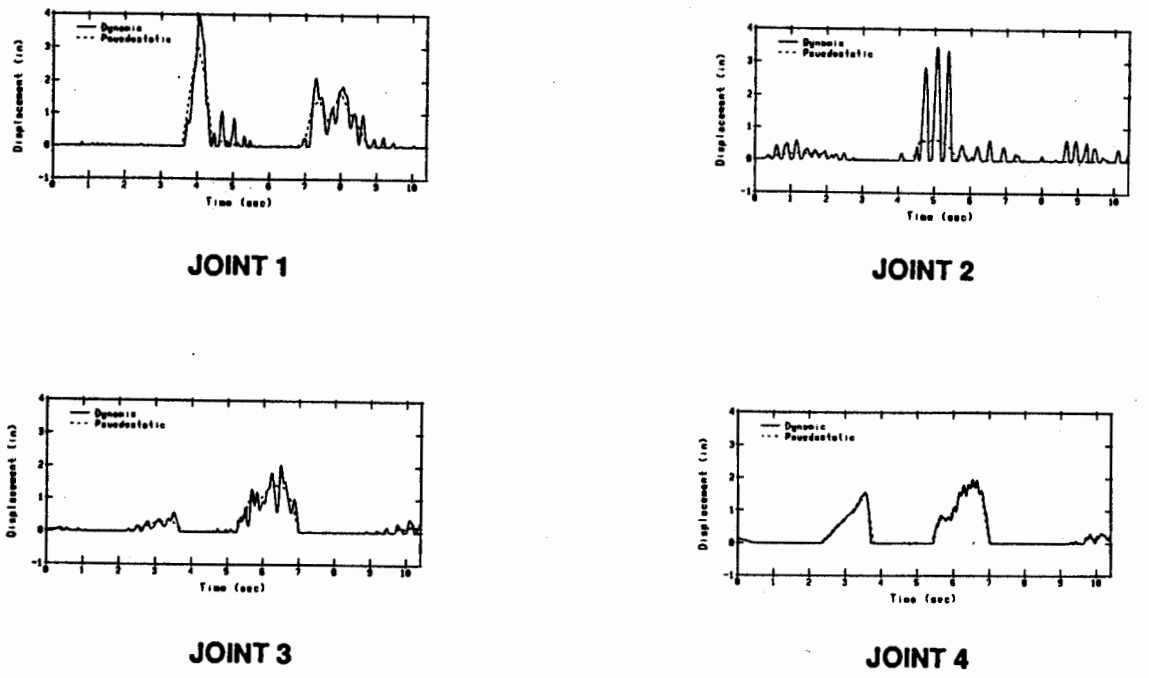

Fig. 9 History of Joint Opening Displacement for Case 4, Open Joint Model and Non–uniform Free–field Ground Motion.

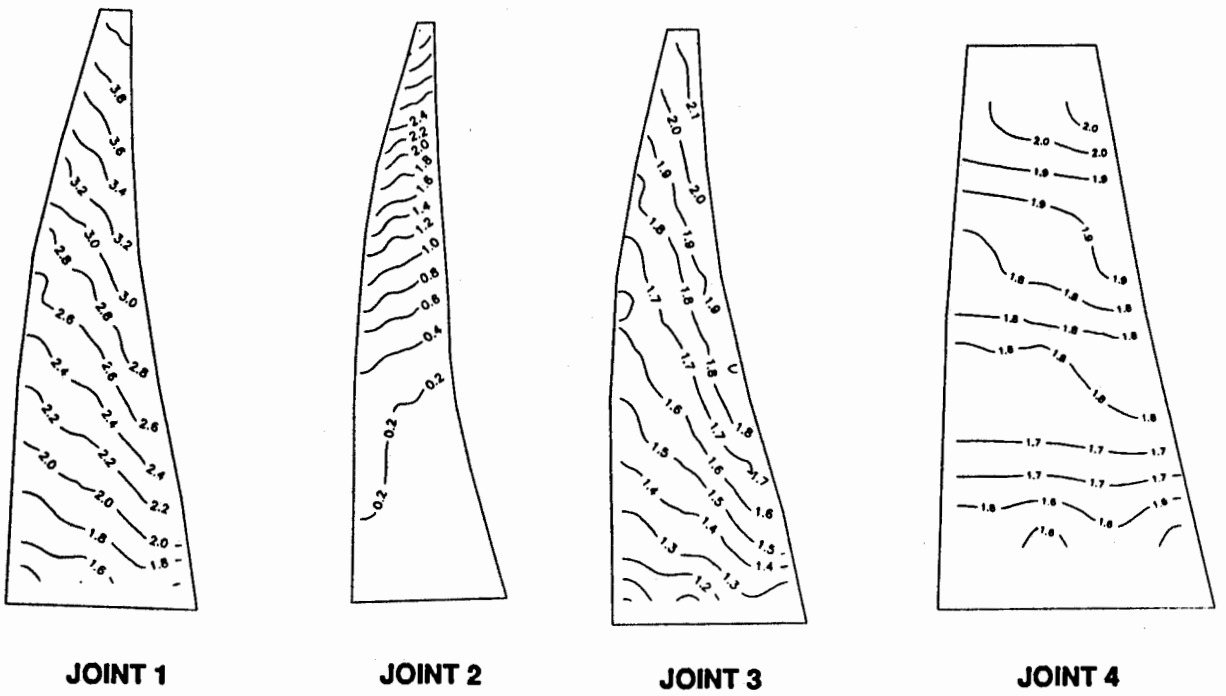

Fig. 10 Contours of Maximum Joint Opening Dispalcement (in inches) for Case 4, Open Joint Model and Non–uniform Free–field Ground Motion.

STRONG MOTION RECORDS FROM THE KOBE, JAPAN EARTHQUAKE OF JAN. 17, 1995, AND IMPLICATIONS FOR SEISMIC HAZARDS IN CALIFORNIA

Paul Somerville

Woodward-Clyde Federal Services
Pasadena, California

ABSTRACT

The strong ground motion characteristics of the Kobe earthquake are very similar to those of California earthquakes. This raises the question of whether losses as large as the $200 billion which occurred in Kobe could occur in an urban earthquake in California.

INTRODUCTION

The January 17, 1995 Hyogo Ken Nanbu Earthquake is the most damaging earthquake to have struck Japan since the great Kanto earthquake destroyed large areas of Tokyo and Yokohama and killed approximately 150,000 people (mostly by fire) in 1923. As of February 17, the toll from the Kobe earthquake had reached 5,368 dead and 26,815 injured. It is estimated that 144,032 buildings were destroyed by ground shaking and 7,456 buildings were destroyed by fire. The number of homeless people requiring shelter was approximately 300,000, which is 20% of the population of Kobe. Current estimates of losses in this city of 1.5 million people are about 20 trillion yen (200 billion dollars). This includes approximately $100 billion estimated by the Hyogo Prefectural Government to restore basic functions, approximately $50 billion in losses of private property, and approximately $50 billion in losses due to economic dislocation and business interruption. This paper describes ground motion data relevant to the question of whether these very large losses, which are an order of magnitude larger than those from the January 17, 1994 Northridge, California earthquake, could occur in an earthquake in an urban region of California.

SOURCE CHARACTERISTICS OF THE KOBE EARTHQUAKE

The tectonic setting and source characteristics of the Kobe earthquake have been described by Kanamori (1995) and Somerville (1995a,b). The time sequence and orientation of faulting during the Kobe earthquake has been inferred from the analysis of strong motion data by Pitarka et al. (1995) and teleseismic data by Kikuchi (1995). The fit of recorded and synthetic velocity waveforms in the Pitarka et al. (1995) model is shown in Figure 1. Southwest of the epicenter, away from Kobe, the earthquake produced 11 km of surface rupture with an average horizontal displacement of 1 to 1.5 meters on the Nojima fault, which runs along the northwest shore of Awaji Island. The strike-slip motion was accompanied by a component of thrust motion, producing a fault scarp dipping down to the southeast, with the northwest side down. This dip is consistent with the offset of the surface rupture by a few km to the northwest from the epicenter, and with the focal mechanism of the first event as inferred by Kikuchi (1995) and Pitarka et al. (1995). The dip direction is reversed on the part of the rupture that extends

northeast from the epicenter toward Kobe. A releveling survey after the earthquake found a decrease in elevation of 26 cm between Tarumi and Suma Wards in western Kobe, inferred to mark the location of subsurface faulting. This down to the southeast faulting on a fault plane dipping down to the northwest is seen in the focal mechanisms of later subevents in the rupture model of Pitarka et al. (1995, Figure 1). Both the Kikuchi and Pitarka rupture models indicate that the propagation of the rupture toward Kobe involved several subevents distributed along the fault at depths of 6 to 8 km. The Pitarka model has uniform strike but variations in dip and rake among three subevents (Figure 1), while the Kikuchi model has variations in strike as well as variations in rake of two subevents.

STRONG MOTION CHARACTERISTICS OF THE KOBE EARTHQUAKE

Strong ground motions were recorded by numerous organizations, including the Committee on Earthquake Observation and Research in the Kansai Area, Japan Rail, Osaka Gas, JMA, Hankyu Railroads, Japan Highways, Building Research Institute, and Port and Harbor Research Institute. The largest recorded peak accelerations were about 0.8g (Figure 2), and were recorded on alluvial sites. The vertical peak accelerations were generally about two-thirds as large as the horizontal at near-fault sites, and much lower at more distant alluvial sites.

The rupture of this strike-slip earthquake directly into downtown Kobe caused near-fault rupture directivity effects which appear to have contributed to the high level of damage. The recorded peak velocities were as large as 175 cm/sec at Takatori in western Kobe, and the largest values occurred in the densely populated urban region, as shown in Figure 3a. Currently, buildings over 60 meters in height in Japan are designed to withstand peak velocities of 50 cm/sec without collapse. The near-fault ground velocity time histories have large, brief pulses of ground motion (Figure 4) that are indicative of rupture directivity effects and are potentially damaging to multi-story buildings and other long-period structures such as bridges. The horizontal motions in the fault normal direction are about twice as large as those in the fault parallel direction, as seen in the time histories in Figure 4 and the response spectra in Figure 5. This feature, which is caused by rupture directivity effects, has been widely observed in near fault strong motion data in California (Somerville and Graves, 1993) and quantified as a modification to empirical attenuation relations by Somerville and Graves (1995).

Severe damage to buildings due to the Kobe earthquake was observed along a strip of land about 30 km long and 1 km wide, and offset about 1 km southeast of the fault. Figure 6 shows the severely damaged area, active faults, and aftershock distribution (Kohketsu, 1995). The hachured zone indicates the area where the rate of collapsed wood-frame buildings is more than 30%; this rate exceeded 70% in the central part of this area. There are few aftershocks and active faults in the severely damaged area, suggesting that the location of the severely damaged area is not explained by its proximity to the fault rupture.

In order to investigate whether these large variations in site response in the Kobe area were attributable to site effects, investigators from Ohsaki Research Institute recorded aftershocks at several sites on alluvium in the heavily damaged area as well as at rock sites on the foot of Rokko mountain in Kobe (Kawase et al, 1995). The locations of their stations are shown in Figure 7a and their study area is shown as an inset in Figure 6. They found that, for six

aftershocks, horizontal peak accelerations recorded at three sites located on a thin layer of soft alluvium (about 10 to 15 meters thick) were about 3 to 5 times larger than those at a reference site on rock, and the Fourier spectral amplitudes for frequencies between 2 and 3 Hz were as much as 20 times higher, as shown in Figure 7b.

IMPLICATIONS FOR SEISMIC HAZARDS IN CALIFORNIA

There are many parallels between the seismic hazard environment in Kobe and those that are present in urban regions in California. Figure 8 shows active faults and the surficial geology of the San Francisco Bay region. The many similarities between Kobe and the East San Francisco Bay region are illustrated by comparison of Figure 8 with Figure 6, and the comparison of geological cross sections through Kobe and Oakland shown in Figure 9. These similarities include the location of strike-slip faults along the base of the mountains; the increasing thickness of alluvial deposits from the mountains to the bay shore; and the highly urbanized areas located on soft sediments between the mountains and the shore.

The recorded peak accelerations and velocities from the Kobe earthquake are generally comparable to those predicted for a strike-slip earthquake using empirical attenuation relations for soil based mainly on California data (Abrahamson and Silva, 1995; Campbell, 1990), as shown in Figure 10. The much larger level of damage that occurred in the Kobe earthquake compared with that of recent earthquakes in California may be partly attributable to the fact that the dense urban region of Kobe was subject to strong rupture directivity effects. As shown in Figure 3a, the largest peak velocities recorded from the Kobe earthquake were in the dense urban region. Equally large peak velocities were recorded during the 1994 Northridge earthquake, as shown in Figure 3b. However, the dense urban regions of the southern San Fernando Valley and the northwest Los Angeles basin were not subject to rupture directivity effects. Almost all of the faulting occurred at depths greater than 10 km, and the great majority of the multi-story buildings in the San Fernando Valley were at least 15 km from the closest part of the fault. Rupture directivity effects were experienced only in the northern San Fernando Valley and Santa Susana Mountains, which are located away from the dense urban region.

There are many densely populated urban regions in California that are located very close to major strike-slip faults. However, California has not experienced a strike-slip earthquake that ruptured directly into a heavily populated urban region since the 1933 Long Beach earthquake, and has no experience of a strike-slip earthquake rupturing into the downtown region of a major city. We do not have data from California on the performance of structures exposed to rupture directivity effects from a strike-slip earthquake that ruptured directly into an urban region, as occurred in Kobe. However, the apparent similarity in earthquake source and strong ground motion characteristics between the Kobe earthquake and California earthquakes indicates that the performance of soils and structures in the Kobe earthquake may be very useful for predicting damage effects from an urban strike-slip earthquake in California.

Given the widespread damage that occurred in Kobe, and the apparent parallels between the strong ground motions experienced there and those that we expect in California, it is important to make loss estimates for urban strike-slip earthquakes in California based on the performance data from Kobe, and to assess whether they may greatly exceed those of the 1994

Northridge earthquake. If it is concluded that losses of Kobe proportions could occur in an urban strike-slip earthquake in California, this could have important implications for code provisions and other policy decisions concerning the reduction of earthquake damage in the United States.

REFERENCES

Kanamori, H. (1995). The Kobe (Hyogo-ken Nanbu), Japan, earthquake of January 16, 1995. Seismological Research Letters 66, 6-10.

Kawase, H., T. Satoh and S. Matsushima (1995). Aftershock measurements and a preliminary analysis of aftershock records in Higashi-Nada Ward in Kobe after the 1995 Hyogo-Ken-Nanbu earthquake, ORI Report 94-04.

Kohketsu, K. (1995). Are predominant period contents of strong-motions the major cause of severe damage by the Kobe earthquake?, Monthly Journal of Science, Kagaku Asahi, No. 652, 11-14.

Kikuchi, M., Teleseismic analysis of the Southern Hyogo (Kobe), Japan, earthquake of January 17, 1995, Yokohama City University Seismological Note #38, 1995.

Pitarka, A., K. Irikura and T. Kagawa (1995). Source complexity of the January 17, 1995 Hyogo-ken-nanbu earthquake from nearfield strong motion modeling: preliminary results. Submitted to Journal of Natural Disaster Science.

Research Group for Active Faults in Japan (1980). Maps of Active Faults in Japan with an Explanatory Text, University of Tokyo Press, Hongo, Bunkyo-ku, Tokyo 113, Japan.

Rogers, J.D. and S.H. Figuers (1991). Engineering geologic site characterization of the greater Oakland-Alameda area. Alameda and San Francisco Counties, California. Final Report to the National Science Foundation, Grant No. BCS-9003785.

Somerville, P.G. (1995a). Kobe Earthquake: an Urban Disaster. EOS 76, 49-51.

Somerville, P.G. (1995b). Kobe Earthquake : Geoscience and Strong Motion Apects, in EERI Reconnaissance Report, Chapter 1, pp. 1-10.

Somerville, P.G. and R.W. Graves (1995). Ground motion potential of the Los Angeles Region. *Proceedings of the 1995 Annual Meeting of the Los Angeles Tall Buildings Structural Design Council*, May 5.

Somerville, P.G. and R.W. Graves (1993). Conditions that give rise to unusually large long period ground motions, *The structural design of tall buildings* 2, 211-232.

Takeo, M. (1995). Rupture model of the Kobe earthquake inferred from strong motion data. Poster presented at the Annual Meeting of the Seismological Society of Japan, March 27-30, Tokyo.

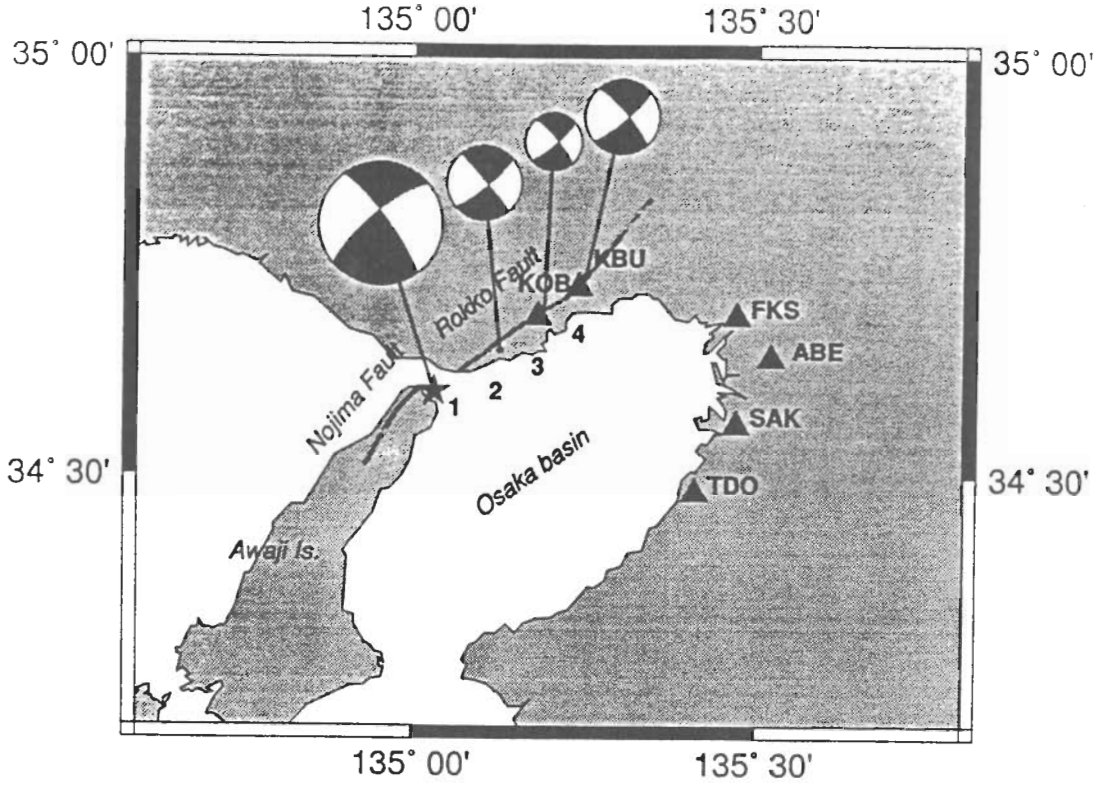

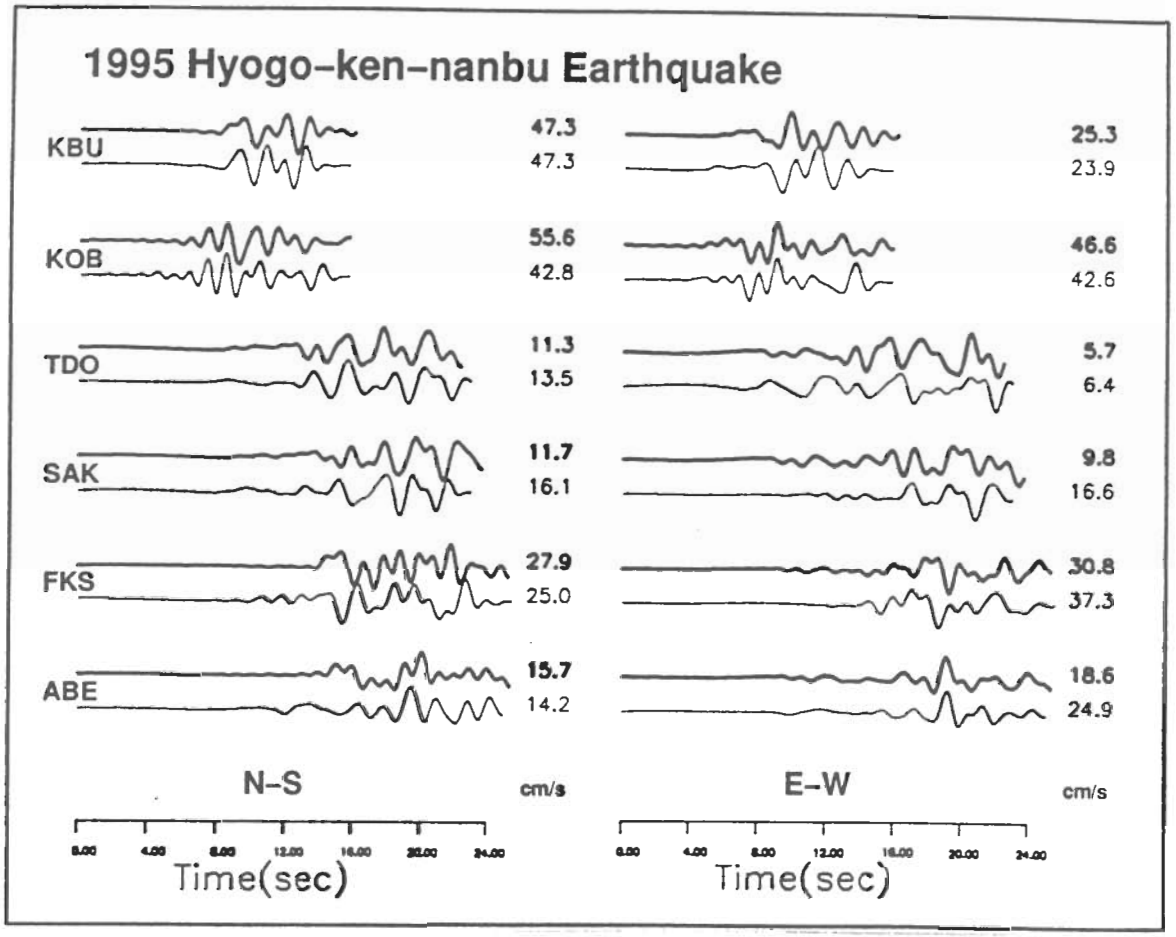

Figure 1. Focal mechanism and source process of the Kobe earthquake. The earthquake consisted of four subevents, whose locations and focal mechanisms are shown at the top. Recorded and synthetic waveforms are compared at the bottom. Source: Pitarka et al., 1995.

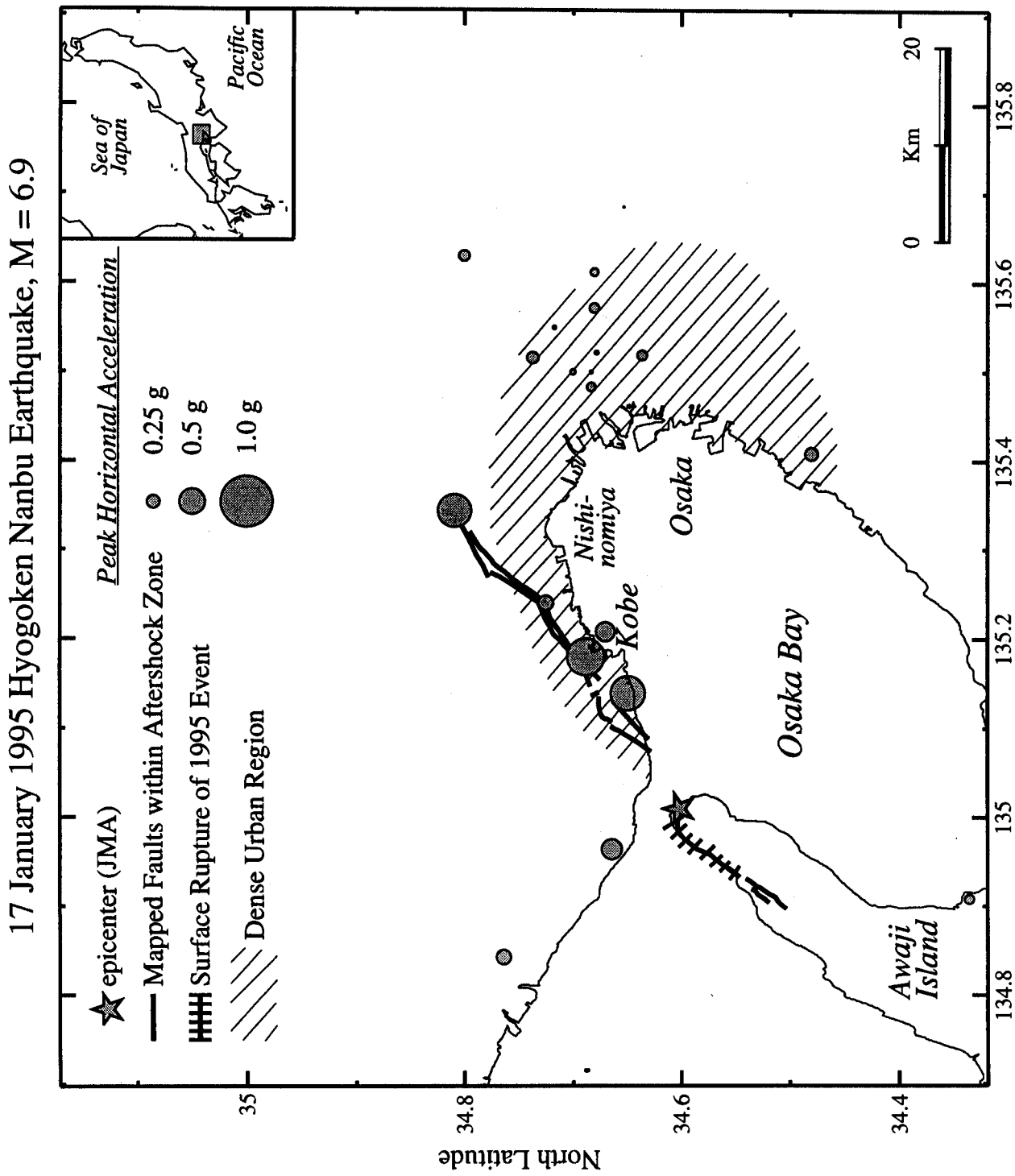

Figure 2. Location of the mainshock epicenter, mapped active faults within the aftershock zone (including surface rupture of the Nojima fault on Awaji Island), the dense urban region, and average horizontal peak accelerations recorded from the 1995 Kobe earthquake.

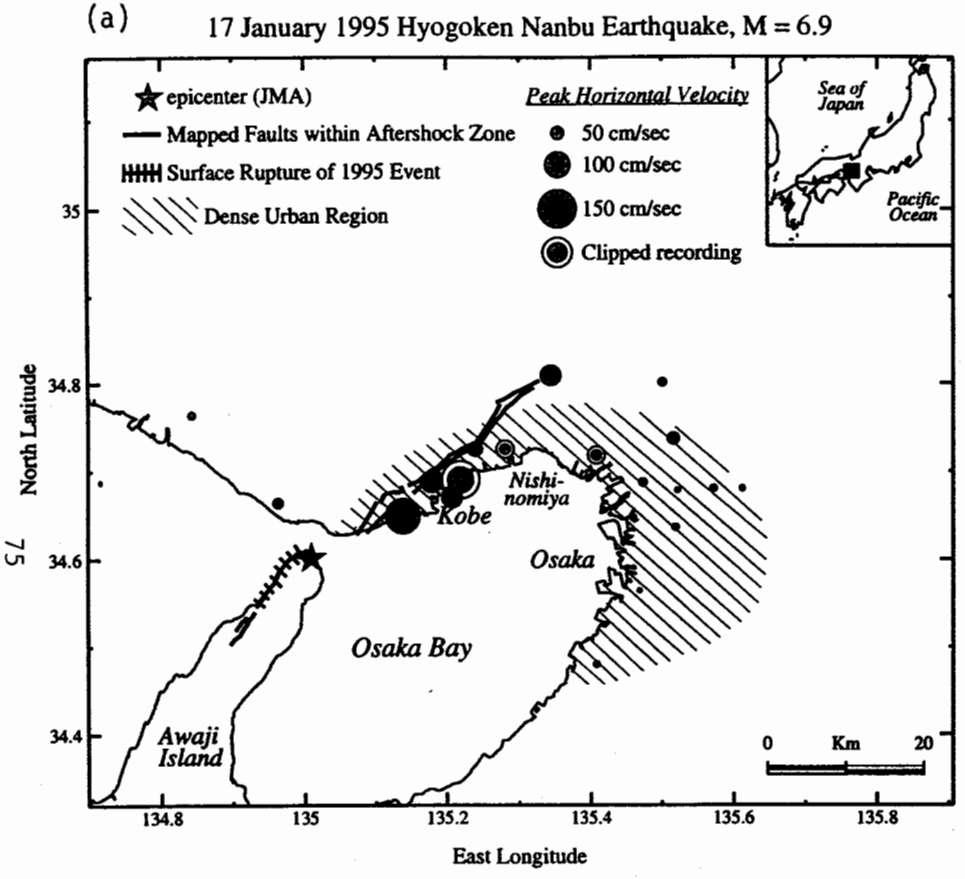

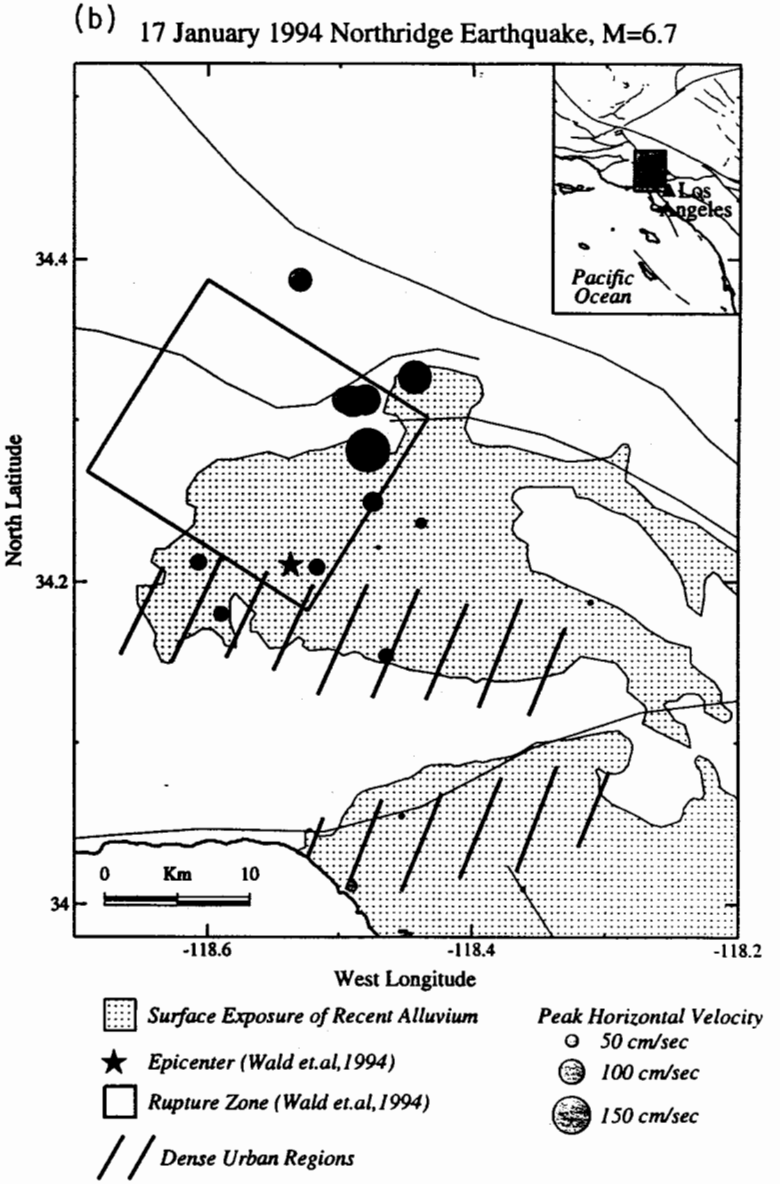

Figure 3 (a) Location of the mainshock epicenter, mapped active faults within the aftershock zone (including surface rupture of the Nojima fault on Awaji Island), the dense urban region, and average horizontal peak velocities recorded from the 1995 Kobe earthquake. (b) Location of the mainshock epicenter, surface projection of the fault rupture model of Wald and Heaton (1994), dense urban regions, and average horizontal peak ground velocities recorded from the 1994 Northridge earthquake.

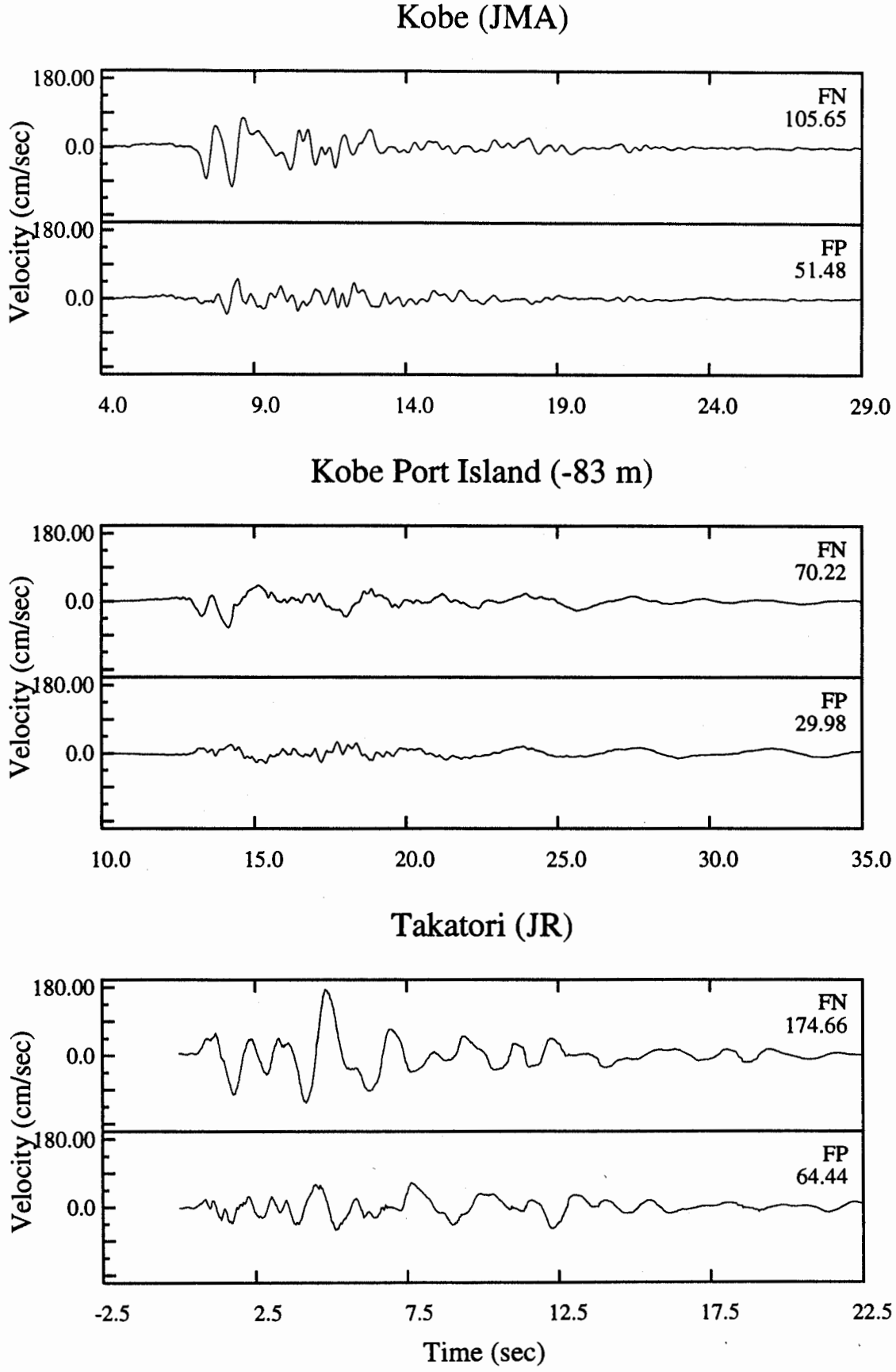

Figure 4. Recorded velocity time histories at Kobe JMA, Port Island -83 meters, and Takatori rotated into fault-normal and fault-parallel components.

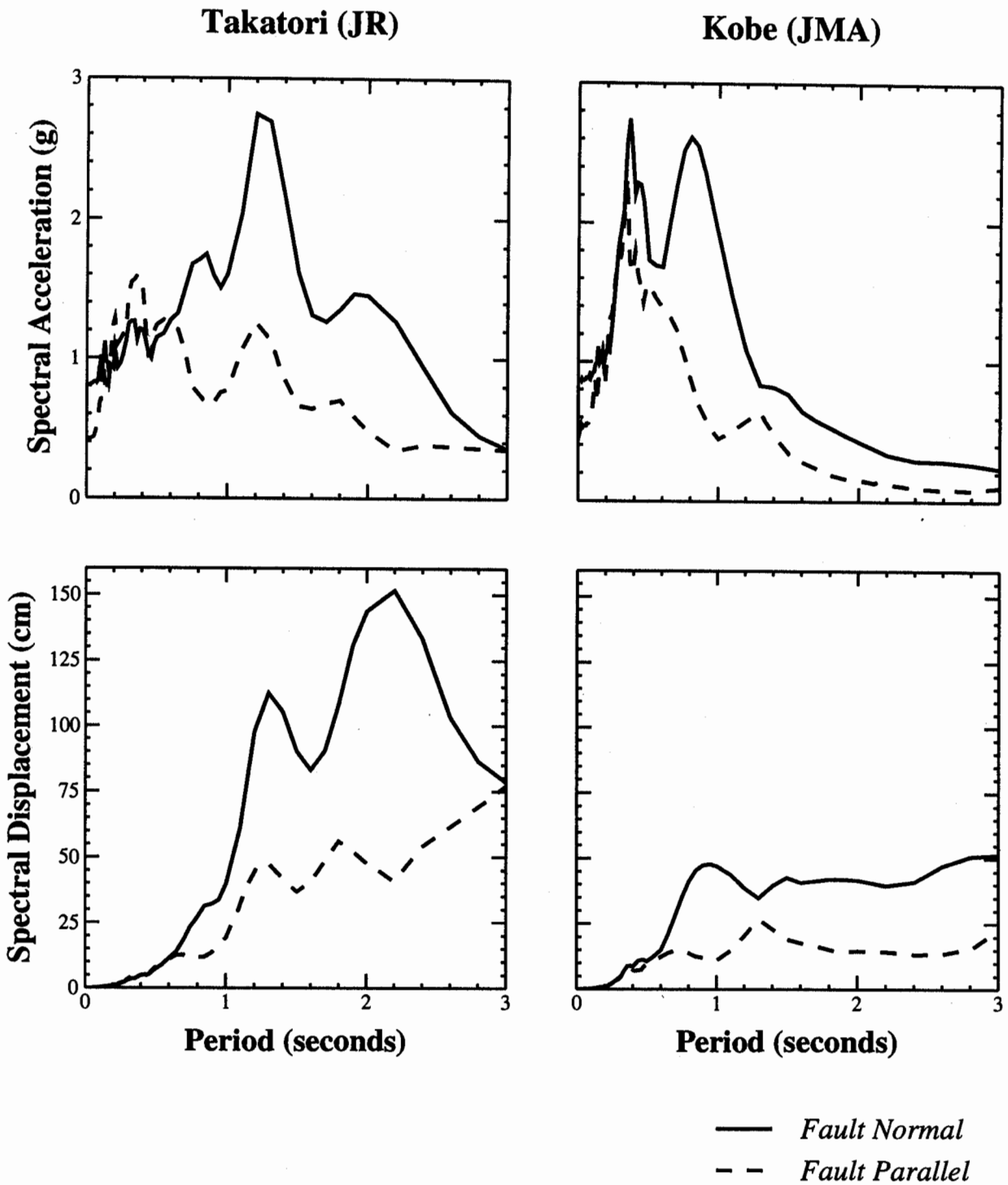

Figure 5. Response spectral acceleration (top) and displacement (bottom) of the fault-normal and fault-parallel components of the Kobe earthquake recorded at Kobe JMA and Takatori.

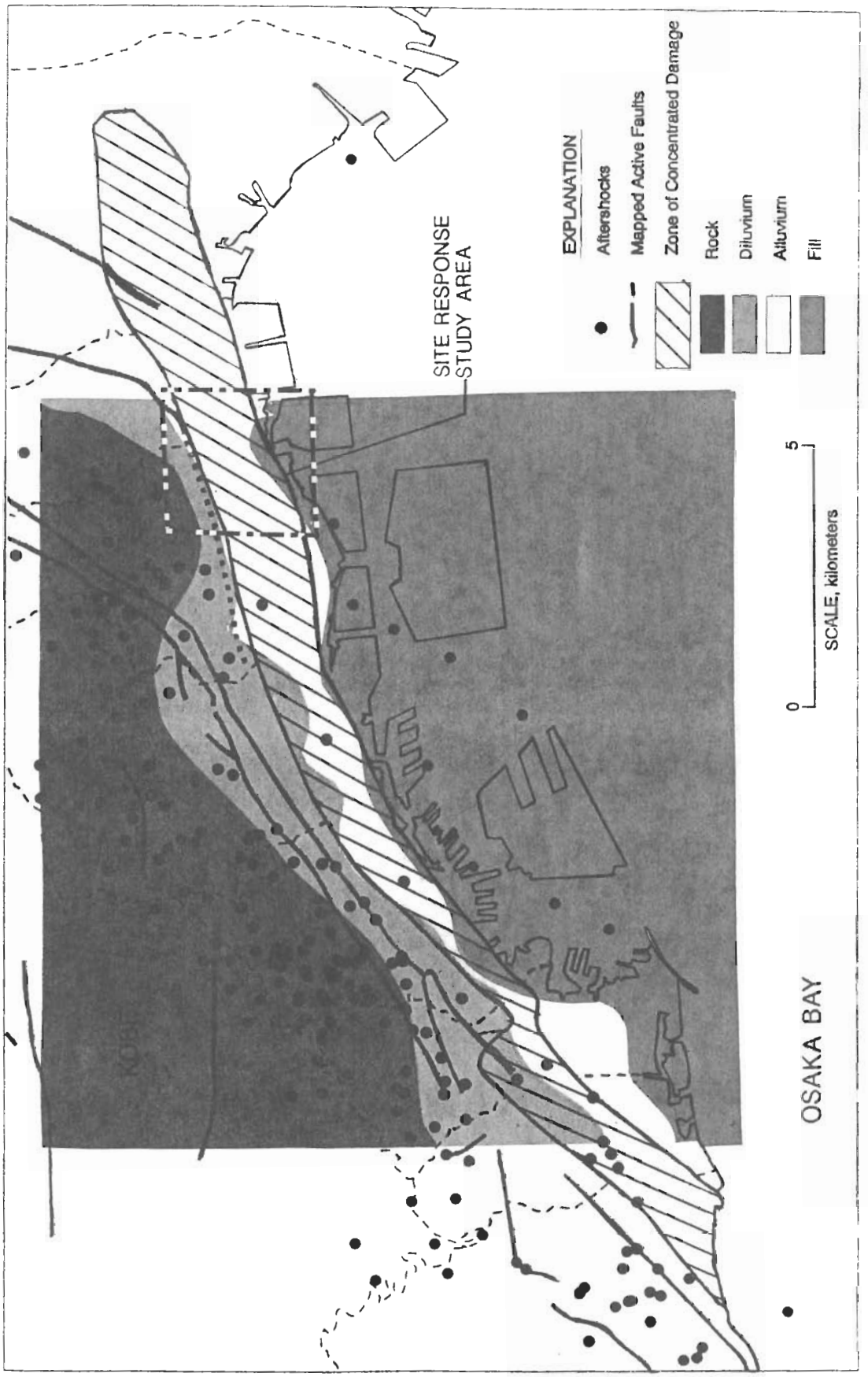

Figure 6. Location of zone of intense destruction in the Kobe area, and its relationship to the location of active faults, the aftershock distribution, and geological site conditions. Modified from Kohketsu, 1995.

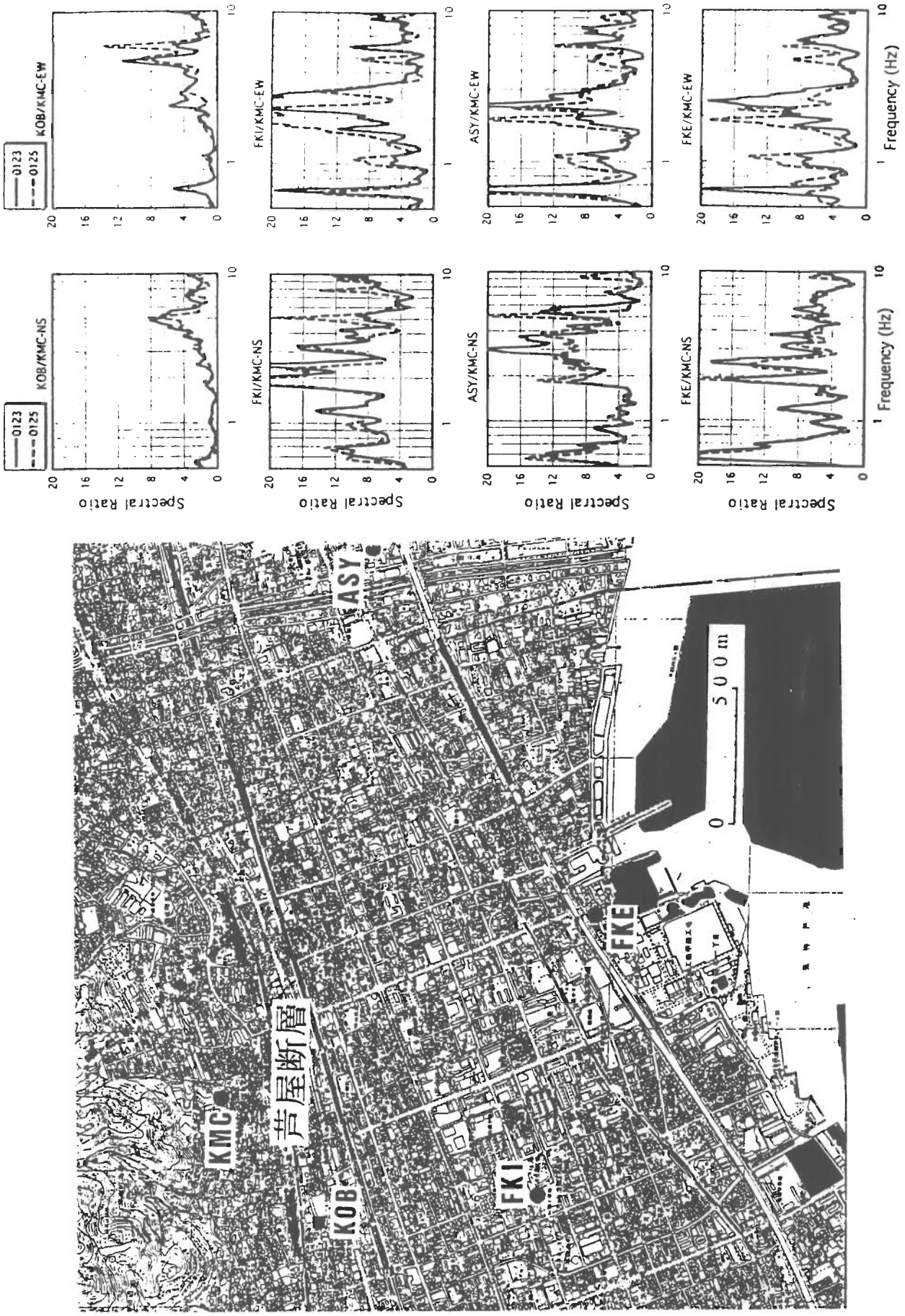

Figure 7. Left: Locations of aftershock recording sites used in the site response study conducted by Kawase et al. (1995). The location of the study area is shown in Figure 6. Right: Fourier spectral ratios for two aftershocks and referenced to rock site KMC for diluvial site KOB, alluvial sites FKI and ASY, and fill site FKE. Source: Kawase et al. (1995).

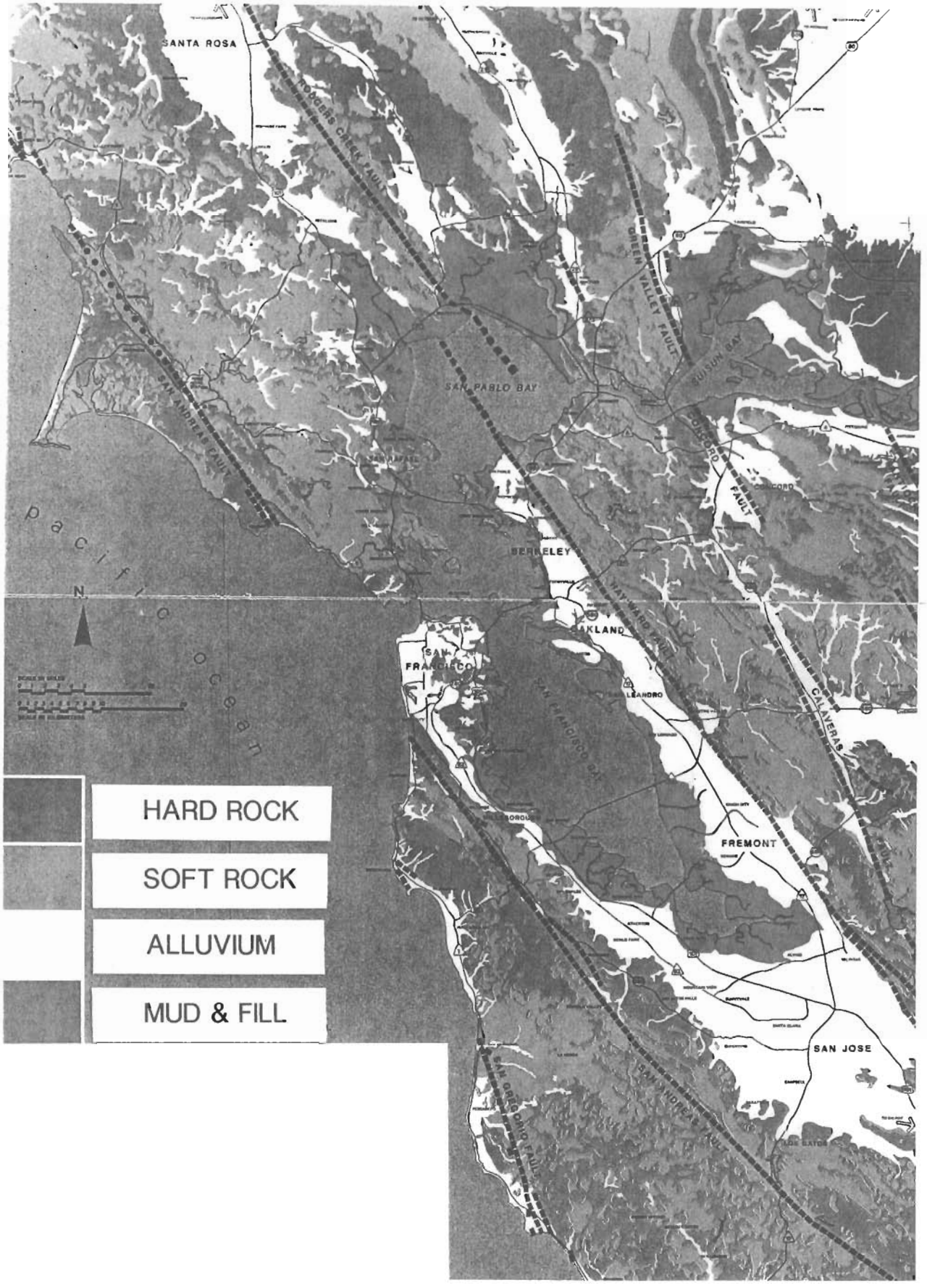

Figure 8. Map of the San Francisco Bay area showing the location of the Hayward fault and the distribution of surface geology. Source: United States Geological Survey.

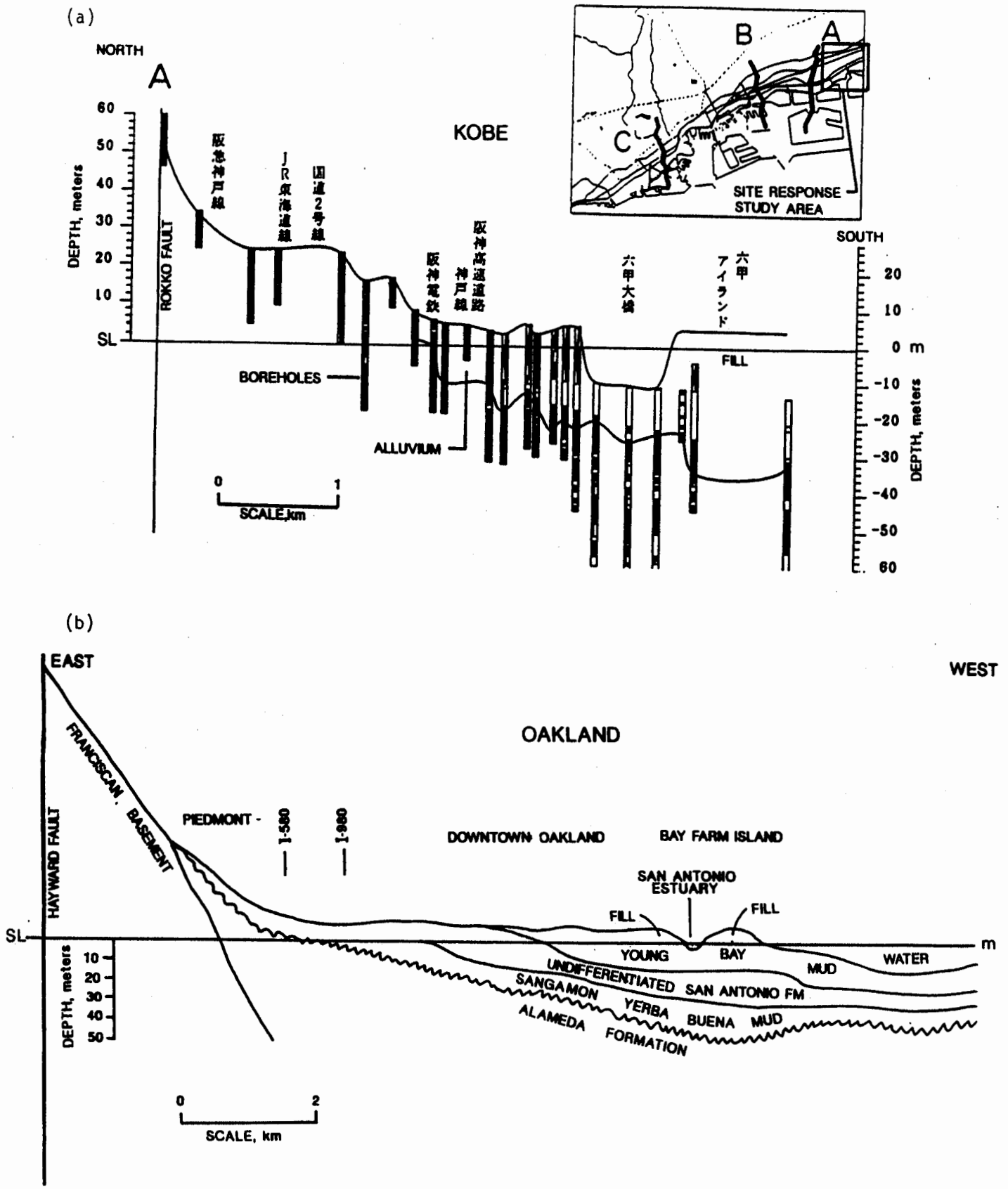

Figure 9. Profiles of shallow geological structure in Kobe (top) and Oakland (bottom; from Rogers and Figuers, 1991), with the Rokko and Hayward faults respectively on the left hand side of the profile. The inset in the Kobe profile locates the profile within the area shown in Figure 6, and also locates the site response study area shown in Figure 7. Both profiles have a vertical exaggeration of 30.

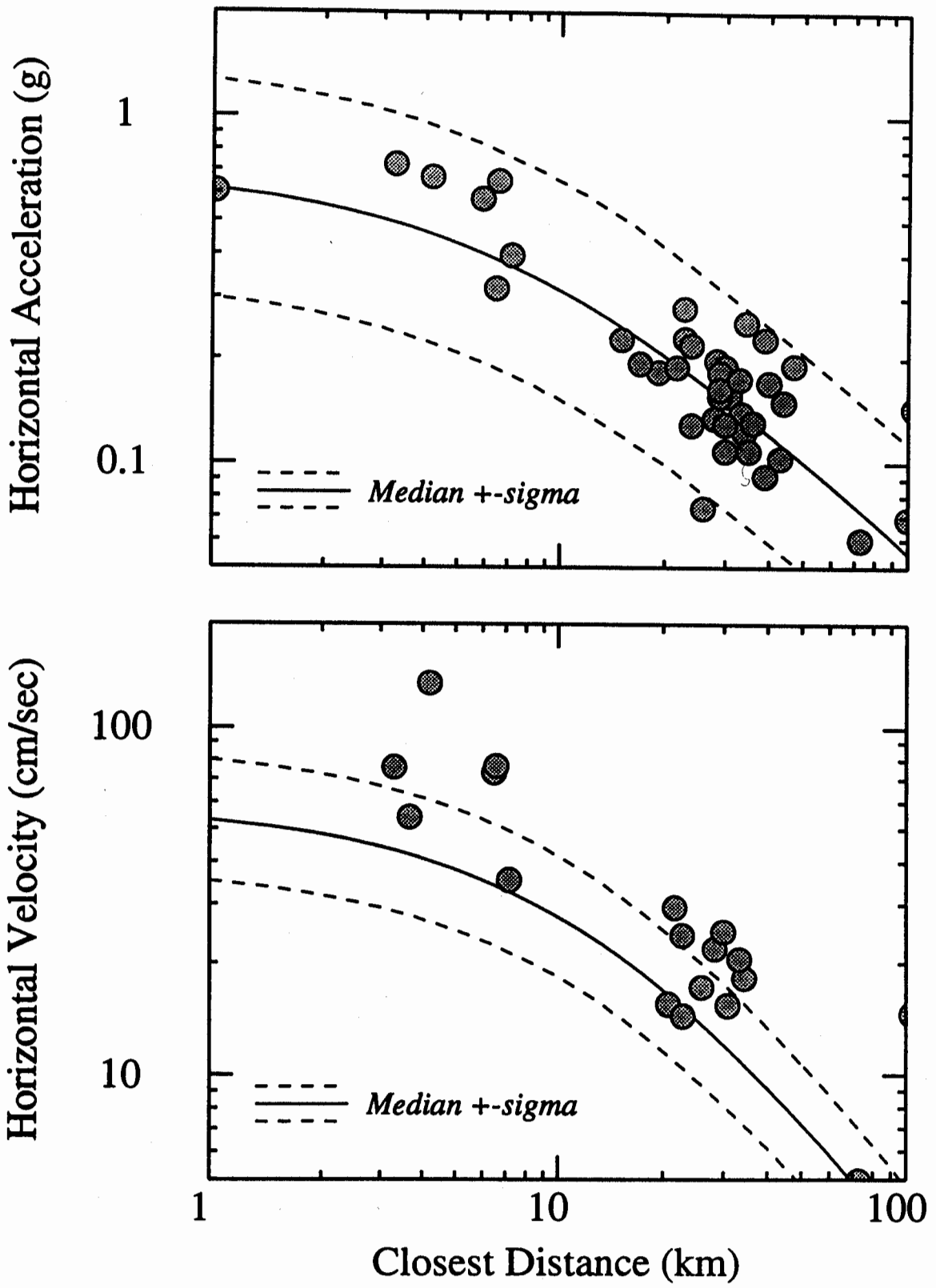

Figure 10. Attenuation of recorded peak acceleration and peak velocity at soil sites from the Kobe earthquake, compared with empirical relations for strike-slip earthquakes recorded on soil based mainly on California data (Abrahamson, 1995 for pga; Campbell, 1990 for pgv).

ASSESSMENT OF THE PERFORMANCE OF STEEL MOMENT FRAME BUILDINGS DURING THE 1994 NORTHRIDGE EARTHQUAKE: TASK 3 OF SAC STEEL PROGRAM

Presented by

James O. Malley
Degenkolb Engineers
and
SAC Project Director for Topical Investigations

INTRODUCTION

Following the January 17, 1994 Northridge earthquake, more than 100 steel buildings with welded moment-resisting frames were found to have experienced beam-to-column connection fractures. The damaged structures cover a wide range of heights ranging from one story to 26 stories; and a wide range of ages spanning from buildings as old as 30 years of age to structures just being erected at the time of the earthquake. The damaged structures are spread over a large geographical area with the highest concentration of reported damage near the epicentral region. Discovery of these extensive connection fractures, often with little associated architectural damage to the buildings, has been very alarming. The discovery has also caused some concern that similar, but undiscovered damage may have occurred in other buildings affected by past earthquakes. Indeed, there have been isolated reports of similar damage having been found in buildings following both the 1971 San Fernando and 1989 Loma Prieta earthquakes.

Welded steel moment frame construction is used commonly throughout the United States and the world, particularly for mid- and high-rise construction. Prior to the Northridge earthquake, this type of construction was considered one of the most seismic-resistant structural systems, due to the fact severe damage to such structures had rarely been reported in past earthquakes, and that only notable collapse of such a structure, the Pino Suarez failure in the 1985 Mexico City earthquake, had ever occurred. That collapse was attributed by investigators to large axial column demands, induced by overly strong bracing in this dual system structure. Subsequent editions of U.S. building codes adopted provisions specifically intended to prevent such failures, and it was presumed by many that buildings designed to these later provisions would be largely collapse resistant. However, the widespread severe structural damage which occurred to such structures calls for re-examination of this premise.

GOALS AND OBJECTIVES

The Structural Engineers Association of California (SEAOC), the Applied Technology Council (ATC) and California Universities for Research in Earthquake Engineering (CUREe) have combined their considerable resources to address and resolve questions relating to the repair, design and retrofit of steel moment frame structures. Their goal for the SAC Steel Program: Reducing Earthquake Hazards in Steel Moment Frame Structures is to:

> *Develop professional practices and recommend standards for the repair, design and retrofit of steel moment frame buildings so that they provide reliable, cost-effective seismic performance in future earthquakes.*

Three objectives must be met to achieve this goal:

1) Characterize and understand what has happened to steel moment frame buildings in the Northridge earthquake.

2) Prepare interim procedures for professional practices and standards:

   - Identify buildings that may have been damaged and require further investigation.
   - Characterize the safety condition of inspected buildings.
   - Rehabilitate damage buildings to provide life-safety.

3) Prepare recommendations for the repair, design and retrofit of buildings based on a rational understanding of seismic behavior.

The SAC Steel Program has been specifically designed to achieve this goal in a time frame consistent with the urgency of the problem. Accomplishing these objectives will require marshaling both what is known about the design and seismic performance of steel structures, and what can be learned through directed investigations and analyses to augment existing knowledge. The technical challenges to be overcome are complex and difficult.

The five thousand SEAOC members, the eight major earthquake engineering research universities of CUREe, and the national technical resources of the Applied Technology Council (ATC) are committed to mobilizing all available national and international resources to rapidly and systematically achieve these objectives. Each of these organizations has a history of distinguished achievement. Together they provide a formidable resource for solving this important problem.

APPROACH

The number and complexity of the technical problems involved, and the importance of the economic and public policy issues raised, suggest that an ad hoc, quick-fix solution is inappropriate and likely to be ineffectual. Indeed, several attempts to date to reach rapid consensus by practicing engineers and researchers have failed - the problems are just too difficult for resolution within the current state of knowledge. A more fundamental investigative approach is needed, one that addresses the full range of associated technical issues and involves the best technical talent and resources available, not only from California, but from throughout U.S.

Restoration of public and professional confidence in the safety and performance of new steel frame buildings and in our ability to evaluate and rehabilitate existing ones requires development and synthesis of knowledge necessary to answer the following simple questions:

- What happened to steel buildings during the Northridge earthquake?
- Why did it happen and can it be predicted?
- How dangerous are damaged structures?
- How can we identify seismically vulnerable structures?
- How can we fix damaged or vulnerable buildings?
- Can this type of damage be avoided in the future?

The SAC Steel Program addresses these questions and will provide answers in the form of recommended standards of practice and draft guidelines. The urgency of these questions and the need for prudent expenditure of funds dictates a short-term program of centrally managed and coordinated investigations.

Achieving the goal and objectives of the project will require a wide array of coordinated individual investigations. These are divided into four basic categories:

Category 1 Immediate investigations to characterize and understand what happened to steel moment frame buildings in the Northridge earthquake.

Category 2: Other short-term investigations and efforts to develop and peer review interim guidelines for professional practices and standards for identification, evaluation and rehabilitation.

Category 3: Near-term investigations and analyses to improve understanding of the important factors contributing tot he structural performance of steel moment frames and identification of effective and economical methods of evaluation, analysis, design and rehabilitation.

Category 4: Investigations focusing on the refinement, confirmation and assessment practices and standards for evaluation, rehabilitation and design of steel moment frame structures that are identified in Task 2 as reliable and cost-effective.

Phase 1 of the program which is currently in progress, is specifically addressing Categories 1 and 2. Categories 3 and 4 will be the focus of the second phase of the project which will commence later this year. SAC is presently attempting to obtain funding for Phase 2.

WORK PLAN

The initially formulated Work Plan includes a large number of actions. The following highlights of the draft Work Plan are given to convey the comprehensive set of actions and investigations that were initially perceived as important to achieving the stated goal:

1) The immediate focus of the work effort is on near-term needs related to inspection, evaluation and repair of steel frame buildings in Los Angeles and includes:

   - Workshop(s) to refine investigation plans and identify experts and resources interested in participating in program.
   - Detailed field surveys of steel frame buildings in the heavily shaken area.
   - Study of ground motion characteristics and influences on response.
   - Synthesis and assessment of current worldwide states of knowledge and practice.
   - Development and evaluation of interim guidelines for inspection, evaluation and repair.

2) Longer range tasks focus on professional practices and recommendation of standards for the repair, design and retrofit of steel moment frame buildings so that they provide reliable, cost-effective seismic performance. These tasks include:

   - Systematically investigate the various technical factors contributing to seismic performance of steel moment-resisting frames, including metallurgy, welding, structural and fracture mechanics, joint design and behavior, structural system behavior, nondestructive evaluation and inspection techniques.
   - Identify effective inspection procedures and nondestructive evaluation tools.

- Develop effective and practical modeling and analysis tools for evaluation of existing steel frames and for the design of new structures.

- Develop, evaluate and document professional practices and recommendations for design guidelines related to repair, evaluation and retrofit, and new construction.

- Assess the cost-effectiveness, performance expectations and practicability of resulting guidelines and practices through detailed case studies of public buildings damaged by the Northridge earthquake.

- Laboratory and field experiments, including large scale component, assemblage and structure tests, will be conducted to gather needed information on performance.

3) Implementation of the developed guidelines and standards of practice will be encouraged through frequent workshops and technical bulletins, training materials, instructional programs, and development of electronic data bases.

TASK 3 OF THE SAC STEEL PROGRAM

Detailed Assessment of the Performance of Selected Buildings

Detailed investigations and analyses (and material and field tests) are being performed on selected buildings to identify the specific causes of failures, to assess the accuracy of available analytical methods, and to identify the conditions under which more severe, life- threatening damage might occur. This activity is building upon previous efforts undertaken by inspectors and engineers following the Northridge earthquake, but is more detailed and focused. Schematic investigations are quantitatively assessing the ability of different types of modeling and analysis procedures to predict dynamic characteristics, and the global and local damage in the building. Also, studies are being undertaken to assess the possible response of the structures considered during hypothetical aftershocks, or other types of future earthquakes to identify conditions that might lead to more severe damage and threaten life-safety. These activities directly support concurrent efforts to develop effective Interim Guidelines and suggest topics for subsequent investigation related to modeling and analysis methods, evaluations procedures, analysis methods, system response and so on.

The overall goals of Task 3 are to:

1) identify the specific causes of failure of selected public and private steel frame buildings;

2) assess the accuracy of available analytical methods to identify seismic hazards and failure modes;

3) identify the conditions under which more severe, life threatening damage might occur; and

4) gather information supporting the development of interim guidelines and standards of practice related to inspection, evaluation, rehabilitation of existing buildings and design of new structures.

This task consists of several inter-related elements:

1) Detailed analytical and experimental investigations of specific buildings identifying the reasons for the observed performance, the adequacy of current analytical procedures and modeling assumptions, and implications for inspection, evaluation, rehabilitation, design and construction practices. (Sub-Tasks 3.1 and 3.2)

2) Detailed histories and an evaluation of the inspection, evaluation, design, and construction process utilized in one or more buildings. (Sub-Task 3.3)

3) A preliminary assessment of the effect of weld and joint fractures on dynamic response and seismic safety. Simple analytical models capable of simulating brittle failures are being developed. (Sub-Task 3.4)

4) Preliminary sensitivity studies will be documented and interpreted to assess the importance of:

   (a) ground motion characteristics (vertical accelerations, near fault effects, bi-directional motions) and structural characteristics (period, irregularity, etc.) on structural performance and

   (b) the effect of hypothetical aftershocks, or other types of future earthquakes to identify conditions that might lead to more severe damage and threaten life-safety. (Sub-Task 3.5)

5) Areas of uncertainty and needed future investigations will be identified.

This paper will address the efforts related to Sub-Task 3.1.

Sub-Task 3.1: **Detailed Investigations of Particular Buildings**

Detailed investigations and analyses of particular buildings are being carried out to develop an understanding of the reasons for the observed damages and the adequacy of various types of models and analysis procedures to predict the severity and distribution of this damage, both globally and locally. In addition, specific analyses are being carried out to identify the conditions under which more severe, life threatening damage might occur.

A solicitation for proposals to perform these detailed analyses was circulated during December 1994. Over thirty proposals were received for this sub-task, which included more than twenty buildings of interest. The following criteria were used in the selection of buildings to be analyzed in this study:

1) Access to detailed information related to a steel moment frame building which had been severely shaken by the Northridge earthquake, and permission of the owner to participate in this investigation.

2) Strong-motion instrumentation within the building, or very near the structure.

3) A distribution of building height among the selected buildings was desired (low, medium and high-rise, e.g.).

4) A geographic distribution among the selected buildings was desired (San Fernando valley, Santa Monica/West Los Angeles, Santa Clarita, e.g.).

5) Different amounts and types of structural and nonstructural damage suffered by the group of selected buildings were desired.

6) Demonstrated capability of the proposer in elastic and inelastic analyses of steel moment frame buildings and familiarity with design of such structures.

7) Collaboration of practicing engineers and academic researchers.

A total of eight Subcontractors were selected, and nine buildings were included in this study. Included within these nine buildings were structures which addressed a wide variety of parameters and issues, including the following:

1) The buildings ranged in height from 2 to 22 stories.

2) The complexity of the different buildings ranged from simple, rectangular plans without any irregularities to irregular, complex configurations which included participation by other structural elements (masonry walls, e.g.) at lower levels.

3) The majority of the buildings were located in the San Fernando Valley. Buildings located in West Los Angeles and Santa Monica were also analyzed.

4) Damage to the different buildings ranged from severe to none at all.

5) Varying amounts of frame redundancy were incorporated into different buildings.

6) Two buildings on the same site with very different levels were analyzed by two of the subcontractors; one at the Cal State Northridge Campus, and the other at a Woodland Hills medical center.

7) Two independent analyses of one building were performed.

8) One building in the survey was structurally complete, but the interior nonstructural elements and finishes were not in place, effectively reducing the building mass and damping.

9) Three of the buildings have strong motion instruments. One only had a basement instrument. One only had a roof instrument. The third had a series of instruments over the height of the building.

Analysis Guidelines

The general capabilities of the four different analytical procedures are intended to be assessed as to their ability to predict damage states and susceptibility to increased aftershock damage. These four procedures include the following:

1) Equivalent static elastic methods

2) Elastic dynamic analysis methods, both response spectrum and time history

3) Static nonlinear analyses ("push-over")

4) Nonlinear dynamic analysis methods

To insure compatibility of the results obtained by different investigators and to provide a direct means of comparing between different buildings within this sub-Task, a standard set of modeling and analysis standards and a common set of ground motion characteristics (response and time histories) were established for use by all of the Subcontractors. These so-called "baseline" analysis procedures were intended to represent simple analytical approaches which would be commonly used in standard building design (centerline frame dimensions, simple foundation models, no slab or non-frame column participation in lateral resistance, etc.). Baseline assumptions were provided for both the elastic and inelastic analyses. The response spectrum specified was an equal hazard spectrum for the Northern San Fernando Valley, with a recurrence interval of 475 years. Baseline time histories included the following: 1940 El Centro, 1978 Tabas Iran, 1994 Northridge Sylmar County Hospital Record, and the 1994 Canoga Park Record. These records were selected for purposes of comparison to previous standard records (El Centro), representative records from the 1994 Northridge earthquake (Sylmar County Hospital and Canoga Park), and a larger near field event which includes a long duration pulse.

In addition to the baseline analyses, the investigators were encouraged to modify their analytical models to represent more accurate representations of the actual structural systems of the building. These improvements took the form of including the participation of panel zones, composite floor slabs, non-frame columns, foundation flexibility, varying levels of damping, etc. The performance of the enhanced analytical models could then be compared with that of the baseline results. In addition, a simple fracture element was developed as part of Sub-Task 3.4 for use in the nonlinear analyses.

A suite of simulated time histories were developed for each of the building sites in this Sub-Task which did not have strong motion instruments. These were prepared as a portion of the work in Task 4 of the SAC Steel program. The suite of time histories included nine records for each site. These time histories were developed to provide a mechanism for estimating the demands to which these buildings were subjected as closely as possible.

Various analytical results were collected and evaluated as indicators of damage. For the elastic analyses, these results included the roof displacement ratio, interstory drift ratios, Demand/Capacity ratios (DCR's) for the various members of the frames, etc. For the inelastic analyses, the roof displacement ratio, interstory drift ratios, and inelastic joint and member demands were evaluated. In addition, various investigators attempted to develop other methods for assessing the results.

Preliminary Assessment of Results

At present, the draft reports for these analyses have been completed and final revisions are being made. While complete analysis of all the data generated by these studies is not yet complete, some preliminary assessments have been performed which have resulted in a number of general observations which will be of use in the development of interim guidelines. Note that these observations were obtained from a review of all of the reports; they should by no means be considered universal, but rather to reflect the preliminary results of this somewhat brief, limited study. A complete analysis of the data and summary report will be developed over the following months, and will be made available with the individual final reports.

The following general trends were identified in these analyses:

1) All of the analytical procedures were able in at least a limited fashion to provide an indication of the location of connection damage. That is, analytical indicators could be identified in all cases which were better than random sampling for damaged joint inspection.

2) None of the procedures or indicators evaluated were very reliable in predicting specific locations for joint damage. Correlation between joint demand indicators and damage was better if incipient root cracks which were likely present prior to the earthquake were removed from the sample.

3) Joint indicators such as DCR or inelastic rotation demand appear to be somewhat more reliable in predicting damage than more global indices such as interstory drift. The postulation of absolute values for DCRs in relation to damage was not possible with the data available.

4) Inelastic analyses tend to provide better reliability than elastic analyses in identifying damage patterns. Examples to the contrary were also found in this sample.

5) In taller buildings, higher mode effects appear to have been the cause of a concentration of damage in the upper stories. Push-over analyses can not identify these effects.

6) Enhanced analytical procedures beyond the simple baseline assumptions led to improved correlation of damage location and type. Global factors such as interstory drift were not materially affected, but local response predictors were modified. The degree of improvement varied greatly from case to case. Three dimensional effects showed a pronounced improvement for buildings which were susceptible to torsional motions.

7) The ground motions generated by the Northridge Earthquake did not generate large interstory drifts, DCRs or inelastic joint rotation demands on the moment frame buildings in this study (maximum drifts on the order of 1.5% or less, DCR with a maximum of 2.5, and joint rotations up to 0.02). Other ground motions considered in the study generated much larger joint demand values and expected interstory drifts.

8) Because of time and budgetary constraints, post-fracture analyses were not completed.

Areas of Needed Future Work

These preliminary observations indicate the need for expanded future efforts with more detailed analytical study and development of procedures and methods which can increase the accuracy of our ability to predict the response and performance of steel moment resisting frames to severe earthquake ground motion. The participation of fracture mechanics concepts in the causes of the connection damage must be better understood, and means to incorporate it into analytical approaches should be developed. Further development of more detailed models of actual buildings should be carried out and compared to building damage. Procedures which can appropriately consider fractured joints must be developed to provide an analytical basis for estimating the reliability of existing steel moment resisting frame structures to provide life safety protection in the event of a future, larger event. Sensitivity studies for various parameters such as ground motions, joint modeling, building configuration, frame redundancy, connection details, etc., should be performed to evaluate design and rehabilitation procedures and building code standards.

Dynamic Analysis of a 13-Story Steel Frame Building Instrumented and Damaged in the 1994 Northridge Earthquake

Chia-Ming Uang [1], Qi-song Yu[1], Ali Sadre [2], David Bonowitz[3], and Nabih Youssef [3]

ABSTRACT

This case study is for an instumented thirteen-story steel moment frame (SMF) building located near the epicenter, which sustained damage to its welded connections during the 1994 Northridge earthquake. The building, which was instrumented on three floors, had been surveyed and data was collected on the fractured joints. One objective of this study was to verify the accuracy of present analytical tools in predicting the extent and severity of connection failures. Elastic time-history analysis showed good correlation with the measured response in E-W direction. In the other direction with strong ground shaking, panel zones had to be modeled in the inelastic time-history analysis in order to achieve good correlation. The inelastic analysis indicated that panel zones must have been a major source of energy dissipation during the Northridge earthquake. From this study, it appears that current analytical tools for both elastic and inelastic analyses can be instrumental in predicting the intensity and pattern of the expected damage during severe seismic events.

INTRODUCTION

The 1994 Northridge event has afforded an opportunity to investigate issues like: near-field effects and cumulative damage; impact from the vertical component of the ground motion; significance of the higher modes and building irregularities; importance of redundancy, overstrength and its relation to rotation ductility demands; influence of slabs and panel zone flexibility; adequacy of available analytical or modeling tools and related design assumptions to accurately predict the extent and location of the observed damage in buildings. The main objective of this paper is to establish the adequacy of current modeling techniques to predict the pattern and the extent of the connection damage observed after the Northridge Earthquake.

BUILDING DESCRIPTION AND AVAILABLE DATA

Building Location and Sturctural System: The case study is for a thirteen-story SMF office building in the San Fernando Valley, built under the 1973 UBC. Lateral stiffness and resistance are provided by SMFs on the perimeter. Figure 1 shows the elevation indicating typical frame member sizes and the story heights. The building is square shaped in plan and box columns are used at the corners. The typical floor and roof system is composite slab. A uniformly distributed dead load of 72.5 psf with 20 psf curtain wall weight was used for reactive mass calculations.

[1] University of California, San Diego
[2] Esgil Corporation, San Diego
[3] Nabih Youssef & Associates, Los Angeles

Observed Damage: Damage pattern to the west side frame of the building is summarized in Figure 1. Joint fractures on this side were more prevalent than the other three sides (Uang et al. 1995). Definition of various damage patterns is depicted in Figure 2. Figure 1 illustrates that the damaged connections were essentially classified as types C_5, G_3, W_1, and W_4. A controversial type of damage, W_1 signifies a crack at the root of the weld, detectable by ultrasonic testing (UT). It is considered a rejectable planar discontinuity of class B or C, per American Welding Society Standards D1.1 (AWS 1994). This type of crack is ordinarily visible once the backing bar is removed. Some speculate that W_1 cracks may easily be misread or could have existed before the earthquake.

Strong Motion Records: Strong motion recording instruments are located on the basement level, the sixth floor, and the twelfth floor. See Figure 3 for recorded accelerations provided by CDMG (Darragh et al. 1994). The peak horizontal accelerations at the basement were 0.41g and 0.32g in the N-S and E-W directions, respectively.

ELASTIC ANALYSES

Objectives: The main objectives of conducting elastic time-history analyses were (1) to correlate the structure's predicted and recorded responses, (2) to compute demand/capacity ratios (DCRs) of beams and columns and correlate with observed damage, and (3) to compute response envelopes for lateral displacements and maximum story drift ratios.

Modeling Assumptions: The following assumptions were made based on the SAC benchmark guidelines: bare steel frame with centerline dimensions and no accidental torsion; use expected yield stress (F_y= 47 ksi) to compute member strength; use LRFD (1994) with ϕ = 1 for calculating DCRs; use 1.0D + 0.5L + 1.0E load case; consider orthogonal effects per 1991 UBC; and consider P-Δ effects.

Input Ground Motions: The basement record, i.e., the Oxnard record, was used as the input motion for both elastic and inelastic time-history correlations. Furthermore, the Sylmar (i.e., Olive View Hospital) record with a peak ground acceleration of 0.84g was also used to predict deformation demand of the structure.

Elastic Time-History Correlation: Translational natural periods were computed from a 3-D model, by SAP90 (Wilson and Habibullah 1992), to be 2.9, 1.0, and 0.6 seconds in the first three modes. Figure 4 indicates that elastic analysis correlates well with the measured response in the E-W direction, but not so well in the N-S direction due to more severe shaking in this direction. The DCRs were also computed. Figure 5 shows the maximum DCR in the N-S frame beams as 1.24, double that in the E-W direction. Beams with higher DCRs are located between levels 2 and 6, correlating reasonably well with the observed damage on the west side frame in Figure 1.

Interpretation of Damage Data Based on DCRs: Some standardizations are made to establish statictical correlations with other buildings with similar plots (Youssef et al. 1995). The elastic beam DCRs are normalized by the maximum building DCR and labeled as NRDCR (see Figure 6). Observe that the maximum beam DCR is 1.24, the mean DCR is 0.64 with a standard

deviation of 0.32, and the normalized average of 0.64/1.24=0.52. The connections are generally categorized for the bottom girder-flange damage (BG). Thus "BGC" damage indicates fracture in BG, or in adjacent column flange (BC). Similarly, "BGCW" connections have BGC damage, or bottom weld fracture (BW). Finally, "$BGCWW_1$" damage includes the above and root cracks at the bottom weld.

Damage Distribution and DCRs: Out of 551 total inspected connections, 22 were found to have BGC damage, 12 had BW damage (thus, BGCW=34), and 20 had BW_1 cracks, which results in $BGCWW_1$=54 (see Figure 6a). Clearly, most of the serious BGC damage is in connections with high DCRs. While this does not necessarily mean that high stresses caused fracture, i.e., fractures not simulated by the elastic model may have occurred at low stresses, it does suggest a useful relationship between the analytical demand and the observed damage.

Cummulative Damage by DCRs: Cumulative distribution of damage subsets by NRDCR are depicted in terms of fractions in Figure 6b. Here 1.00 represents 551 total connections, 22 BGC, 34 BGCW, or 54 $BGCWW_1$ in respective categories. If damage was not related to DCR, one would expect the curve for any reasonably sized subset of connections to follow the curve of "All" connections. The steep slope of the BGC curve, at the right end, strongly suggests that this critical damage is closely tied to DCR. Further, when BW and BW_1 damage are added, the subset curves approach the "All" curve, suggesting that root cracks are less related to DCR.

Damage Distribution Ratios: The ratio of damaged connections to total connections for each group are shown in Figure 6c with DCR larger than those plotted on the abscissa. For example, the BGC ratio at DCR=0.7 is about 0.1, i.e., 10% of all connections with DCR $\geq$ 0.7 have BGC damage. While the $BGCWW_1$ ratio doubles as DCR increases from zero to 1.0, the BGC ratio increases from 4% to 20%. If BW_1 and BGCW fractures were not related, one would find at least some root cracks in each DCR group. However, no BW_1 damage is found among the 108 connections with DCR $\geq$ 0.9. This suggests that original defects in connections became fractures during the earthquake. Also the overall BW_1 ratio is only about 4%, much lower than 20% BGCW for high DCRs, suggesting that poor initial quality alone is not sufficient to cause damage even under high stresses. The patterns of damage seem to be both *quality-based* and *demand-based;* the question is how are the two linked.

Response Envelopes: Time-history analyses were conducted to obtain the envelopes of both story drift ratios and lateral displacements. In the N-S direction, the Oxnard record produces a roof drift ratio of 1.1% with a story drift ratio as high as 1.7%. The Sylmar record produces a roof drift ratio of 2.0% and a story drift ratio of 2.7% (see Figure 7).

Observations: For the N-S component of the Oxnard record, floor levels 2 through 7 with story drift ratios larger than 1.3% correspond to DCRs $\geq$ 1.0 and correlate reasonably well with the observed damage in the N-S frame. Thus, it appears that both story drfit ratios and DCRs are reliable indicators of the damage pattern.

INELASTIC ANALYSES

Objectives: The main objectives of conducting inelastic time-history analyses were to (1) correlate the recorded and predicted responses, (2) to predict stroy drifts, plastic rotation demands in beams, columns, and panel zones, and (3) to correlate predicted response with observed damage.

Modeling Assumptions: The DRAIN-2DX (Prakash et al. 1993) computer program was used. Beams and columns with rigid offsets were modeled by Element 2, while semi-rigid Element 4 was used to model panel zones (Krawinkler 1978). Rayleigh damping with a 5% damping factor was assigned to the first and third modes and a 2% strain hardening ratio was assumed for beams.

Inelastic Time-History Correlation: With the basement record of the building as the input motion, the predicted lateral displacements are compared with the recorded displacements (see Figure 8).

In the E-W direction, a comparison of Figures 8a and 4a (elastic analysis) indicates a slight improvement in the correlation. In the N-S direction — a direction of strong shaking and significant damage — a comparison of Figures 8b and 4b shows a very dramatic improvement in the correlation with a much closer matching in amplitude and phase. The plastic rotation demand for the N-S component of the Oxnard record is depicted in Figure 9a; note that most of the yielding is concentrated in the panel zones. The maximum plastic rotations in the panel zones and beams are 0.013 and 0.006 radians, respectively.

It appears from this dynamic analysis that panel zones must have played a very important role in dissipating energy during the 1994 Northridge earthquake, although shear yielding with the magnitue of plastic rotation demand shown in Figure 9a is difficult to detect visually in the field. To test this hypothesis, a separate inelastic time-history analysis was conducted without modeling the panel zones, which worsened the correlation between the predicted and recorded response (see Figure 10).

Story Drift Ratios and Plastic Rotation Demand: Figure 11 shows the envelopes of lateral displacements and story drift ratios for both the Oxnard and Sylmar records. The maximum story drift ratios produced by the Oxnard and Sylmar records were about 1.6% and 2% while the roof drift ratios were around 0.75% and 1.1%, respectively. The maximum panel zone plastic rotation is 0.013 radians for the Oxnard record (see Figure 9a) and is 0.015 radians for the Sylmar record (see Figure 12a).

CONCLUSIONS

Based on the results of time-history analyses, recorded building response, and observed joint damage, the following conclusions can be drawn.

Elastic Analyses: The SAP90 elastic analyses, which considered the center-line dimension bare steel frames in the perimeter of the building, resulted in the following conclusions.

(1) The elastic response correlated very well with the measured building response in the E-W direction. The intensity of the basement motion in the N-S direction was about 50% higher

than that in the E-W direction. Since the elastic model could not simulate the yielding and damage of moment connections, the elastic time-history correlation was poor in the N-S direction.

(2) Demand/capacity ratios (DCRs) computed from the elastic model provided a reasonable correlation to the observed damage. Field inspections and survey data indicated generally a higher incidence of welded connection failure in the N-S direction as oppose to the E-W direction. The maximum DCRs were 1.24 and 0.63 in the N-S and E-W directions, respectively.

(3) Frame members with higher DCRs were concentrated between floor levels 2 and 6, which correlated reasonably well with the observed damage to the west side frame in the N-S direction.

(4) The Sylmar record has much higher damage potential to the building frame. The maximum DCR was about 2, the maximum roof drift ratio was nearly 2.0%, and the maximum story drift ratio was around 2.7%.

Inelastic Analyses: The mathematical model for the DRAIN-2DX inelastic analyses incorporated panel zone elements. The following conclusions can be made.

(1) The DRAIN-2DX time-history analysis drastically improved the correlation in the N-S direction. For the type of regular building investigated in this study, DRAIN-2DX or similar computer programs is a very useful tool to predict the seismic damage and deformation demand of steel moment frames.

(2) The time-history correlation study indicated that most of the inelastic actions were concentrated in the panel zones, not beams. It implies that panel zones must have played an important role to dissipate earthquake input energy during the Northridge earthquake.

(3) The maximum story drift ratio and plastic rotation that developed during the Northridge earthquake were estimated to be 1.6% and 0.013 radians, respectively. The sylmar record would produce a stroy drift ratio of 2% and a plasitc rotation of 0.015 radians.

ACKNOWLEDGEMENTS

This report was made possible by a grant through the SAC Joint Venture, which is a cooperative effort between the Structural Engineers Association of California (SEAOC), Applied Technology Council (ATC) and California State Universities for Research in Earthquake Engineering (CUREe). Also thanks to Dr. Huang with the Office of Strong Motion Studies, Division of Mines and Geology, Department of Conservation for providing the processed records.

REFERENCES

1. AISC, *Load and resistance factor design (LRFD)*, Amer. Inst. of Steel Constr., Chicago, Ill., 1994.
2. AWS, "Structural welding code - steel," *ANSI/AWS D1.1 - 94*, AWS, Miami,FL., 1994.
3. Krawinkler, H., "Shear in beam-column joints in seismic design of steel frames," *Engrg.J.* vol. 15, no. 3, 1978.
4. Prakash, V., Powell, G.H., and Filippou, F.C., "DRAIN-2DX," *User Guide*, U. C. Berkeley, Ca., 1993.
5. Uang, C.-M., Yu, Q.-S., Sadre, A., Bonowitz, D., and N. Youssef, "Performance of a 13-story steel moment-resisting frame damaged in the 1994 Northridge earthquake," Report No. SSRP-95/04, Univ. Of Calif., San Diego, La Jolla, CA, 1994.
6. *Uniform Building Code (UBC)*, Int. Conf. of Bldg. Officials, Whittier, Calif., 1991.
7. Wilson, E. L. and Habibullah, A., *SAP90 - Structural analysis users manual*, CSI, Berkeley, CA, 1992
8. Youssef, N. F. G., Bonowitz, D., and Gross, J. L., "A survey of steel moment-resisting frame buildings affected by the 1994 Northridge earthquake," *Report No. NISTIR 5625*, NIST, Gaithersburg, MD, 1995.

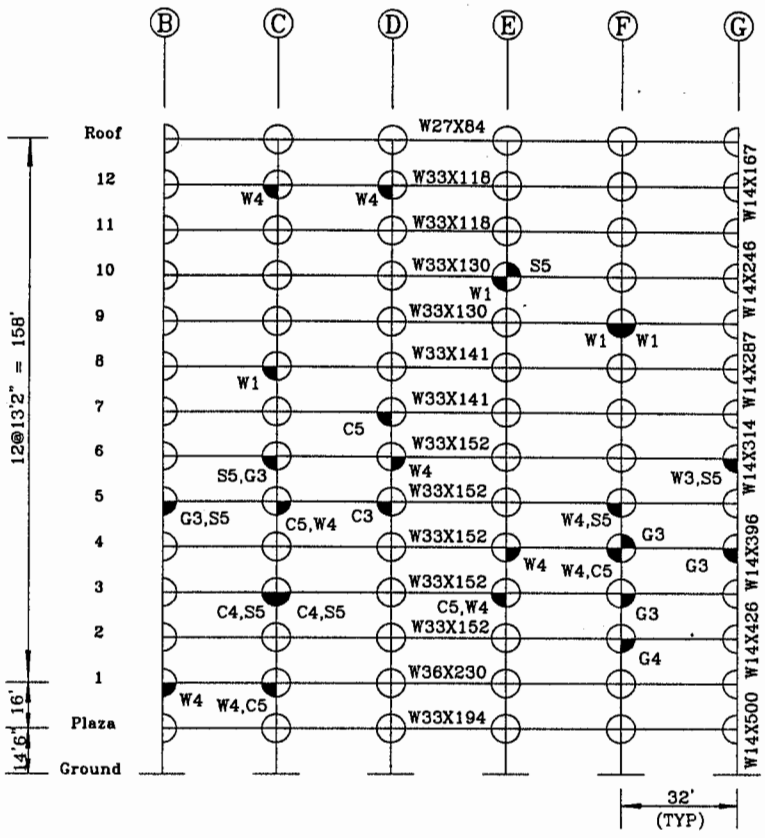

Figure 1 Elevation and Damage Pattern of the Frame (West Side)

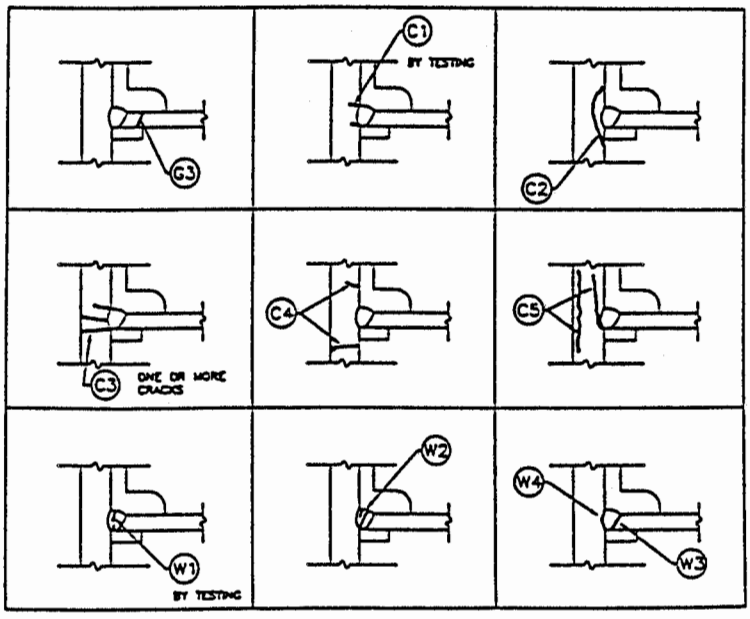

Figure 2 Moment-Resisting Frame Damage Type

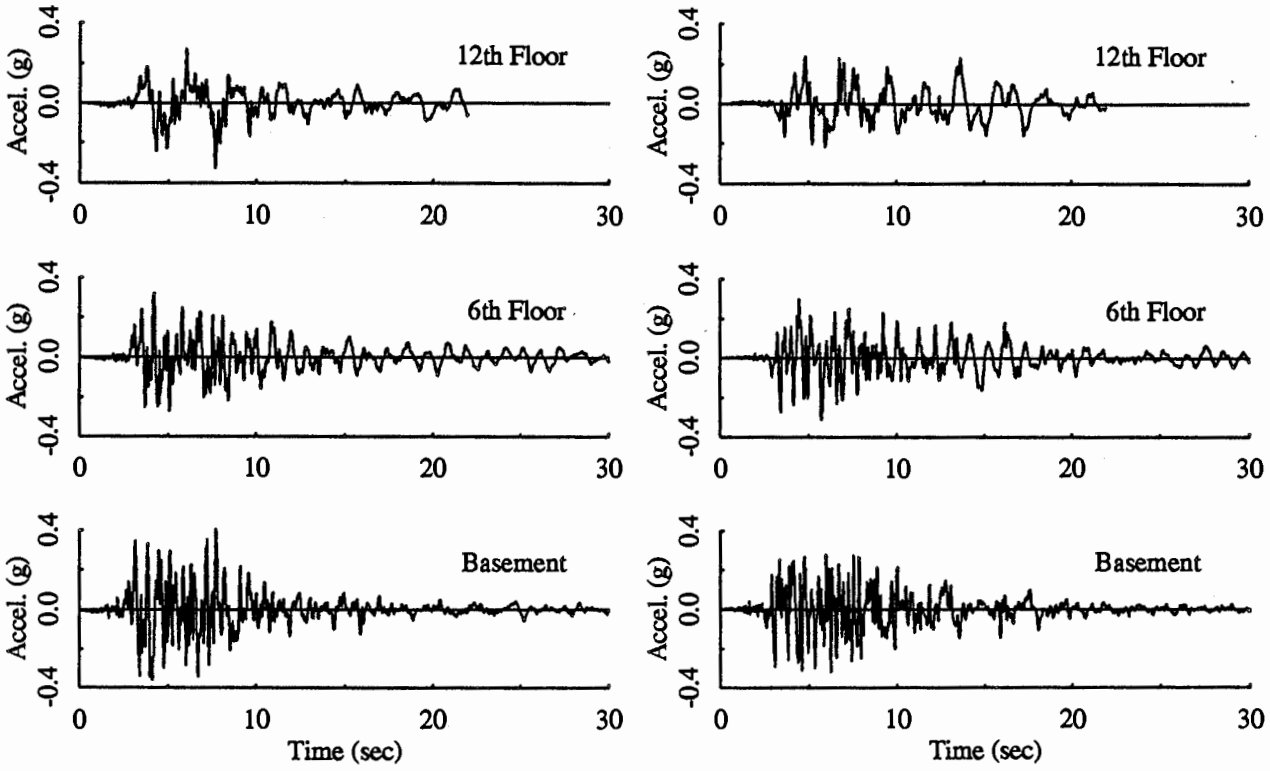

(a) N-S Components (b) E-W Components

Figure 3 Recorded Absolute Accelerations (Oxnard Record, 1994 Northridge)

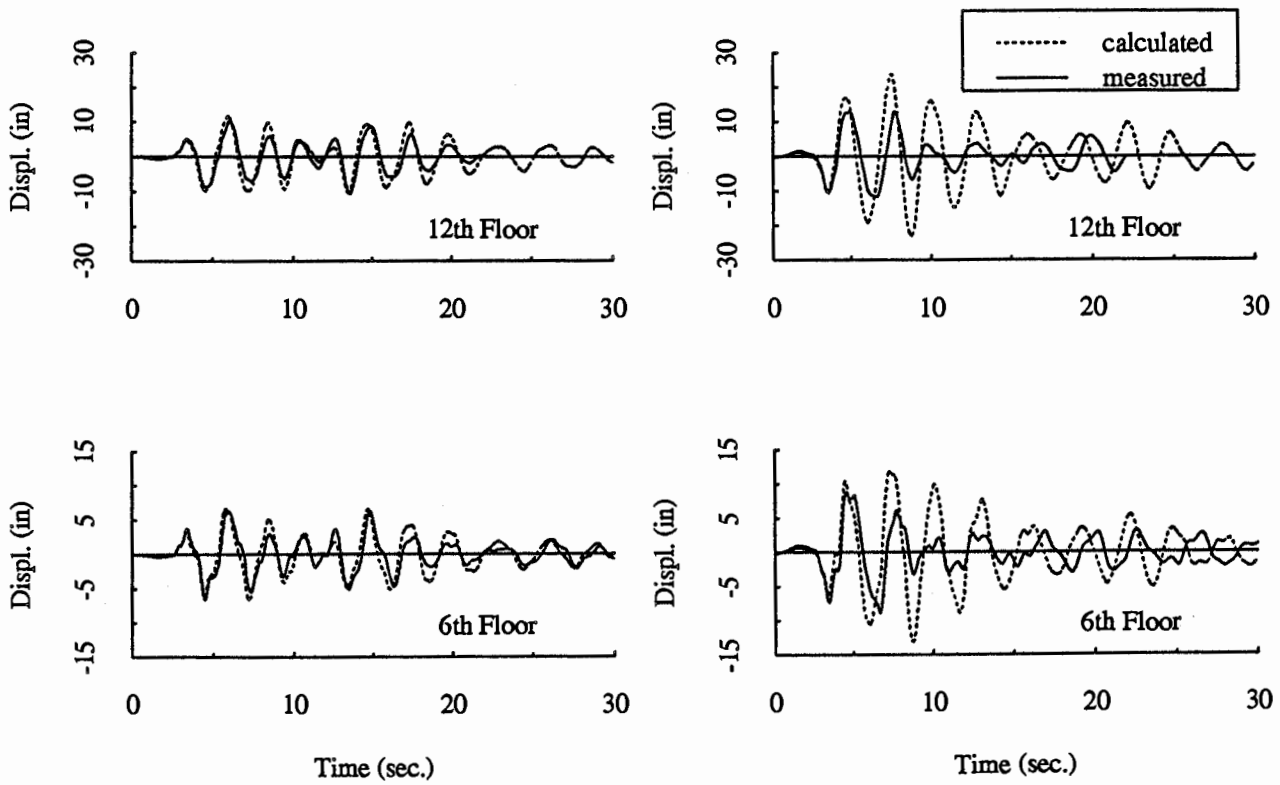

(a) E-W Direction (b) N-S Direction

Figure 4 Elastic Time-History Correlation (Oxnard Record, 1994 Northridge)

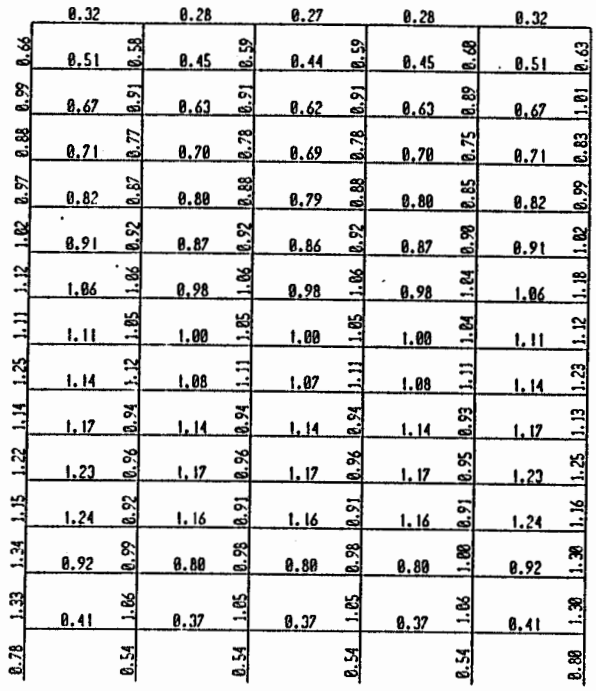

Figure 5 Demand/Capacitiy Ratio (N-S)

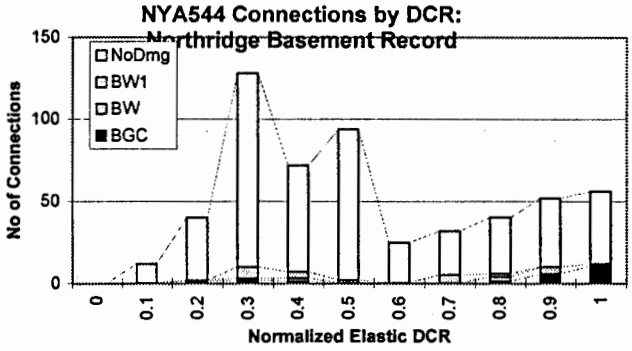

Distribution of Inspected and Analyzed (Case 6) Connections by Normalized DCR							
NRDCR	ALL	BGC	BGCW	BGCWW1	BW	BW1	No Dmg
0	0	0	0	0	0	0	0
0.1	12	0	0	0	0	0	12
0.2	40	1	2	2	1	0	38
0.3	128	2	3	10	1	7	118
0.4	72	1	3	7	2	4	65
0.5	94	0	0	2	0	2	92
0.6	25	0	0	0	0	0	25
0.7	32	0	0	5	0	5	27
0.8	40	1	4	6	3	2	34
0.9	52	6	10	10	4	0	42
1	56	11	12	12	1	0	44
Total:	551	22	34	54	12	20	497

(a) Distribution of Inspected and Analyzed Connections with DCRs

Figure 6 Distribution of Inspected Connections with Normalized DCRs (continued)

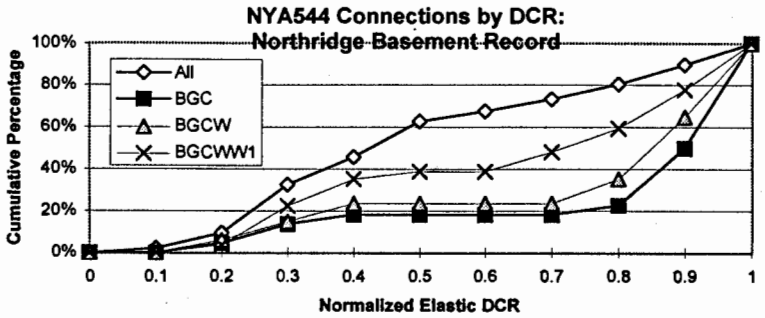

Cumulative Distribution of Inspected and Analyzed (Case 6) Connections by Normalized DCR				
CUMULATIVE VALUES				
NRDCR	All	BGC	BGCW	BGCWW1
0	0.00	0.00	0.00	0.00
0.1	0.02	0.00	0.00	0.00
0.2	0.09	0.05	0.06	0.04
0.3	0.33	0.14	0.15	0.22
0.4	0.46	0.18	0.24	0.35
0.5	0.63	0.18	0.24	0.39
0.6	0.67	0.18	0.24	0.39
0.7	0.73	0.18	0.24	0.48
0.8	0.80	0.23	0.35	0.59
0.9	0.90	0.50	0.65	0.78
1	1.00	1.00	1.00	1.00

(b) Cumulative Distribution of Inspected Connections with Normalize DCR

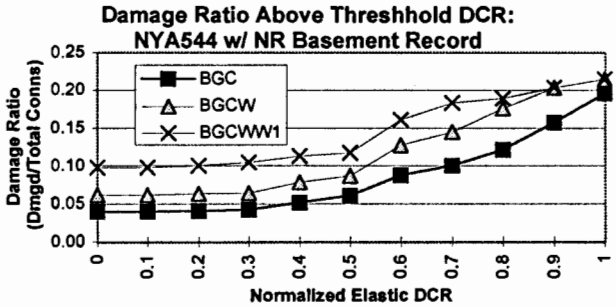

Damage Ratios of Inspected and Analyzed (Case 6) Connections above Threshold Normalized DCR							
NRDCR	All	Cum BGC	Cum BGCW	Cum BGCWW1	BGC	BGCW	BGCWW1
0	551	22	34	54	0.04	0.06	0.10
0.1	551	22	34	54	0.04	0.06	0.10
0.2	539	22	34	54	0.04	0.06	0.10
0.3	499	21	32	52	0.04	0.06	0.10
0.4	371	19	29	42	0.05	0.08	0.11
0.5	299	18	26	35	0.06	0.09	0.12
0.6	205	18	26	33	0.09	0.13	0.16
0.7	180	18	26	33	0.10	0.14	0.18
0.8	148	18	26	28	0.12	0.18	0.19
0.9	108	17	22	22	0.16	0.20	0.20
1	56	11	12	12	0.20	0.21	0.21

(c) Distribution of Damage Ratios

Figure 6 Distribution of Inspected Connections with Normalized DCRs

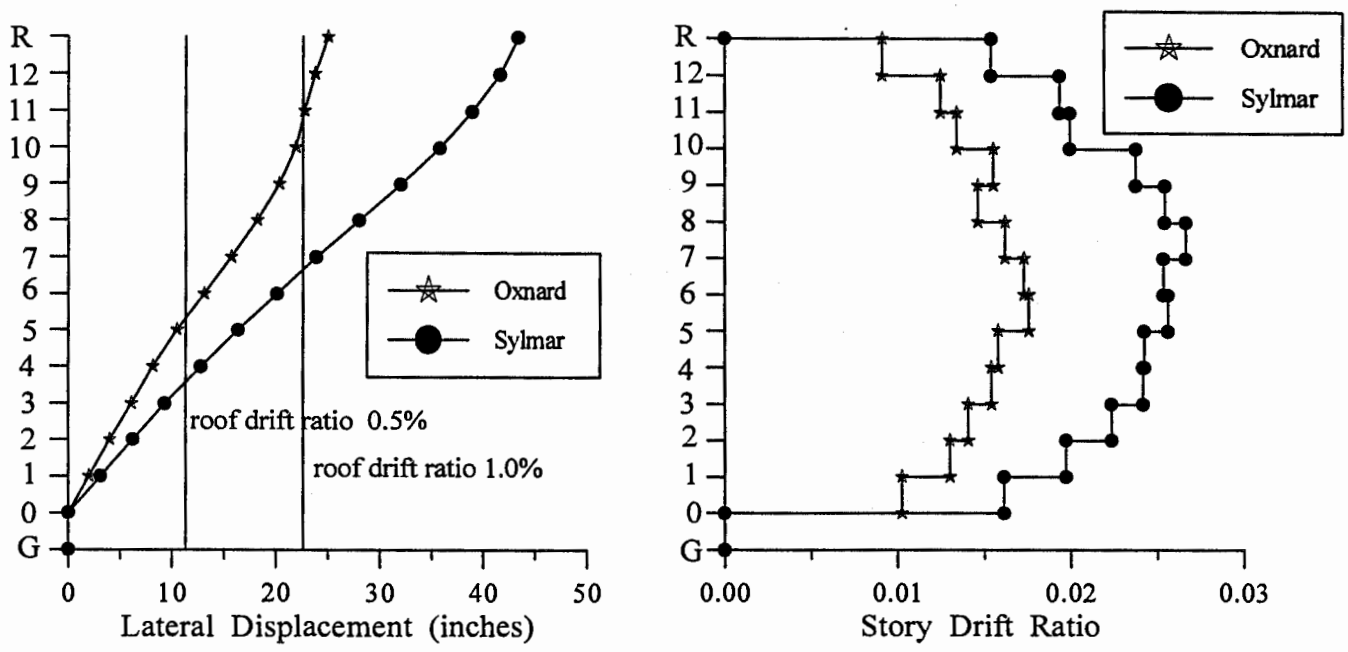

Figure 7 Elastic Response Envelopes (N-S)

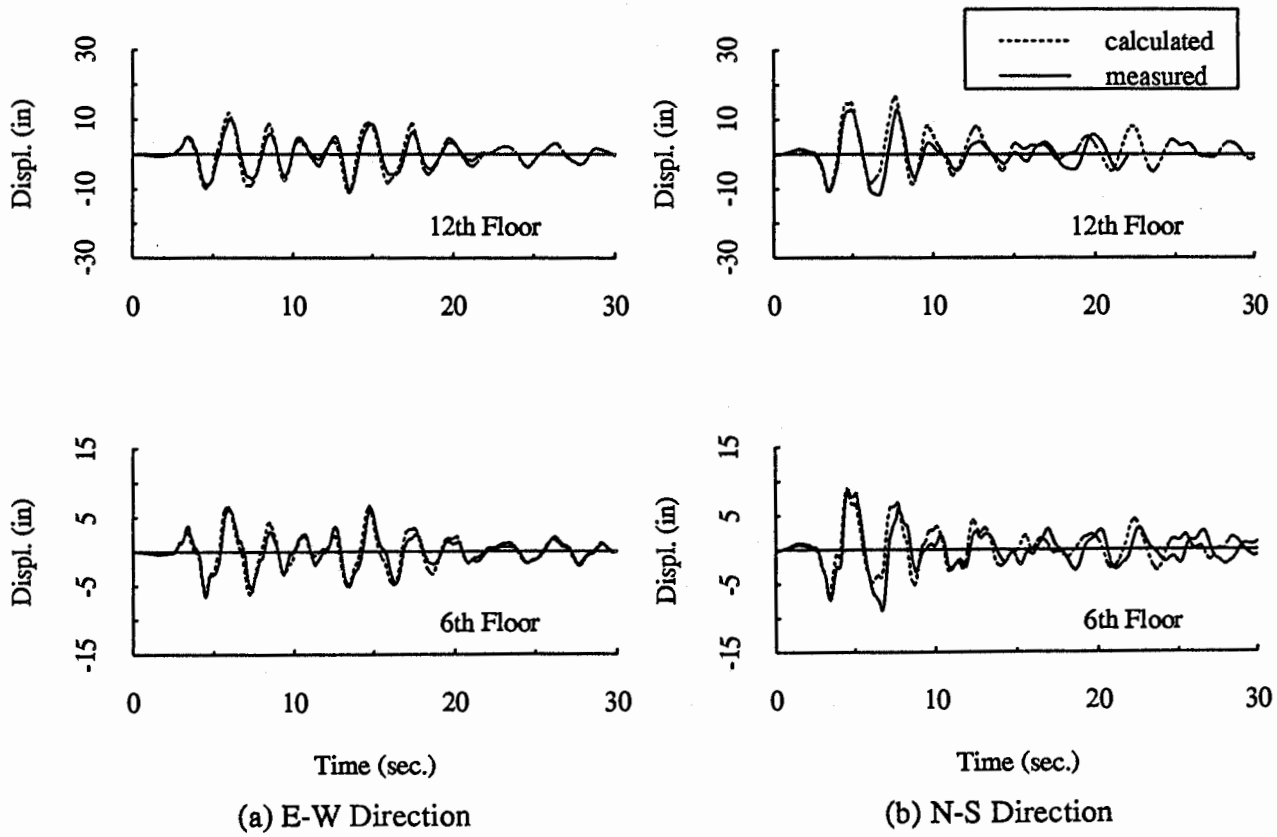

Figure 8 Inelastic Time-History Correlation (Oxnard Record, 1994 Northridge)

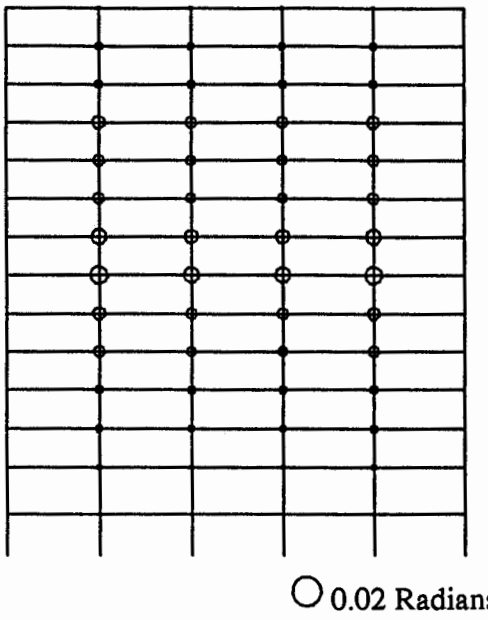

(a) Panel Zones

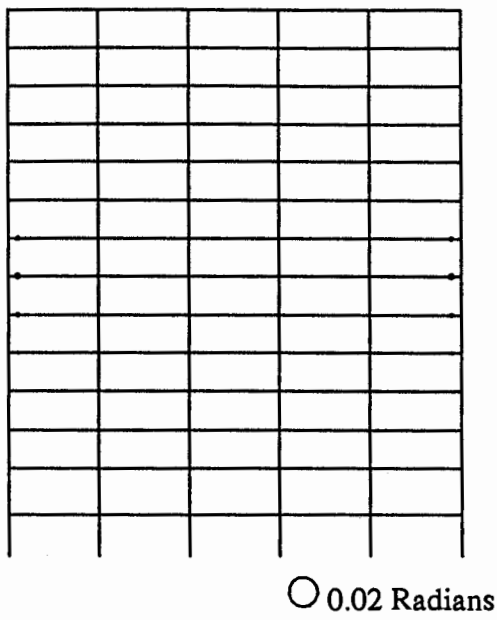

(b) Beams and Columns

Figure 9 Distributions of Maximum Plastic Rotations
(N-S Comp. Of Oxnard Record, 1994 Northridge)

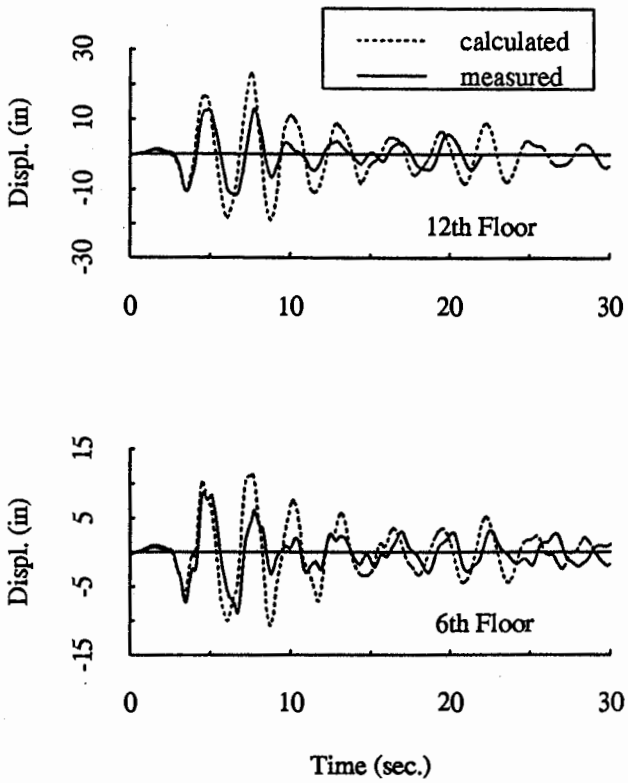

(a) Displacement Time-History Correlation

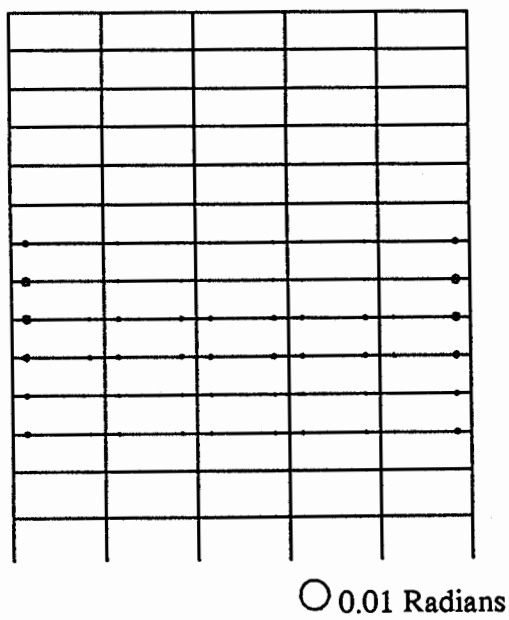

(b) Plastic Rotations

Figure 10 Inelastic Time-History Correlation *without* Modeling Panel Zones

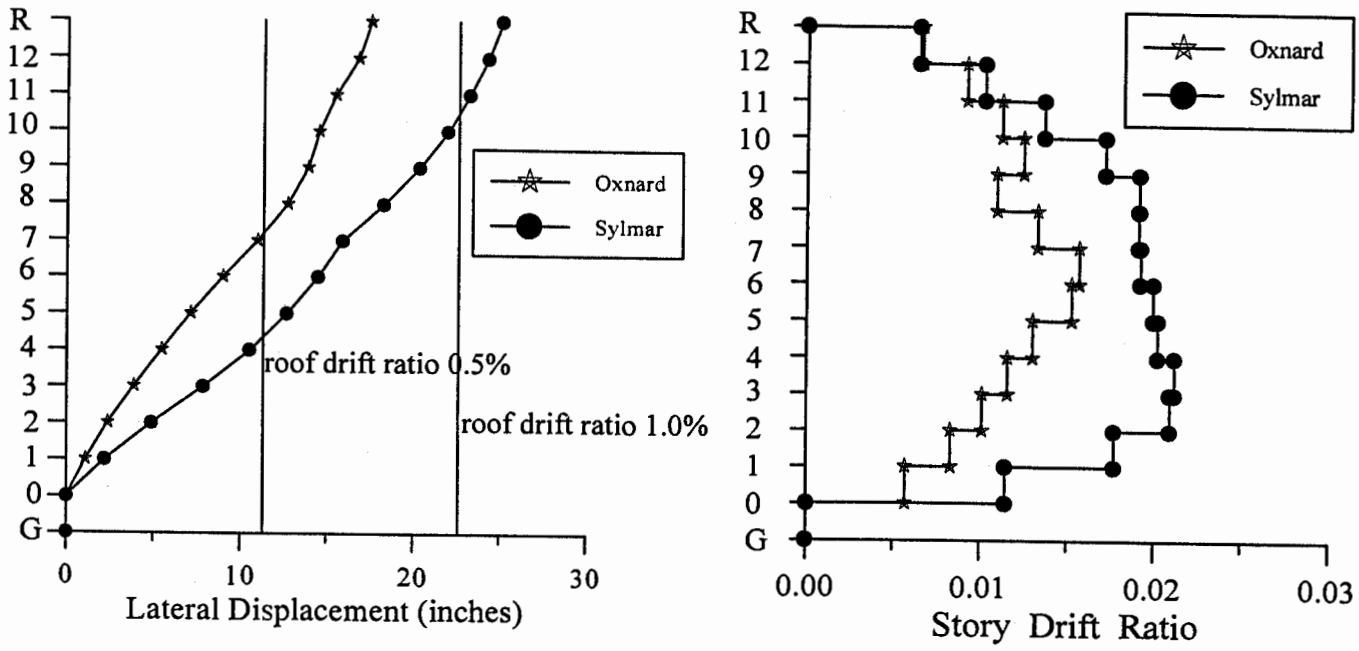

Figure 11 Inelastic Response Envelopes (N-S)

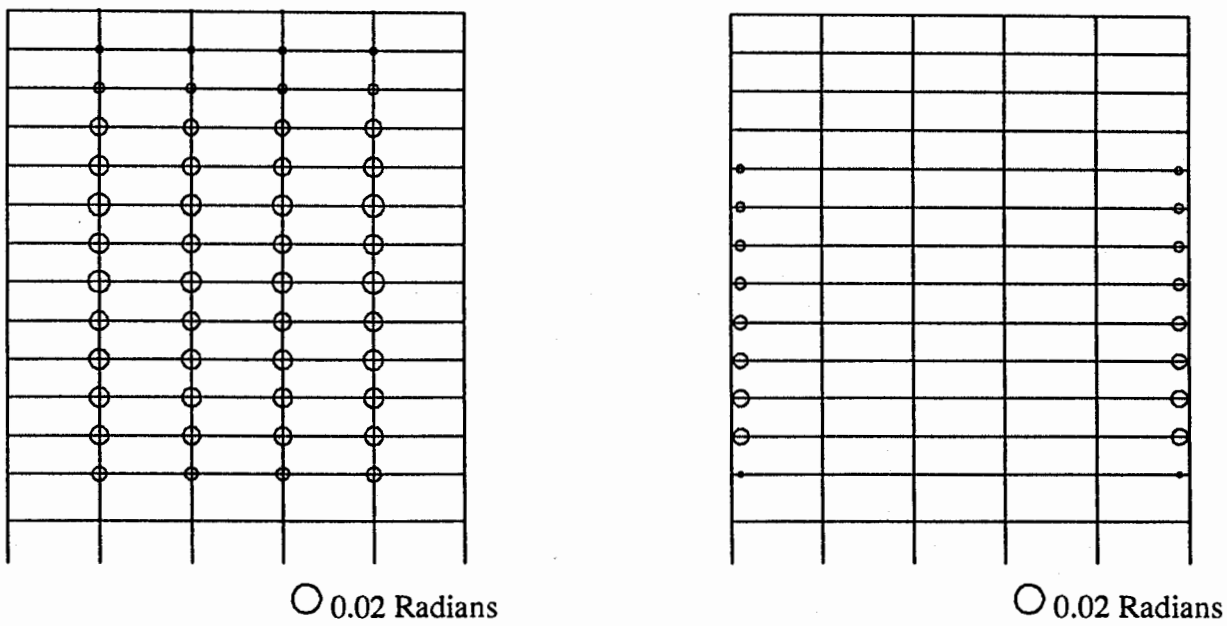

(a) Panel Zones

(b) Beams and Columns

Figure 12 Distributions of Maximum Plastic Rotations
(N-S Comp. Of Sylmar Record, 1994 Northridge)